



# Engineering Journal IJOER

Volume-10, Issue-8, August 2024

ISSN: 2395-6992



## Preface

We would like to present, with great pleasure, the inaugural volume-10, Issue-8, August 2024, of a scholarly journal, *International Journal of Engineering Research & Science*. This journal is part of the AD Publications series *in the field of Engineering, Mathematics, Physics, Chemistry and science Research Development*, and is devoted to the gamut of Engineering and Science issues, from theoretical aspects to application-dependent studies and the validation of emerging technologies.

This journal was envisioned and founded to represent the growing needs of Engineering and Science as an emerging and increasingly vital field, now widely recognized as an integral part of scientific and technical investigations. Its mission is to become a voice of the Engineering and Science community, addressing researchers and practitioners in below areas:

Chemical Engineering	
Biomolecular Engineering	Materials Engineering
Molecular Engineering	Process Engineering
Corrosion Engineering	
Civil Engineering	
Environmental Engineering	Geotechnical Engineering
Structural Engineering	Mining Engineering
Transport Engineering	Water resources Engineering
Electrical Engineering	
Power System Engineering	Optical Engineering
Mechanical Engineering	
Acoustical Engineering	Manufacturing Engineering
Optomechanical Engineering	Thermal Engineering
Power plant Engineering	Energy Engineering
Sports Engineering	Vehicle Engineering
Software Engineering	
Computer-aided Engineering	Cryptographic Engineering
Teletraffic Engineering	Web Engineering
System Engineering	
Mathematics	
Arithmetic	Algebra
Number theory	Field theory and polynomials
Analysis	Combinatorics
Geometry and topology	Topology
Probability and Statistics	Computational Science
Physical Science	Operational Research
Physics	
Nuclear and particle physics	Atomic, molecular, and optical physics
Condensed matter physics	Astrophysics
Applied Physics	Modern physics
Philosophy	Core theories

Chemistry	
Analytical chemistry	Biochemistry
Inorganic chemistry	Materials chemistry
Neurochemistry	Nuclear chemistry
Organic chemistry	Physical chemistry
Other Engineering Areas	
Aerospace Engineering	Agricultural Engineering
Applied Engineering	Biomedical Engineering
Biological Engineering	Building services Engineering
Energy Engineering	Railway Engineering
Industrial Engineering	Mechatronics Engineering
Management Engineering	Military Engineering
Petroleum Engineering	Nuclear Engineering
Textile Engineering	Nano Engineering
Algorithm and Computational Complexity	Artificial Intelligence
Electronics & Communication Engineering	Image Processing
Information Retrieval	Low Power VLSI Design
Neural Networks	Plastic Engineering

Each article in this issue provides an example of a concrete industrial application or a case study of the presented methodology to amplify the impact of the contribution. We are very thankful to everybody within that community who supported the idea of creating a new Research with IJOER. We are certain that this issue will be followed by many others, reporting new developments in the Engineering and Science field. This issue would not have been possible without the great support of the Reviewer, Editorial Board members and also with our Advisory Board Members, and we would like to express our sincere thanks to all of them. We would also like to express our gratitude to the editorial staff of AD Publications, who supported us at every stage of the project. It is our hope that this fine collection of articles will be a valuable resource for *IJOER* readers and will stimulate further research into the vibrant area of Engineering and Science Research.



Mukesh Arora  
(Chief Editor)

## **Board Members**

### **Mr. Mukesh Arora (Editor-in-Chief)**

BE (Electronics & Communication), M.Tech (Digital Communication), currently serving as Assistant Professor in the Department of ECE.

### **Prof. Dr. Fabricio Moraes de Almeida**

Professor of Doctoral and Master of Regional Development and Environment - Federal University of Rondonia.

### **Dr. Parveen Sharma**

Dr Parveen Sharma is working as an Assistant Professor in the School of Mechanical Engineering at Lovely Professional University, Phagwara, Punjab.

### **Prof. S. Balamurugan**

Department of Information Technology, Kalaingar Karunanidhi Institute of Technology, Coimbatore, Tamilnadu, India.

### **Dr. Omar Abed Elkareem Abu Arqub**

Department of Mathematics, Faculty of Science, Al Balqa Applied University, Salt Campus, Salt, Jordan, He received PhD and Msc. in Applied Mathematics, The University of Jordan, Jordan.

### **Dr. AKPOJARO Jackson**

Associate Professor/HOD, Department of Mathematical and Physical Sciences, Samuel Adegboyega University, Ogwa, Edo State.

### **Dr. Ajoy Chakraborty**

Ph.D.(IIT Kharagpur) working as Professor in the department of Electronics & Electrical Communication Engineering in IIT Kharagpur since 1977.

### **Dr. Ukar W. Soelistijo**

Ph D, Mineral and Energy Resource Economics, West Virginia State University, USA, 1984, retired from the post of Senior Researcher, Mineral and Coal Technology R&D Center, Agency for Energy and Mineral Research, Ministry of Energy and Mineral Resources, Indonesia.

### **Dr. Samy Khalaf Allah Ibrahim**

PhD of Irrigation &Hydraulics Engineering, 01/2012 under the title of: "Groundwater Management under Different Development Plans in Farafra Oasis, Western Desert, Egypt".

### **Dr. Ahmet ÇİFCİ**

Ph.D. in Electrical Engineering, Currently Serving as Head of Department, Burdur Mehmet Akif Ersoy University, Faculty of Engineering and Architecture, Department of Electrical Engineering.

## **Dr. M. Varatha Vijayan**

Annauniversity Rank Holder, Commissioned Officer Indian Navy, Ncc Navy Officer (Ex-Serviceman Navy), Best Researcher Awardee, Best Publication Awardee, Tamilnadu Best Innovation & Social Service Awardee From Lions Club.

## **Dr. Mohamed Abdel Fatah Ashabrawy Moustafa**

PhD. in Computer Science - Faculty of Science - Suez Canal University University, 2010, Egypt.

Assistant Professor Computer Science, Prince Sattam bin AbdulAziz University ALkharj, KSA.

## **Prof.S.Balamurugan**

Dr S. Balamurugan is the Head of Research and Development, Quants IS & CS, India. He has authored/co-authored 35 books, 200+ publications in various international journals and conferences and 6 patents to his credit. He was awarded with Three Post-Doctoral Degrees - Doctor of Science (D.Sc.) degree and Two Doctor of Letters (D.Litt) degrees for his significant contribution to research and development in Engineering.

## **Dr. Mahdi Hosseini**

Dr. Mahdi did his Pre-University (12<sup>th</sup>) in Mathematical Science. Later he received his Bachelor of Engineering with Distinction in Civil Engineering and later he Received both M.Tech. and Ph.D. Degree in Structural Engineering with Grade "A" First Class with Distinction.

## **Dr. Anil Lamba**

Practice Head – Cyber Security, EXL Services Inc., New Jersey USA.

Dr. Anil Lamba is a researcher, an innovator, and an influencer with proven success in spearheading Strategic Information Security Initiatives and Large-scale IT Infrastructure projects across industry verticals. He has helped bring about a profound shift in cybersecurity defense. Throughout his career, he has parlayed his extensive background in security and a deep knowledge to help organizations build and implement strategic cybersecurity solutions. His published researches and conference papers has led to many thought provoking examples for augmenting better security.

## **Dr. Ali İhsan KAYA**

Currently working as Associate Professor in Mehmet Akif Ersoy University, Turkey.

**Research Area:** Civil Engineering - Building Material - Insulation Materials Applications, Chemistry - Physical Chemistry – Composites.

## **Dr. Parsa Heydarpour**

Ph.D. in Structural Engineering from George Washington University (Jan 2018), GPA=4.00.

## **Dr. Heba Mahmoud Mohamed Afify**

Ph.D degree of philosophy in Biomedical Engineering, Cairo University, Egypt worked as Assistant Professor at MTI University.

### **Dr. Aurora Angela Pisano**

Ph.D. in Civil Engineering, Currently Serving as Associate Professor of Solid and Structural Mechanics (scientific discipline area nationally denoted as ICAR/08—"Scienza delle Costruzioni"), University Mediterranea of Reggio Calabria, Italy.

### **Dr. Faizullah Mahar**

Associate Professor in Department of Electrical Engineering, Balochistan University Engineering & Technology Khuzdar. He is PhD (Electronic Engineering) from IQRA University, Defense View, Karachi, Pakistan.

### **Prof. Viviane Barrozo da Silva**

Graduated in Physics from the Federal University of Paraná (1997), graduated in Electrical Engineering from the Federal University of Rio Grande do Sul - UFRGS (2008), and master's degree in Physics from the Federal University of Rio Grande do Sul (2001).

### **Dr. S. Kannadhasan**

Ph.D (Smart Antennas), M.E (Communication Systems), M.B.A (Human Resources).

### **Dr. Christo Ananth**

Ph.D. Co-operative Networks, M.E. Applied Electronics, B.E Electronics & Communication Engineering Working as Associate Professor, Lecturer and Faculty Advisor/ Department of Electronics & Communication Engineering in Francis Xavier Engineering College, Tirunelveli.

### **Dr. S.R.Boselin Prabhu**

Ph.D, Wireless Sensor Networks, M.E. Network Engineering, Excellent Professional Achievement Award Winner from Society of Professional Engineers Biography Included in Marquis Who's Who in the World (Academic Year 2015 and 2016). Currently Serving as Assistant Professor in the department of ECE in SVS College of Engineering, Coimbatore.

### **Dr. PAUL P MATHAI**

Dr. Paul P Mathai received his Bachelor's degree in Computer Science and Engineering from University of Madras, India. Then he obtained his Master's degree in Computer and Information Technology from Manonmanium Sundaranar University, India. In 2018, he received his Doctor of Philosophy in Computer Science and Engineering from Noorul Islam Centre for Higher Education, Kanyakumari, India.

### **Dr. M. Ramesh Kumar**

Ph.D (Computer Science and Engineering), M.E (Computer Science and Engineering).

Currently working as Associate Professor in VSB College of Engineering Technical Campus, Coimbatore.

### **Dr. Maheshwar Shrestha**

Postdoctoral Research Fellow in DEPT. OF ELE ENGG & COMP SCI, SDSU, Brookings, SD Ph.D, M.Sc. in Electrical Engineering from SOUTH DAKOTA STATE UNIVERSITY, Brookings, SD.

### **Dr. D. Amaranatha Reddy**

Ph.D. (Postdoctoral Fellow, Pusan National University, South Korea), M.Sc., B.Sc. : Physics.

## **Dr. Dibya Prakash Rai**

Post Doctoral Fellow (PDF), M.Sc., B.Sc., Working as Assistant Professor in Department of Physics in Pachhungga University College, Mizoram, India.

## **Dr. Pankaj Kumar Pal**

Ph.D R/S, ECE Deptt., IIT-Roorkee.

## **Dr. P. Thangam**

PhD in Information & Communication Engineering, ME (CSE), BE (Computer Hardware & Software), currently serving as Associate Professor in the Department of Computer Science and Engineering of Coimbatore Institute of Engineering and Technology.

## **Dr. Pradeep K. Sharma**

PhD., M.Phil, M.Sc, B.Sc, in Physics, MBA in System Management, Presently working as Provost and Associate Professor & Head of Department for Physics in University of Engineering & Management, Jaipur.

## **Dr. R. Devi Priya**

Ph.D (CSE), Anna University Chennai in 2013, M.E, B.E (CSE) from Kongu Engineering College, currently working in the Department of Computer Science and Engineering in Kongu Engineering College, Tamil Nadu, India.

## **Dr. Sandeep**

Post-doctoral fellow, Principal Investigator, Young Scientist Scheme Project (DST-SERB), Department of Physics, Mizoram University, Aizawl Mizoram, India- 796001.

## **Dr. Roberto Volpe**

Faculty of Engineering and Architecture, Università degli Studi di Enna "Kore", Cittadella Universitaria, 94100 – Enna (IT).

## **Dr. S. Kannadhasan**

Ph.D (Smart Antennas), M.E (Communication Systems), M.B.A (Human Resources).

**Research Area:** Engineering Physics, Electromagnetic Field Theory, Electronic Material and Processes, Wireless Communications.

## **Mr. Amit Kumar**

Amit Kumar is associated as a Researcher with the Department of Computer Science, College of Information Science and Technology, Nanjing Forestry University, Nanjing, China since 2009. He is working as a State Representative (HP), Spoken Tutorial Project, IIT Bombay promoting and integrating ICT in Literacy through Free and Open Source Software under National Mission on Education through ICT (NMEICT) of MHRD, Govt. of India; in the state of Himachal Pradesh, India.

## **Mr. Tanvir Singh**

Tanvir Singh is acting as Outreach Officer (Punjab and J&K) for MHRD Govt. of India Project: Spoken Tutorial - IIT Bombay fostering IT Literacy through Open Source Technology under National Mission on Education through ICT (NMEICT). He is also acting as Research Associate since 2010 with Nanjing Forestry University, Nanjing, Jiangsu, China in the field of Social and Environmental Sustainability.

## **Mr. Abilash**

M.Tech in VLSI, BTech in Electronics & Telecommunication engineering through A.M.I.E.T.E from Central Electronics Engineering Research Institute (C.E.E.R.I) Pilani, Industrial Electronics from ATI-EPI Hyderabad, IEEE course in Mechatronics, CSHAM from Birla Institute Of Professional Studies.

## **Mr. Varun Shukla**

M.Tech in ECE from RGPV (Awarded with silver Medal By President of India), Assistant Professor, Dept. of ECE, PSIT, Kanpur.

## **Mr. Shrikant Harle**

Presently working as a Assistant Professor in Civil Engineering field of Prof. Ram Meghe College of Engineering and Management, Amravati. He was Senior Design Engineer (Larsen & Toubro Limited, India).

## **Zairi Ismael Rizman**

Senior Lecturer, Faculty of Electrical Engineering, Universiti Teknologi MARA (UiTM) (Terengganu) Malaysia Master (Science) in Microelectronics (2005), Universiti Kebangsaan Malaysia (UKM), Malaysia. Bachelor (Hons.) and Diploma in Electrical Engineering (Communication) (2002), UiTM Shah Alam, Malaysia.

## **Mr. Ronak**











**Qualification:** M.Tech. in Mechanical Engineering (CAD/CAM), B.E.

Presently working as a Assistant Professor in Mechanical Engineering in ITM Vocational University, Vadodara. Mr. Ronak also worked as Design Engineer at Finstern Engineering Private Limited, Makarpura, Vadodara.



# Table of Contents

Volume-10, Issue-8, August 2024

S. No	Title	Page No.
1	<b>Experimental Investigation on Super Alloys using Al7178 Metal Matrix Tools (Aluminum Oxide Materials of Different Weight Percentages 3%, 6%, 9%, 12%) on Electrical Discharge Machining</b> <b>Authors:</b> G. Sravan Kumar, Dr. L. Siva Rama Krishna, Dr. S. Gajanana  <b>DOI:</b> <a href="https://dx.doi.org/10.5281/zenodo.13604924">https://dx.doi.org/10.5281/zenodo.13604924</a>  <b>DIN Digital Identification Number:</b> IJOER-AUG-2024-1	01-20
2	<b>Properties of Symmetry of Space and Time, Hamilton's Principle and the Invariants</b> <b>Authors:</b> Korotkevich S.V.  <b>DOI:</b> <a href="https://dx.doi.org/10.5281/zenodo.13605206">https://dx.doi.org/10.5281/zenodo.13605206</a>  <b>DIN Digital Identification Number:</b> IJOER-AUG-2024-3	21-30
3	<b>Legal and Regulatory Structure Prevailing in the UK related to Data Privacy and Public Surveillance</b> <b>Authors:</b> Amarachukwu Grace Nwosu  <b>DOI:</b> <a href="https://dx.doi.org/10.5281/zenodo.13605416">https://dx.doi.org/10.5281/zenodo.13605416</a>  <b>DIN Digital Identification Number:</b> IJOER-AUG-2024-6	31-39
4	<b>Enhancing Material Removal Rate in EDM with Green Dielectrics: A Regression Modeling Approach</b> <b>Authors:</b> M. Sirisha, Dr. S. Gajanana, Dr. P. Laxminarayana  <b>DOI:</b> <a href="https://dx.doi.org/10.5281/zenodo.13605569">https://dx.doi.org/10.5281/zenodo.13605569</a>  <b>DIN Digital Identification Number:</b> IJOER-AUG-2024-7	40-48
5	<b>Solving the Node-Weighted Steiner Tree Problem using Reinforcement Learning</b> <b>Authors:</b> Zongbo Yang  <b>DOI:</b> <a href="https://dx.doi.org/10.5281/zenodo.13605810">https://dx.doi.org/10.5281/zenodo.13605810</a>  <b>DIN Digital Identification Number:</b> IJOER-AUG-2024-8	49-58

# Experimental Investigation on Super Alloys using Al7178 Metal Matrix Tools (Aluminum Oxide Materials of Different Weight Percentages 3%, 6%, 9%, 12%) on Electrical Discharge Machining

G. Sravan Kumar<sup>1\*</sup>, Dr. L. Siva Rama Krishna<sup>2</sup>, Dr. S. Gajanana<sup>3</sup>

<sup>1</sup>Research Scholar, Department of Mechanical Engineering, Osmania University, Hyderabad, India

<sup>2</sup>Professor, Department of Mechanical Engineering, Osmania University, Hyderabad, India

<sup>3</sup>Professor, Department of Mechanical Engineering, MVSR, Hyderabad, India

\*Corresponding Author

Received: 03 August 2024/ Revised: 10 August 2024/ Accepted: 16 August 2024/ Published: 31-08-2024

Copyright © 2024 International Journal of Engineering Research and Science

This is an Open-Access article distributed under the terms of the Creative Commons Attribution

Non-Commercial License (<https://creativecommons.org/licenses/by-nc/4.0>) which permits unrestricted

Non-commercial use, distribution, and reproduction in any medium, provided the original work is properly cited.

**Abstract**— The primary nonferrous metals consist of aluminum, copper, lead, nickel, chromium, manganese, magnesium, titanium, zinc, and alloys like brass. These metals are typically extracted from minerals such as sulfides, carbonates, and silicates. The addition of alloying elements enhances their properties when added in appropriate quantities. Non-ferrous metals are widely utilized due to their favorable characteristics, such as lightweight (e.g. aluminum), high electrical conductivity (e.g. copper), non-magnetism, and corrosion resistance (e.g. zinc). One of the most significant nonferrous alloys is the Al 7178 series alloy, which is commonly used in technical applications. EDM is a method for controlled removal of metal that uses electrical discharge. This process uses an electric spark to erode the workpiece and shape the finished part. Metal removal is accomplished by applying a pulsed charge (ON/OFF) to the workpiece through an electrode using a high-frequency current. The workpiece is subjected to controlled erosion, resulting in the removal of tiny metal fragments. Typically, electrodes made of copper, graphite, and brass are utilized in EDM. The current project investigates the use of the metal matrix material Al7 178 (Al<sub>2</sub>O<sub>3</sub>-reinforced Al7178) as a tool/electrode for machining the superalloy Superni 90. In this study, aluminum alloy 7178 is utilized as the base metal, Al<sub>2</sub>O<sub>3</sub> is chosen as the reinforcement material, weight fraction 3%, 6%, 9%, 12% as the tool material, and nickel-based alloy as the workpiece being studied. Superni90 has been selected. Material removal rate, surface roughness and tool wear rate in electrical machining discharge. Regression models were developed for MRR and TWR based on experimental data. The Mitutoyo surface roughness measuring machine is utilized to measure the surface roughness of the processed workpiece. The geometric accuracy of the surfaces created on the workpiece is evaluated using MATLAB software.

**Keywords**— Electric discharge machining, Current (I), Voltage(V), Pulse on time (Ton), Pulse off time (Toff), Surface Roughness (SR), Tool Wear Rate (TWR), Material Removal Rate (MRR), % error, Regression models Electrical Conductivity.

## I. INTRODUCTION

Modern technology has led to an explosion of lightweight materials, particularly in the realms of aerospace and automobile. The research on new high-strength aluminum alloys is being undertaken by numerous countries and corporations. The aim is to decrease It is crucial to minimize the weight of the materials as much as possible, while still maintaining the stability of mechanics and corrosion resistance for the overall structure, in order to substitute traditional materials such as iron. Numerous modern materials utilized in space exploration, weaponry, and nuclear industries have been produced in the past few years. Due to their increased hardness, toughness, strength, and resistance to heat and wear, these materials cannot be processed using conventional machining methods. The emergence of New Machining Procedures, or Unconventional Machining Procedures, is a direct outcome of the advancement of innovative metal removal techniques. These procedures enable the fabrication of intricate and sophisticated shapes on the workpiece, regardless of the material's strength, hardness, toughness, or brittleness.

These methods are frequently employed for:

- Working with materials that are hard to machine through conventional methods.

- Efficiently producing complex surfaces.
- Additionally, achieving very high surface qualities.

The processes can produce intricate and detailed shapes on the workpiece and are unaffected by the strength, hardness, toughness, or brittleness of the materials. Heat treatment can be used to strengthen Al 7XXX alloys, which are primarily composed of the Zn element. The alloy Al-Zn- Mg, which contains magnesium, is a weldable and high-strength aluminum alloy with excellent thermal deformation characteristics and a broad quenching range. By applying the appropriate heat treatment, it is possible to achieve increased strength, enhanced welding capabilities, and improved corrosion resistance. Incorporating Cu into the Al-Zn-Mg alloy results in the creation of the Al-Zn-Mg-Cu alloy. This alloy demonstrates enhanced strength when compared to Al 2XXX alloys, which is why it is commonly referred to as an ultra-high-strength aluminum alloy, this material exhibits similar yield and tensile strengths, leading to a remarkably high specific strength. However, its plasticity and high-temperature strength are somewhat lacking. It is best suited for use as a load-bearing structural component at or below room temperature or below 120°C. It is easily processed, provides good corrosion resistance, and exhibits high toughness.

## II. EXPERIMENTAL PROCEDURE

### 2.1 EDM Process:

EDM utilizes spark erosion to burn tiny holes in metal through electrical sparks. In order for the process to work properly, both the workpiece and the electrode need to be conductive materials.

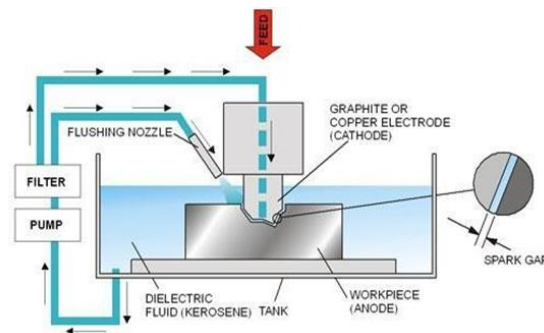


**FIGURE 1: EDM Process**

The controlled metal-removal technique known as Electrical Discharge Machining (EDM) relies on electric spark erosion to eliminate metal. The workpiece is shaped into the desired form of the final product using an electric spark as the cutting tool in this process. High-frequency current is applied through the electrode to the workpiece in the metal-removal process, involving a pulsating electrical charge.

### 2.2 Superni90 Super Alloy:

Superalloys are recognized for their outstanding mechanical strength, resistance to creep at elevated temperatures, surface stability, and corrosion and oxidation resistance. These corrosion-resistant super alloys are extensively employed in extreme environments where high heat and corrosion resistance are essential for the integrity of the final product. Sectors like chemical and petrochemical processing, aero-engines, power plants, and oil and gas industries frequently utilize these super alloys. Superalloys with a nickel base are considered a specialized type of high-performance alloys characterized by a significant nickel content. Differences in nickel-based superalloys are usually apparent in the material composition, which is adjusted to create specific properties according to the intended use.

**TABLE 1  
Properties of Superni90 work material**

S. No.	Property	Metric System
1	Density	8.18g/cm <sup>3</sup>
2	Melting point Temperature	850°C
3	Tensile Strength	1010MPa
4	Yield Strength	755MPa



**FIGURE 1: Superni 90**

### 2.3 Stir Casting:

The stir casting process involves the continuous stirring of the melt, and the aluminum melt surface is exposed to the atmosphere, causing continuous oxidation of the melt. To melt the Al 7178 alloy, a furnace, crucible, blower, coal, and other materials are required. The furnace is heated up to 800°C, while the melting point of Aluminum 7178 is 660°C.

In this study, Aluminum alloy was reinforced with Aluminum Oxide materials at different weight percentages of 3%, 6%, 9%, and 12% of Al<sub>2</sub>O<sub>3</sub>. The process was carried out using a Resistance furnace equipped with a stirring system, at a constant speed of 100 rpm and a stirring duration of 10-15 minutes, at a casting temperature was precisely 750±5°C. The mixing equipment was composed of a driving motor capable of generating a rotation speed ranging from 100rpm. Balanced Aluminum 7178 alloys were melted in a graphite crucible, while the Al<sub>2</sub>O<sub>3</sub> particle was preheated in a muffle furnace set at a temperature of 900°C for around one hour to eliminate surface impurities.

The ceramic particle Al<sub>2</sub>O<sub>3</sub> was poured slowly and continuously into the molten metal, which was being stirred at 100 rpm, in order to prepare metal matrix composites through the stir casting method.

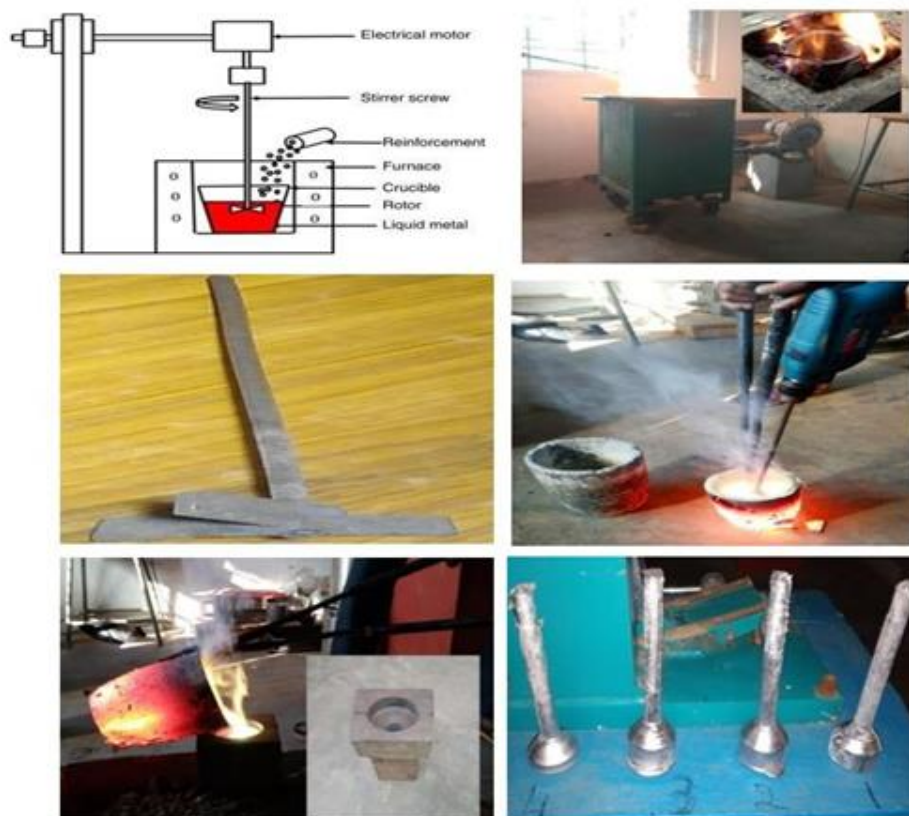


**FIGURE 2: Process of Stir Casting and Al 7178 MMC's**

## 2.4 Aluminum 7178 Alloy and Machining of MMC's:

Aluminum, the most abundant and widely recognized metal globally, is the second most widely used material after steel. It is commonly utilized for foil and conductor links, but the addition of other elements is crucial for various applications. Aluminum alloy combinations are identified by four digits: the first digit represents a primary alloying component, the second indicates the base composite, and the third and fourth signify individual compounds. Aluminum 7178 alloy has exceptional uses in Aviation field, Automobile sector, and Structural industries. Subsequently in this study, Al 7178 alloy has been chosen for investigation.

After the casting process, the specimen samples are machined on lathe machine. The optimum composition of AL7178 material as electrode and Nickel based Super Alloy - Superni90 for machining investigations and process parameter optimization. The machined specimens of metal matrix composites are shown in figure.



**FIGURE 3: Machined Al7178 MMC's**

## 2.5 Surface Roughness (Ra):

The roughness of a surface is a measurement of the texture of a floor, which is determined by deviations in the direction of a surface's normal vector from its perfect form. Large deviations indicate roughness, while small deviations indicate smoothness. Surface metrology typically regards roughness as the high-frequency, short-wavelength features of a surface being assessed. However, in practical applications, understanding both the amplitude and frequency is vital to ensure that a floor is suitable for a specific purpose.



**FIGURE 4: Mitutoyo Surface Roughness Tester**

## 2.6 Electrical Discharge Machining (Experimental Process):

(EDM) is an unconventional and non-contact machining operation utilized in industries such as manufacturing, aerospace, automotive, communication, and biotechnology to produce precision products. The method represented in the image is very useful for machining hard and brittle conductive materials because it can melt any electrically conductive substance, regardless of hardness. EDM is a type of thermal machining in which material is removed from the workpiece using thermal energy produced by an electric spark. The tool and the workpiece are skillfully immersed in a dielectric medium, like kerosene, deionized water, or any other suitable fluid. The non-contact nature of the system, combined with nearly force-free machining, facilitates the gentle and precise machining of electrode materials to shape very hard, delicate, or thin work pieces.

## III. RESULTS AND DISCUSSION

### 3.1 Experimentation:

The experiments were performed on EDM, EDM oil is selected as dielectric. The material is selected as Superni90 having dimension of 120mm diameter and 10mm thickness. Aluminum 7178 alloy. With the optimum composition of AL7178 material

as electrode and Al7178 with 3% Al<sub>2</sub>O<sub>3</sub>, 6% Al<sub>2</sub>O<sub>3</sub>, 9% Al<sub>2</sub>O<sub>3</sub>, 12% Al<sub>2</sub>O<sub>3</sub> and Nickel based Super Alloy - Superni 90 for machining investigations and optimization of process parameters.



**FIGURE 5: Working process of EDM machining**

### 3.2 Material Removal Rate (MRR):

MRR is the ratio of the difference of weight of the workpiece material before and after machining to the machining time.

$$MRR = [(W_{wpbm} - W_{wpam}) / (t * \rho)] \text{ mm}^3/\text{min}$$

$W_{wpbm}$  - Weight of workpiece Before machining;  $W_{wpam}$  - Weight of workpiece After machining

$t$  - Machining period Time 10min

### 3.3 Tool Wear Rate (TWR):

Tool Wear Rate (TWR): TWR is the ratio of the difference of weight of the tool before and after machining to the machining time.

$$TWR = [(W_{etbm} - W_{etam}) / (t * \rho)] \text{ mm}^3/\text{min}$$

$W_{etbm}$  - Weight of electrode Before machining;  $W_{etam}$  - Weight of electrode After machining

$t$  - Machining period Time 10min  $\rho$  - Density of Tool material

### 3.4 Experimentation on Superni90:

The work material selected for experimental investigation is a super alloy which has wide applications in defence with commercial name as Superni90. The electrode material chosen for machining on work material is Al7178 with 3% Al<sub>2</sub>O<sub>3</sub>, 6% Al<sub>2</sub>O<sub>3</sub>, 9% Al<sub>2</sub>O<sub>3</sub>, 12% Al<sub>2</sub>O<sub>3</sub> and the experiment done according to the procedure. Researchers conduct experiments across a wide range of disciplines, usually with the aim of gaining insights into a specific process or system. An experiment involves conducting a trial or a series of trials in which deliberate changes are made to the input variables of a process or system to facilitate the observation and identification of the reasons for changes in the output.



**FIGURE 6: Experimentation on Superni90 work material with Aluminium and Al<sub>2</sub>O<sub>3</sub> 3%, 6%, 9%, 12% as Electrodes on EDM**

Experiment design is the process of determining the number of trails and running circumstances that are necessary and adequate to solve the problem with the requisite accuracy

### 3.5 Linear Regression:

The field of image processing is continuously evolving, aiming to enhance images and extract important information through a series of operations. This method of signal processing involves taking an image as input and generating either the image itself or its relevant characteristics as output. Image analysis is crucial for structural characterization of porous substances and has applications in various fields.

The structural properties of media can be represented by statistical and morphology aspects, such as dimensions and shapes, or topological properties. Image processing in MATLAB is used to analyze the trueness of diameter.

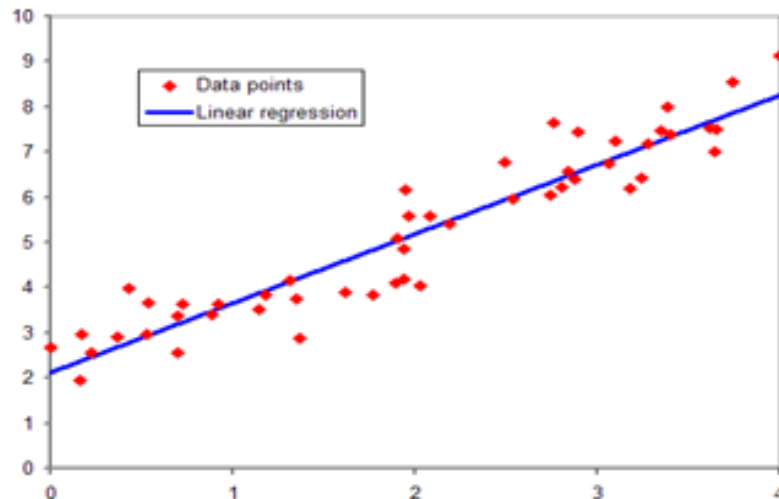


FIGURE 7: Linear Regression

### 3.6 Results:

The Tool Material is Al7178 with 3% Al<sub>2</sub>O<sub>3</sub>, 6% Al<sub>2</sub>O<sub>3</sub>, 9% Al<sub>2</sub>O<sub>3</sub>, 12% Al<sub>2</sub>O<sub>3</sub> is performed on the workpiece material i.e., Superni90 super alloy on Electrical Discharge Machining process. The obtained values of Material Removal Rate (MRR), Tool Wear Rate (TWR) and Surface Roughness (SR) for the Aluminum alloy Al7178 with 3% Al<sub>2</sub>O<sub>3</sub>, 6% Al<sub>2</sub>O<sub>3</sub>, 9% Al<sub>2</sub>O<sub>3</sub>, 12% Al<sub>2</sub>O<sub>3</sub> Metal matrix composite which is performed on Superni90 super alloy on Electrical Discharge Machining are listed in below table for Al7178 with 3% Al<sub>2</sub>O<sub>3</sub>.

#### 3.6.1 Case-1 : Electrode Al7178 + Al<sub>2</sub>O<sub>3</sub> (3%):

Aluminum Oxide with 3% of material removal rate, tool wear rate and surface roughness are compared is shown in figure.

TABLE 2  
MRR, TWR & SR of Al7178+ Al<sub>2</sub>O<sub>3</sub> (3%)

S.No.	Current (I) Amps	Pulse on time (T <sub>on</sub> ) μs	Pulse off time (T <sub>off</sub> ) μs	Voltage (V) Volts	MRR (mm <sup>3</sup> /min)	TWR (mm <sup>3</sup> /min)	SR (μm)
1	4	100	50	30	3.454	0.506	2.581
2	4	450	75	45	1.466	1.265	2.883
3	4	1000	100	60	0.733	1.012	2.973
4	8	100	75	60	1.1	1.518	3.787
5	8	450	100	30	2.2	1.772	2.981
6	8	1000	50	45	0.855	1.265	3.732
7	12	100	100	45	2.078	0.759	3.654
8	12	450	50	60	1.711	3.037	3.048
9	12	1000	75	30	1.222	0.506	3.024

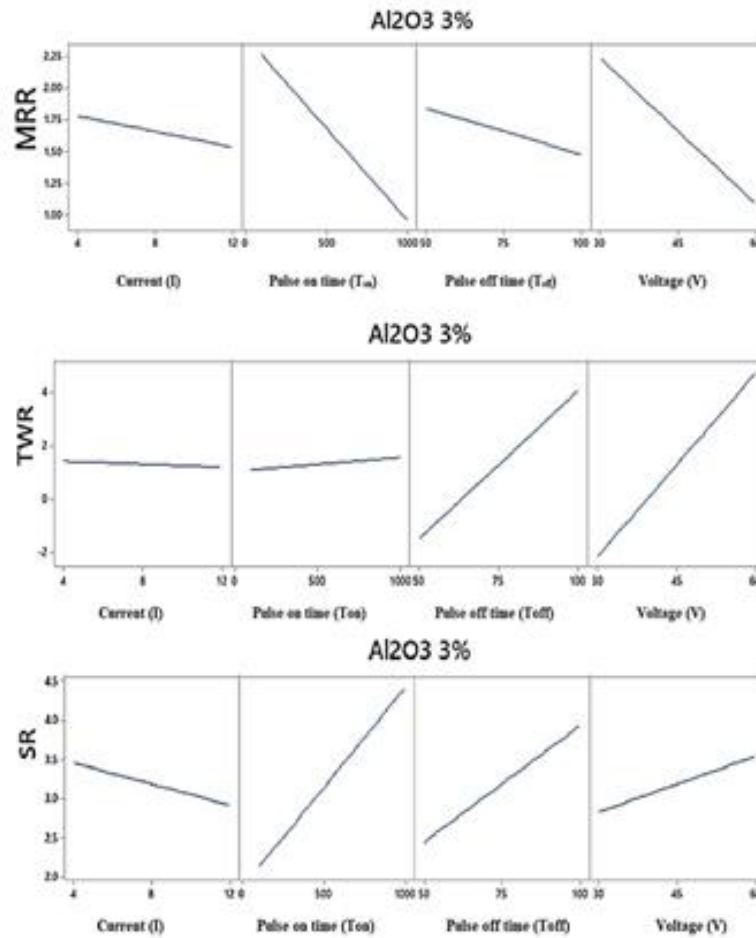


**FIGURE 8: Graphical relation among input parameters and MRR, TWR,SR (Al2O3 3%)**

Aluminum Oxide with 3% of material removal rate, tool wear rate and surface roughness are compared is shown in figure.

**Comparison Graph for MRR, TWR & SR**

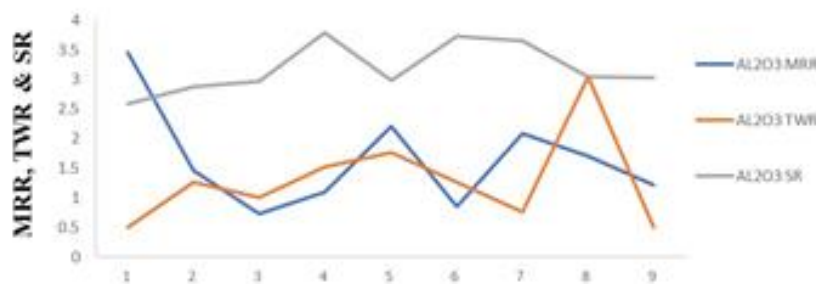


**FIGURE 9: Comparison graph for MRR, TWR & SR**

For 3% Al<sub>2</sub>O<sub>3</sub>, the Material Removal Rate is high (3.45mm<sup>3</sup>/min), Surface Roughness is less for Trail 1 which is 2.581µm. Hence, the optimum condition for 3% Al<sub>2</sub>O<sub>3</sub> is Trail 1 (**Parameters:** current 12amps, pulse on time 1000µs, pulse off time 75µs, voltage 30volts).

Similarly for all the remaining three trails of Al<sub>7178</sub> with 3% Al<sub>2</sub>O<sub>3</sub>, 6% Al<sub>2</sub>O<sub>3</sub>, 9% Al<sub>2</sub>O<sub>3</sub>, 12% Al<sub>2</sub>O<sub>3</sub> are performed and evaluated.

**Geometric Analysis:**

The trueness of the diameter is analyzed by imageprocessing in MATLAB.



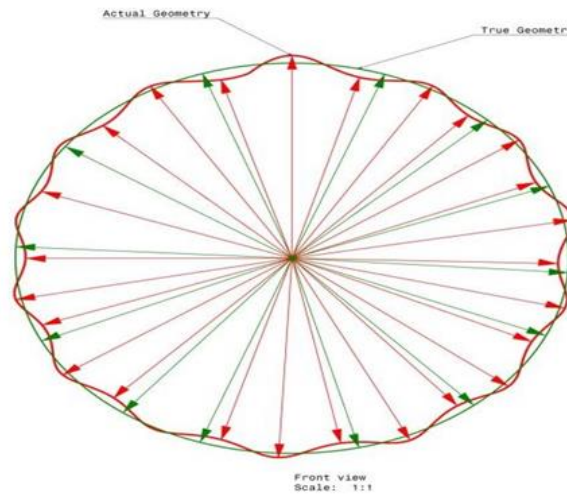


**FIGURE 10: 2D image of centroid location**

The evaluation of this image processing can be performed using MAT Lab software. The six images which are obtained using MATLAB for surface roughness are named as crop image, Black & white, Histogram, Normalized, Normalized Histogram and Binary.

Geometric Analysis (Circularity Accuracy) for Al7178 with 3% Al<sub>2</sub>O<sub>3</sub> tool input parameters (V = 30, I = 4, Ton =100, Toff =50) images are obtained for 3% Al<sub>2</sub>O<sub>3</sub> for Trails (3A1 to 3A9) by using image processing in MATLAB and the percentage error obtained for 3% Al<sub>2</sub>O<sub>3</sub> are shown below:

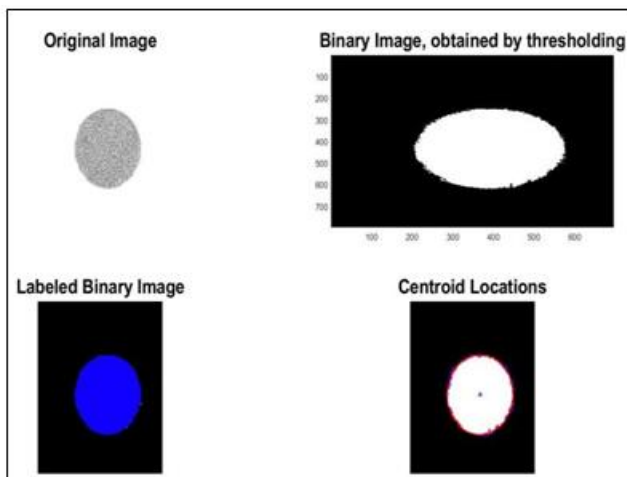


**FIGURE 11: 3% Al<sub>2</sub>O<sub>3</sub> for Trail 1**

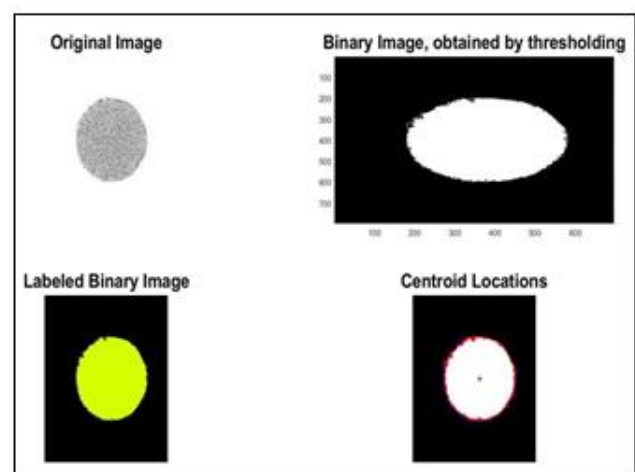


**FIGURE 12: 3% Al<sub>2</sub>O<sub>3</sub> for Tail 2**

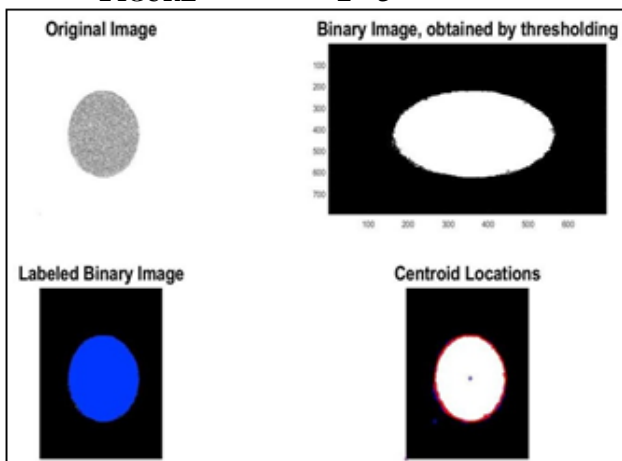


**FIGURE 13: 3% Al<sub>2</sub>O<sub>3</sub> for Trail 5**

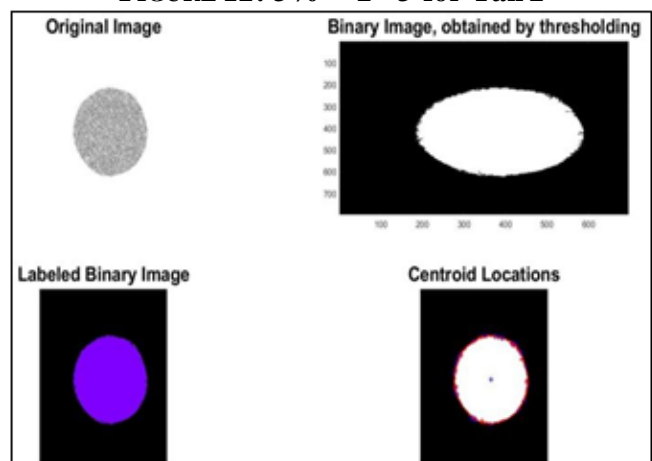


**FIGURE 14: 3% Al<sub>2</sub>O<sub>3</sub> for Trail 3**

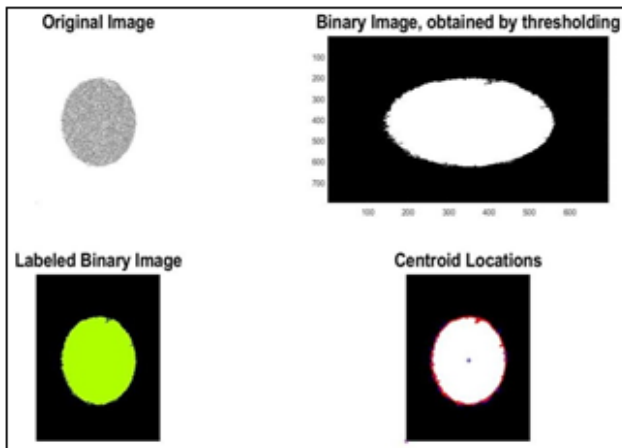


**FIGURE 15: 3% Al<sub>2</sub>O<sub>3</sub> for Trail 6**

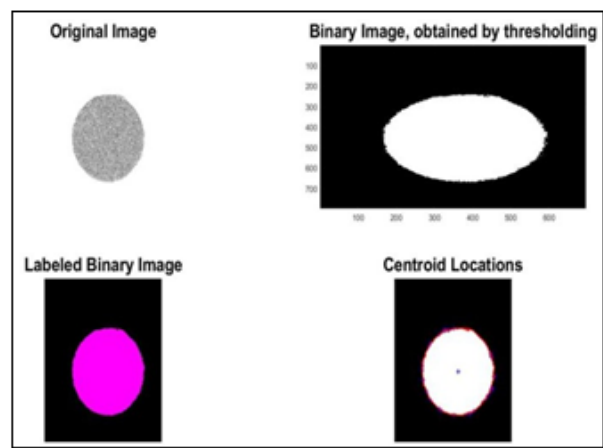


**FIGURE 16: 3% Al<sub>2</sub>O<sub>3</sub> for Trail 4**

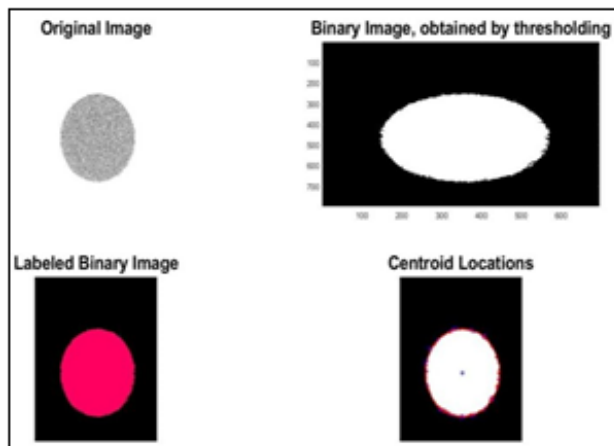


**FIGURE 17: 3% Al<sub>2</sub>O<sub>3</sub> for Trail 7**

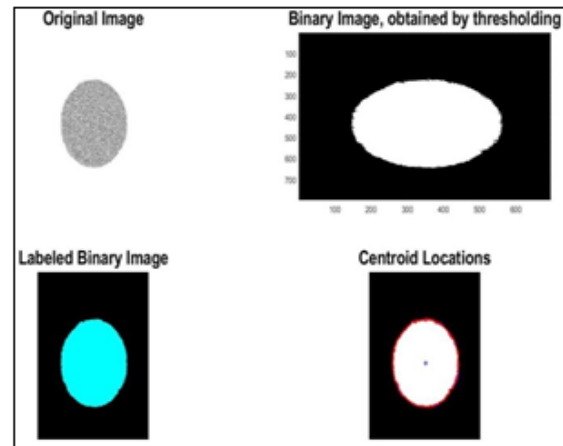


**FIGURE 18: 3% Al<sub>2</sub>O<sub>3</sub> for Trail 8**

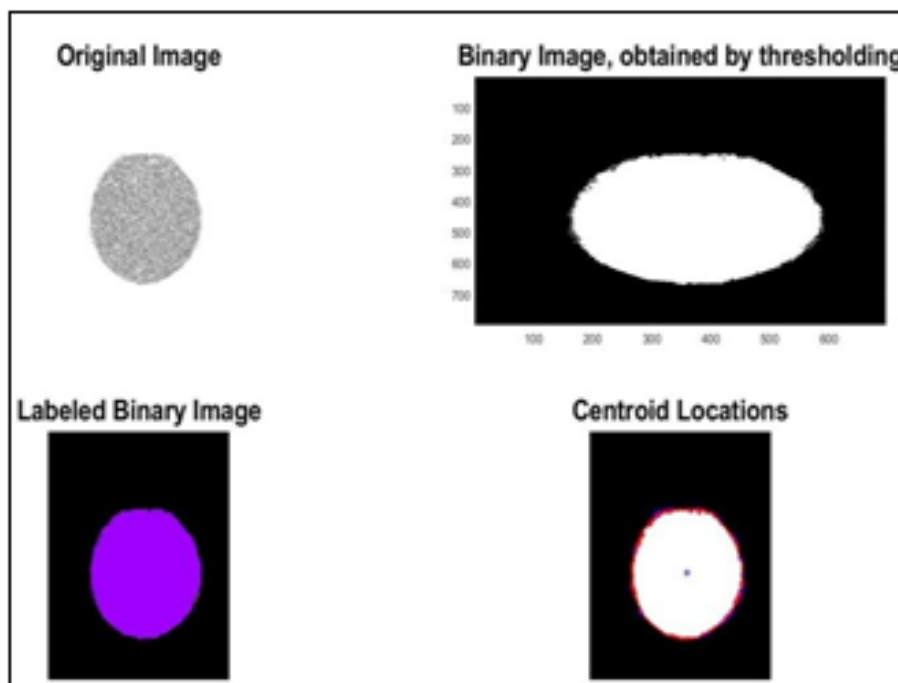


**FIGURE 19: 3% Al<sub>2</sub>O<sub>3</sub> for Trail 9**

All nine trails of Al<sub>7</sub>178 with 3% Al<sub>2</sub>O<sub>3</sub> are evaluated for Geometric Analysis using MATLAB. And Geometric Analysis for Al<sub>7</sub>178 + Al<sub>2</sub>O<sub>3</sub> (3%) is shown below table.

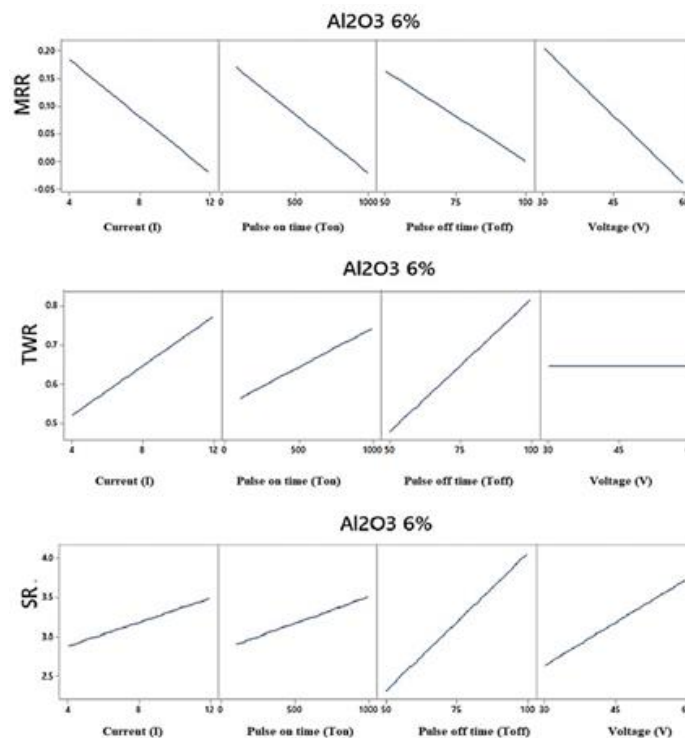
**TABLE 3**  
**Geometric Analysis for Al7178 + Al2O3 (3%)**

S.No.	Current (I) Amps	Pulse on time (T <sub>on</sub> ) μs	Pulse off time (T <sub>off</sub> ) μs	Voltage (V) Volts	MRR (mm <sup>3</sup> /min)	Average Distance (Radius)	% Error	Standard Deviation
1	4	100	50	30	3.454	5.074	1.479	0.086
2	4	450	75	45	1.466	5.08	1.591	0.096
3	4	1000	100	60	0.733	5.119	2.368	0.091
4	8	100	75	60	1.1	4.993	0.125	0.06
5	8	450	100	30	2.2	5.028	0.569	0.068
6	8	1000	50	45	0.855	5.174	3.433	0.117
7	12	100	100	45	2.078	5.023	0.478	0.066
8	12	450	50	60	1.711	5.047	0.939	0.061
9	12	1000	75	30	1.222	5.071	1.415	0.089

**3.6.2 Case-2 : Electrode Al7178 + Al2O3 (6%)**

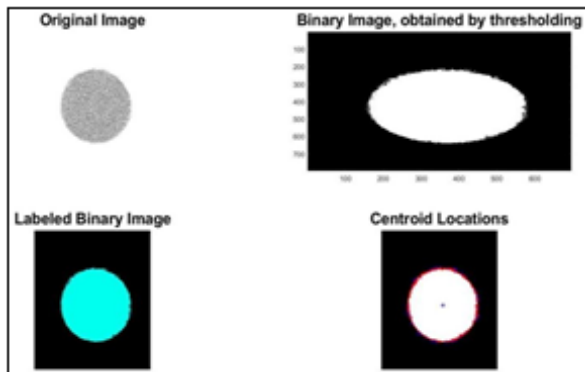
**TABLE 4**  
**MRR, TWR & S of Al7178+ Al2O3 (6%)**

S.No.	Current (I) Amps	Pulse on time (T <sub>on</sub> ) μs	Pulse off time (T <sub>off</sub> ) μs	Voltage (V) Volts	MRR (mm <sup>3</sup> /min)	TWR (mm <sup>3</sup> /min)	SR (μm)
1	4	100	50	30	0.611	0.253	3.21
2	4	450	75	45	0	0.506	2.577
3	4	1000	100	60	0	0.759	3.452
4	8	100	75	60	0	0.506	3.549
5	8	450	100	30	0.122	0.759	4.123
6	8	1000	50	45	0	0.759	2.398
7	12	100	100	45	0	1.012	3.743
8	12	450	50	60	0	0.506	3.267
9	12	1000	75	30	0	0.759	2.301

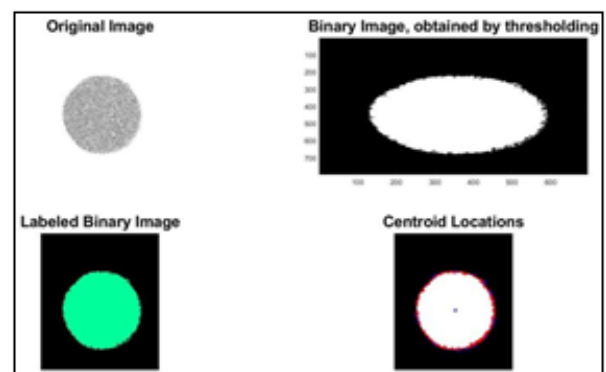


**FIGURE 20: Graphical relation among input parameters and MRR, TWR,SR (Al2O3 6%).**

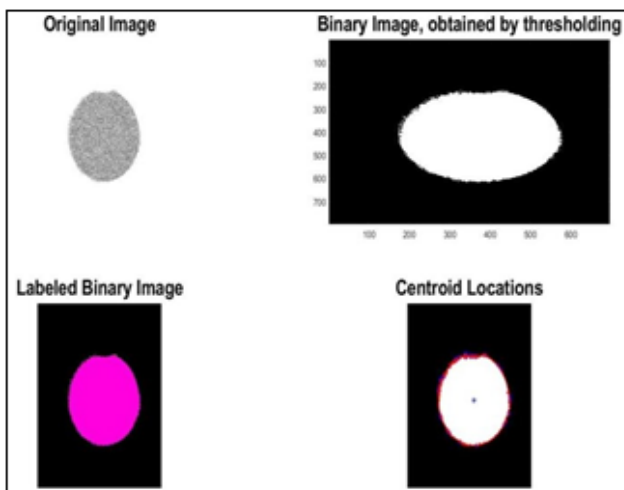
Geometric Analysis (Circularity Accuracy) for Al7178 with 6% Al2O3 tool input parameters ( $V = 30, I = 4, T_{on} = 100, T_{off} = 50$ ) images are obtained for 6% Al2O3 for Trails (6A1 to 6A9) by using image processing in MATLAB and the percentage error obtained for 6% Al2O3 are shown below:



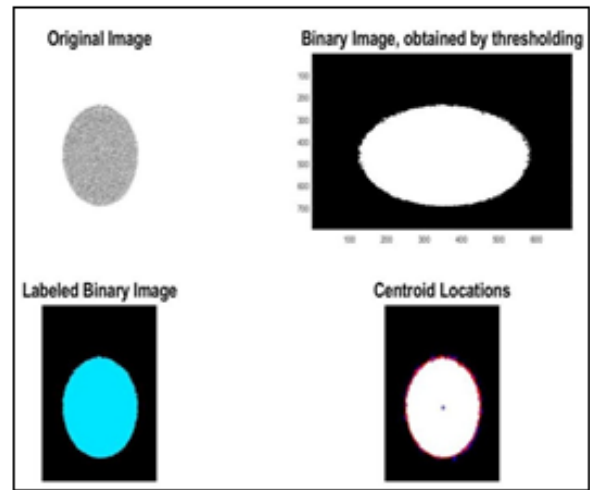
**FIGURE 21: 6% Al2O3 for Trail 1**



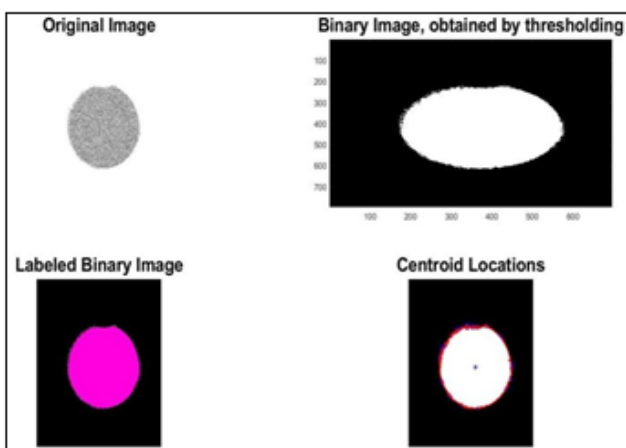
**FIGURE 22: 6% Al2O3 for Trail 2**



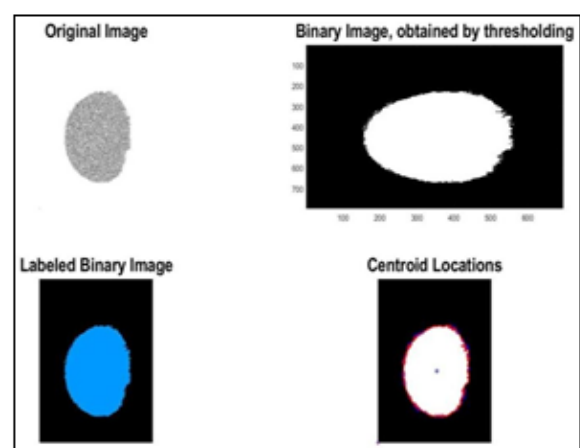
**FIGURE 23: 6% Al2O3 for Trail 3**



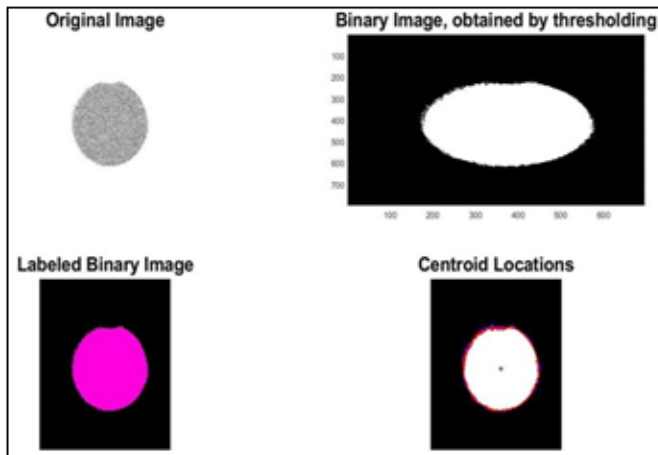
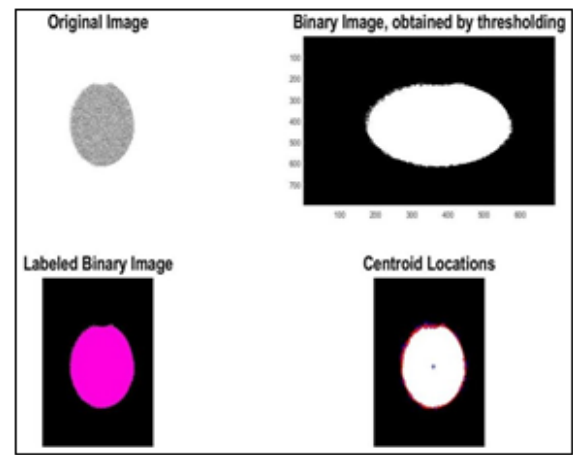
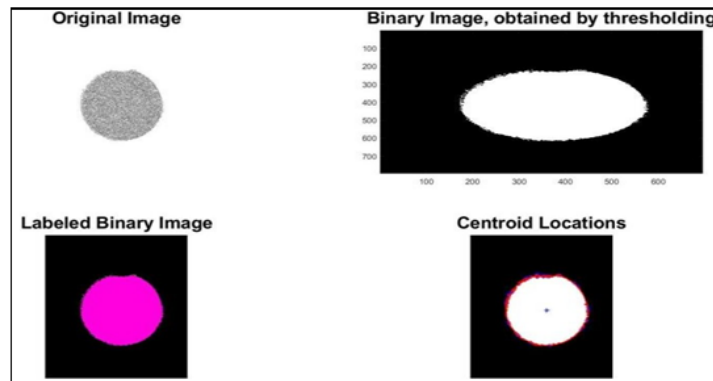
**FIGURE 24: 6% Al2O3 for Trail 4**



**FIGURE 25: 6% Al2O3 for Trail 5**



**FIGURE 26: 6% Al2O3 for Trail 6**

FIGURE 25: 6% Al<sub>2</sub>O<sub>3</sub> for Trail 7FIGURE 26: 6% Al<sub>2</sub>O<sub>3</sub> for Trail 8FIGURE 27: 6% Al<sub>2</sub>O<sub>3</sub> for Trail 9

All nine trails of Al7178 with 6% Al<sub>2</sub>O<sub>3</sub> are evaluated for Geometric Analysis using MATLAB. And Geometric Analysis Al7178 + Al<sub>2</sub>O<sub>3</sub> (6%) is shown below table:

**TABLE 5**  
Geometric Analysis for Al7178 + Al<sub>2</sub>O<sub>3</sub> (6%)

S.No.	Current (I) Amps	Pulse on time (T <sub>on</sub> ) μs	Pulse off time (T <sub>off</sub> ) μs	Voltage (V) Volts	MRR (mm <sup>3</sup> /min)	Average Distance (Radius)	% Error	Standard Deviation
1	4	100	50	30	0.611	5.033	0.672	0.085
2	4	450	75	45	0	5.184	3.631	0.141
3	4	1000	100	60	0	5.055	1.104	0.101
4	8	100	75	60	0	5.06	1.196	0.067
5	8	450	100	30	0.122	5.045	0.908	0.09
6	8	1000	50	45	0	5.063	1.256	0.081
7	12	100	100	45	0	5.058	1.159	0.1
8	12	450	50	60	0	5.031	0.627	0.257
9	12	1000	75	30	0	5.157	3.094	0.148

3.6.3 Case-3: Electrode Al7178 + Al2O3 (9%):

**TABLE 6**  
**MRR, TWR & SR of Al7178+ Al2O3 (9%)**

S.No.	Current (I) Amps	Pulse on time (Ton) $\mu$ s	Pulse off time (Toff) $\mu$ s	Voltage (V) Volts	MRR (mm <sup>3</sup> /min)	TWR (mm <sup>3</sup> /min)	SR ( $\mu$ m)
1	4	100	50	30	3.056	10.886	3.917
2	4	450	75	45	0	0	3.774
3	4	1000	100	60	0.122	0.253	2.604
4	8	100	75	60	0.244	0	3.463
5	8	450	100	30	5.012	0.253	1.539
6	8	1000	50	45	0.366	0.253	3.602
7	12	100	100	45	0.122	2.531	3.483
8	12	450	50	60	0	0.759	3.269
9	12	1000	75	30	0.122	0.759	2.951

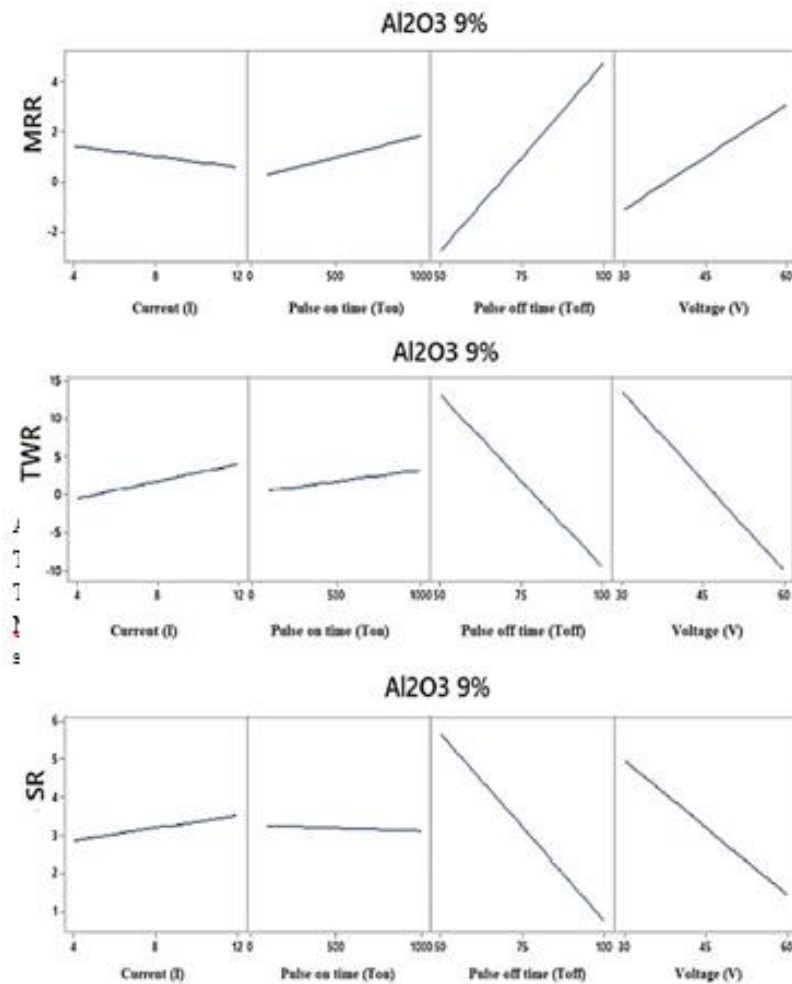


**FIGURE 28: Graphical relation among input parameters and MRR, TWR,SR (Al2O3 9%)**

Geometric Analysis (Circularity Accuracy) for Al7178 with 9% Al2O3 tool input parameters (V = 30, I = 4, Ton =100, Toff =50) images are obtained for 9% Al2O3 for Trails (9A1 to 9A9) by using image processing in MATLAB and the percentage error obtained for 9% Al2O3 are shown below:

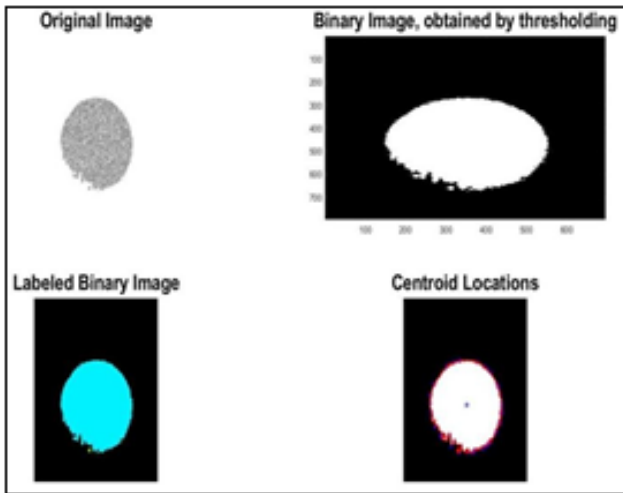


FIGURE 29: 9% Al<sub>2</sub>O<sub>3</sub> for Trail 1

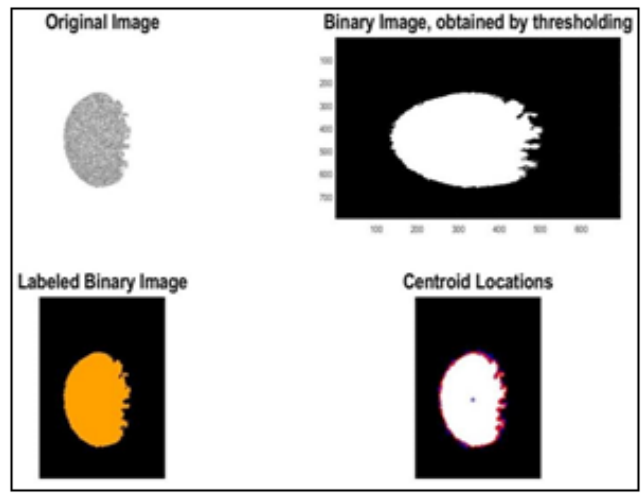


FIGURE 30: 9% Al<sub>2</sub>O<sub>3</sub> for Trail 2

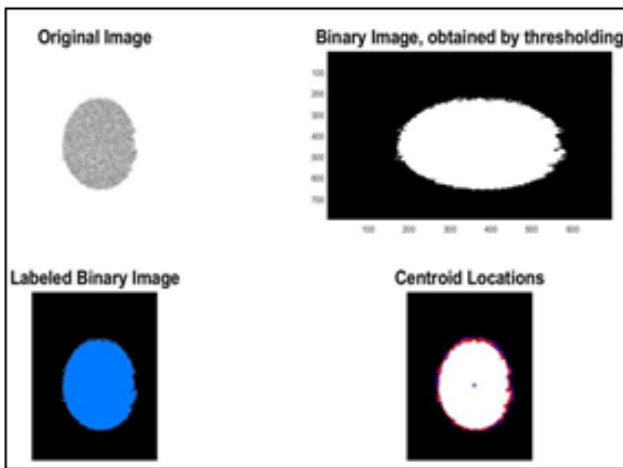


FIGURE 31: 9% Al<sub>2</sub>O<sub>3</sub> for Trail 3

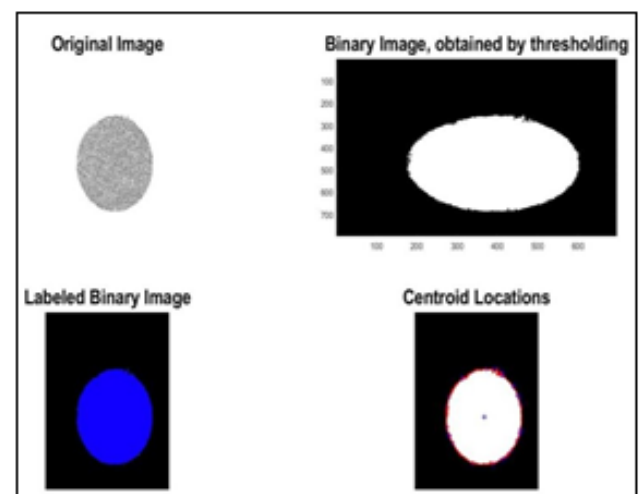


FIGURE 32: 9% Al<sub>2</sub>O<sub>3</sub> for Trail 4

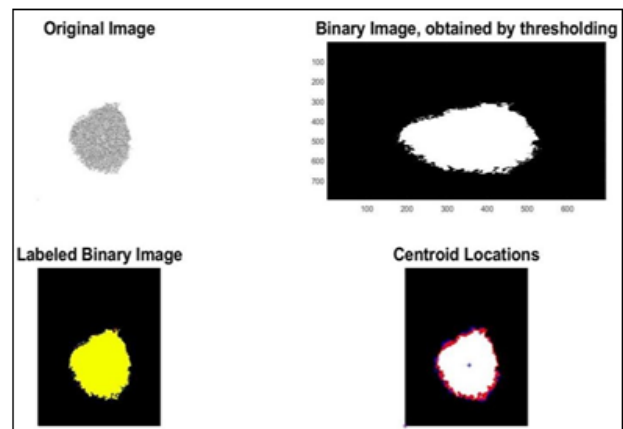


FIGURE 33: 9% Al<sub>2</sub>O<sub>3</sub> for Trail 5

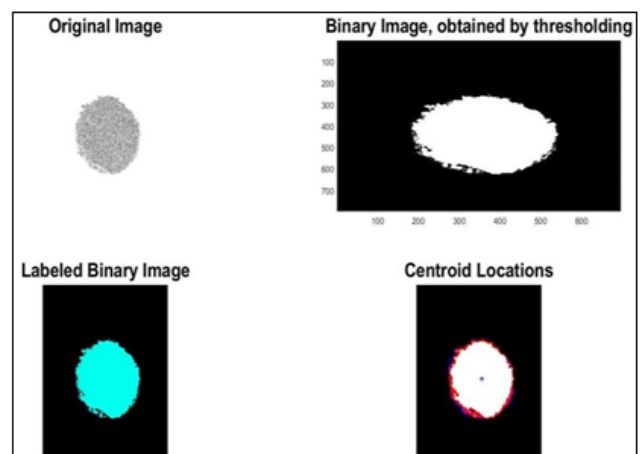
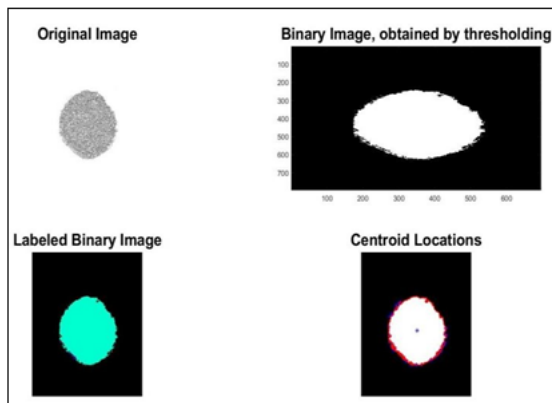
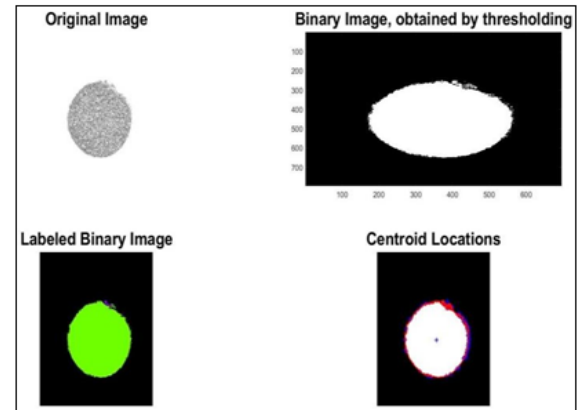
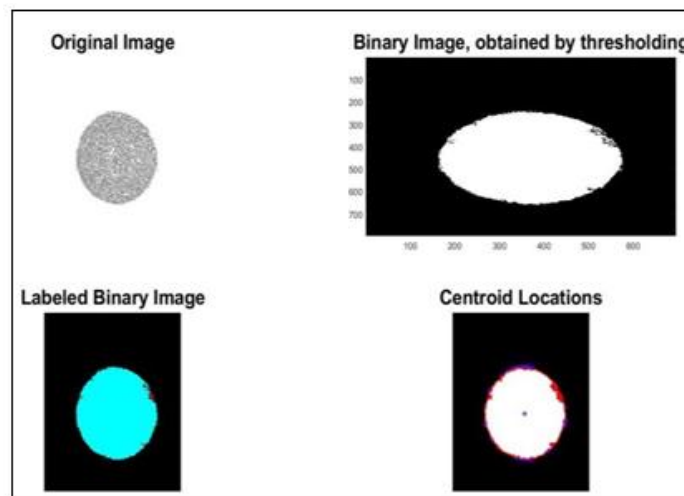


FIGURE 34: 9% Al<sub>2</sub>O<sub>3</sub> for Trail 6

FIGURE 35: 9% Al<sub>2</sub>O<sub>3</sub> for Trail 7FIGURE 36: 9% Al<sub>2</sub>O<sub>3</sub> for Trail 8FIGURE 37: 9% Al<sub>2</sub>O<sub>3</sub> for Trail 9

All nine trails of Al7178 with 9% Al<sub>2</sub>O<sub>3</sub> are evaluated for Geometric Analysis using MATLAB. And Geometric Analysis for Al7178 + Al<sub>2</sub>O<sub>3</sub> (9%) is shown below table:

**TABLE 7**  
**Geometric Analysis for Al7178 + Al<sub>2</sub>O<sub>3</sub> (9%)**

S.No.	Current (I) Amps	Pulse on time (T <sub>on</sub> ) μs	Pulse off time (T <sub>off</sub> ) μs	Voltage (V) Volts	MRR (mm <sup>3</sup> /min)	Average Distance (Radius)	% Error	Standard Deviation
1	4	100	50	30	3.056	5.294	5.728	0.241
2	4	450	75	45	0	5.211	4.133	0.472
3	4	1000	100	60	0.122	5.189	3.714	0.201
4	8	100	75	60	0.244	4.985	0.3	0.074
5	8	450	100	30	5.012	4.786	4.372	0.351
6	8	1000	50	45	0.366	5.001	0.031	0.245
7	12	100	100	45	0.122	5.069	1.389	0.203
8	12	450	50	60	0	5.129	2.559	0.139
9	12	1000	75	30	0.122	5.124	2.453	0.167



## 3.6.4 Case-4 : Electrode Al7178 + Al2O3 (12%)

**TABLE 8**  
**MRR, TWR & SR of Al7178+ Al2O3 (12%)**

S.No.	Current (I) Amps	Pulse on time (T <sub>on</sub> ) μs	Pulse off time (T <sub>off</sub> ) μs	Voltage (V) Volts	MRR (mm <sup>3</sup> /min)	TWR (mm <sup>3</sup> /min)	SR (μm)
1	4	100	50	30	0.611	11.139	3.425
2	4	450	75	45	0	0	3.919
3	4	1000	100	60	0.122	0.253	2.386
4	8	100	75	60	0.244	0.253	2.54
5	8	450	100	30	0.122	0	3.331
6	8	1000	50	45	0.611	0.506	2.306
7	12	100	100	45	0.366	0.759	3.727
8	12	450	50	60	0.611	0.759	4.588
9	12	1000	75	30	0.366	0.506	2.803

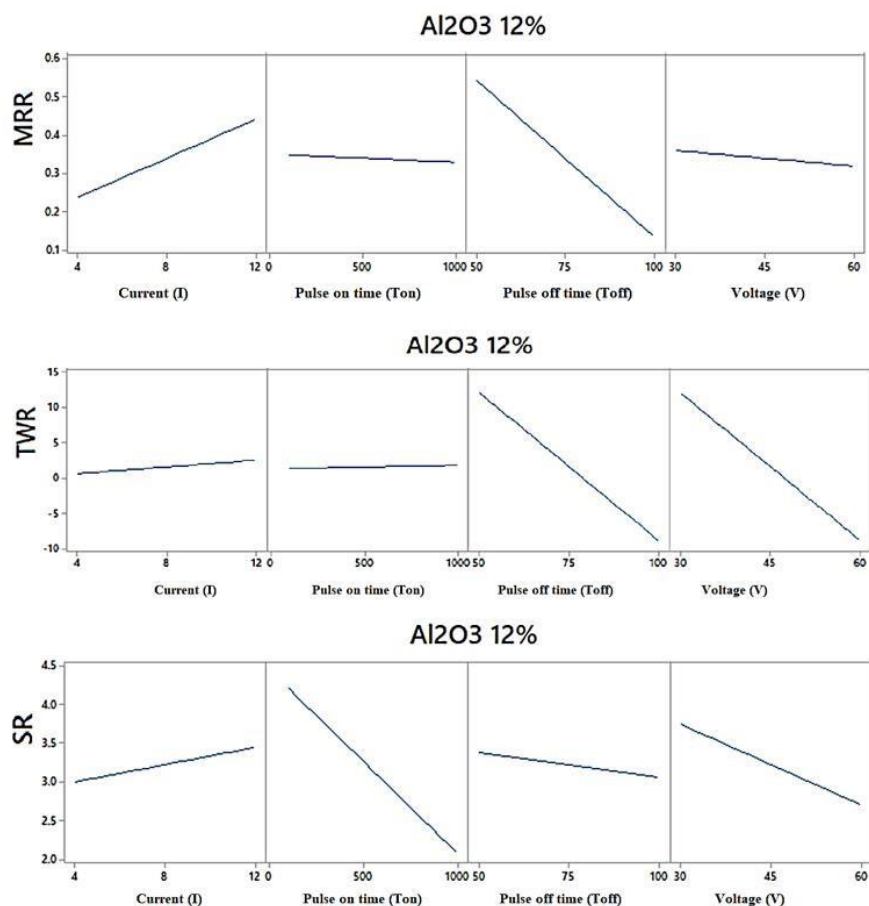


**FIGURE 38: Graphical relation among input parameters and MRR, TWR,SR (Al<sub>2</sub>O<sub>3</sub> 12%)**

Geometric Analysis (Circularity Accuracy) for Al7178 with 12% Al<sub>2</sub>O<sub>3</sub> tool input parameters (V = 30, I = 4, T<sub>on</sub> =100, T<sub>off</sub> =50) images are obtained for 12% Al<sub>2</sub>O<sub>3</sub> for Trails (12A1 to 12A9) by using image processing in MATLAB the percentage error obtained for 12% Al<sub>2</sub>O<sub>3</sub> are shown below:

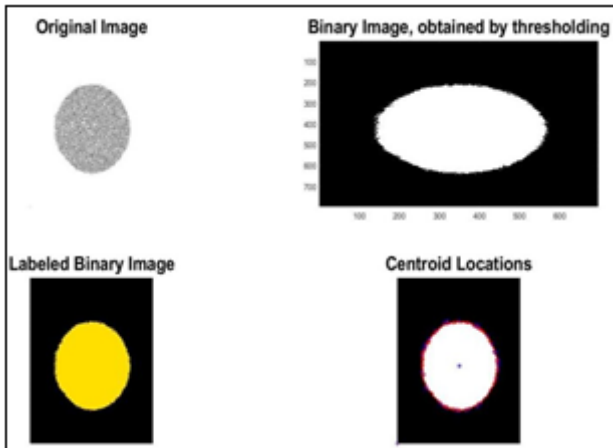


FIGURE 39: 12% Al<sub>2</sub>O<sub>3</sub> for Trail 1

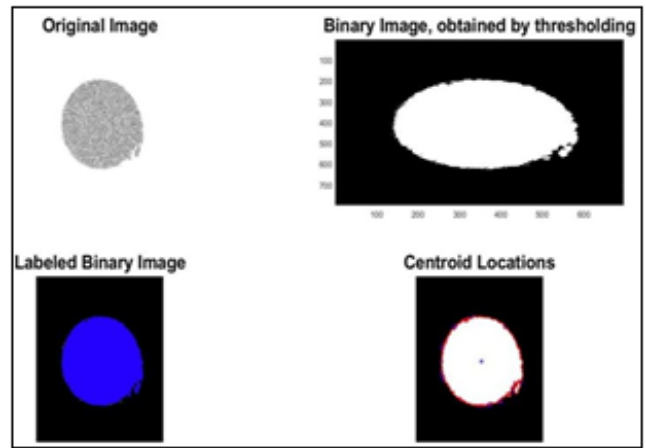


FIGURE 40: 12% Al<sub>2</sub>O<sub>3</sub> for Trail 2

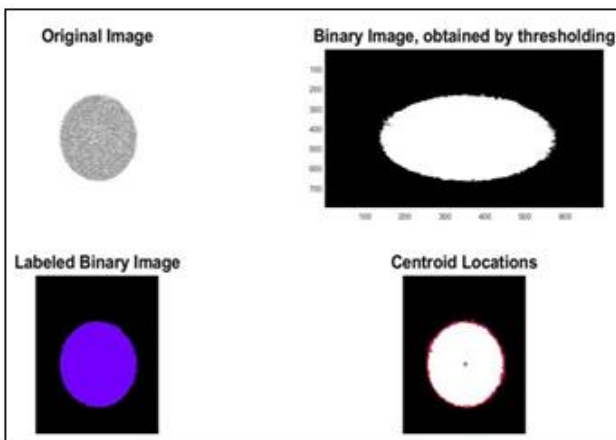


FIGURE 41: 12% Al<sub>2</sub>O<sub>3</sub> for Trail 3

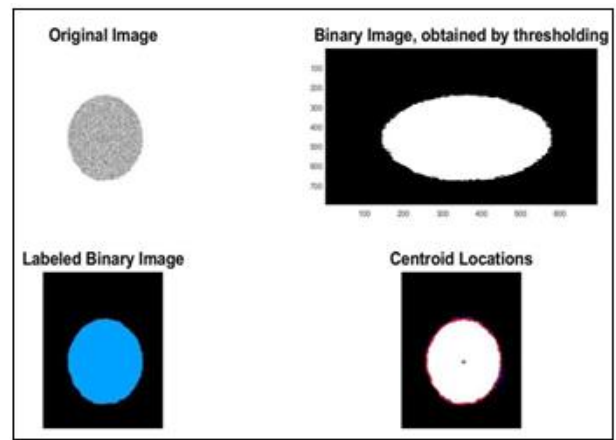


FIGURE 42: 12% Al<sub>2</sub>O<sub>3</sub> for Trail 4

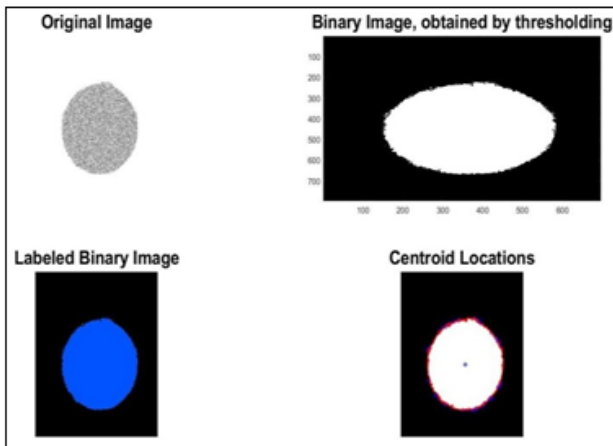


FIGURE 43: 12% Al<sub>2</sub>O<sub>3</sub> for Trail 5

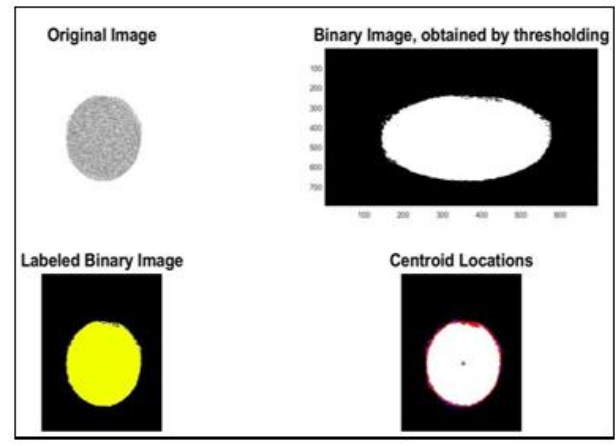


FIGURE 44: 12% Al<sub>2</sub>O<sub>3</sub> for Trail 6

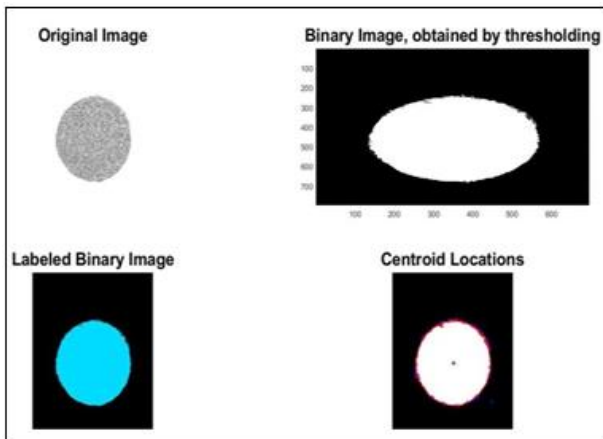


FIGURE 45: 12% Al<sub>2</sub>O<sub>3</sub> for Trail 7

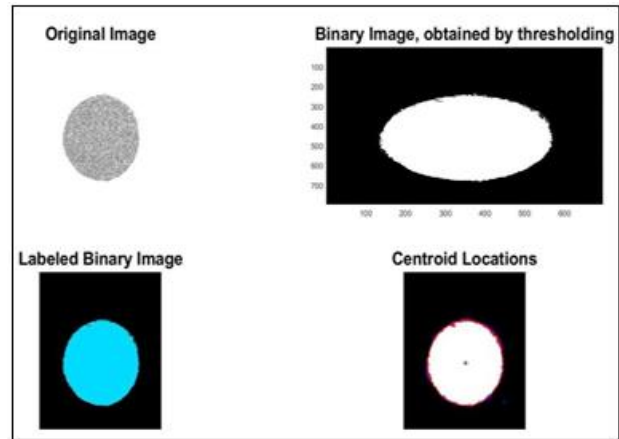


FIGURE 46: 12% Al<sub>2</sub>O<sub>3</sub> for Trail 8

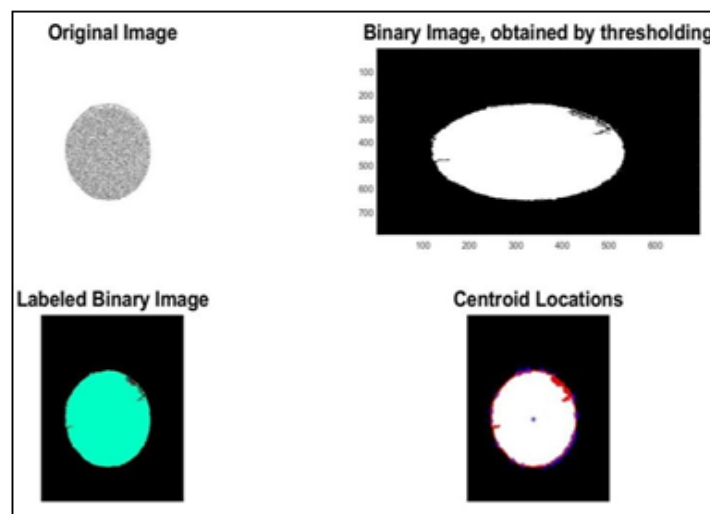


FIGURE 47: 12% Al<sub>2</sub>O<sub>3</sub> for Trail 9

All nine trails of Al<sub>7</sub>178 with 12% Al<sub>2</sub>O<sub>3</sub> are evaluated for Geometric Analysis using MATLAB. And Geometric Analysis for Al<sub>7</sub>178 + Al<sub>2</sub>O<sub>3</sub> (12%) is shown below table:

TABLE 9  
Geometric Analysis for Al<sub>7</sub>178 + Al<sub>2</sub>O<sub>3</sub> (12%)

S.No.	Current (I) Amps	Pulse on time (T <sub>on</sub> ) μs	Pulse off time (T <sub>off</sub> ) μs	Voltage (V) Volts	MRR (mm <sup>3</sup> /min)	Average Distance (Radius)	% Error	Standard Deviation
1	4	100	50	30	0.611	5.003	0.065	0.076
2	4	450	75	45	0	4.792	4.232	0.168
3	4	1000	100	60	0.122	5.087	1.735	0.075
4	8	100	75	60	0.244	5.018	0.375	0.067
5	8	450	100	30	0.122	4.941	1.171	0.089
6	8	1000	50	45	0.611	5.103	2.043	0.125
7	12	100	100	45	0.366	5.142	2.803	0.088
8	12	450	50	60	0.611	5.396	7.618	0.229
9	12	1000	75	30	0.366	5.043	0.871	0.078

**3.6.5 Consolidated Table & Graph for % error in Geometrical Accuracy:**

The consolidated results for percentage error for four cases of Aluminum Oxide 3%, 6%, 9% and 12% are shown in below table:

**TABLE 10  
Consolidated Table for % error**

S.No.	Geometrical Accuracy for different % of Al <sub>2</sub> O <sub>3</sub>			
	Al <sub>2</sub> O <sub>3</sub> 3%	Al <sub>2</sub> O <sub>3</sub> 6%	Al <sub>2</sub> O <sub>3</sub> 9%	Al <sub>2</sub> O <sub>3</sub> 12%
1	1.479	0.672	5.728	0.065
2	1.591	3.631	4.133	4.232
3	2.368	1.104	3.714	1.735
4	0.125	1.196	0.3	0.375
5	0.569	0.908	4.372	1.171
6	3.433	1.256	0.031	2.043
7	0.478	1.159	1.389	2.803
8	0.939	0.627	2.559	7.618
9	1.415	3.094	2.453	0.871

**Comparison Graph for % error**

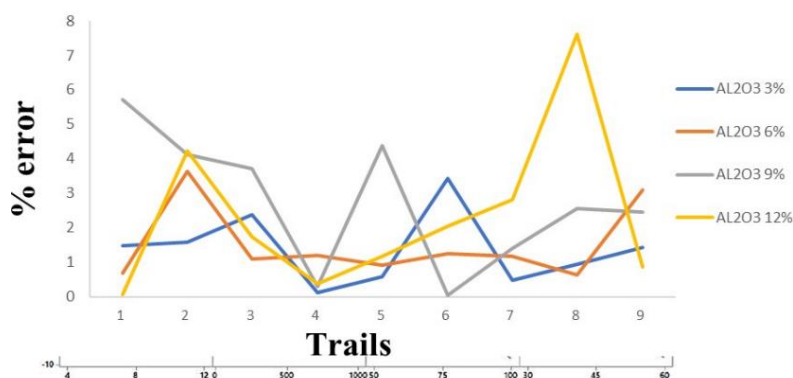


**FIGURE 48: Consolidated graph for percentage error for four cases of Aluminum Oxide 3%, 6%, 9% and 12%**

After performing the nine trails of four cases of Al<sub>7178</sub> + Al<sub>2</sub>O<sub>3</sub> 3%, Al<sub>2</sub>O<sub>3</sub> 6%, Al<sub>2</sub>O<sub>3</sub> 9% and Al<sub>2</sub>O<sub>3</sub> 12% the higher percentage error is obtained at Al<sub>2</sub>O<sub>3</sub> 9% in trail 1 i.e., 5.728 and the lower percentage error is obtained at Al<sub>2</sub>O<sub>3</sub> 12% in trail 1 i.e., 0.065 by using MATLAB and the comparison graph for percentage error for four cases of Aluminum Oxide 3%, 6%, 9% and 12% are shown in figure.

The comparison graph for MRR, TWR, SR and percentage error for 3% Aluminum Oxide (3% Al<sub>2</sub>O<sub>3</sub>) is shown in figure:

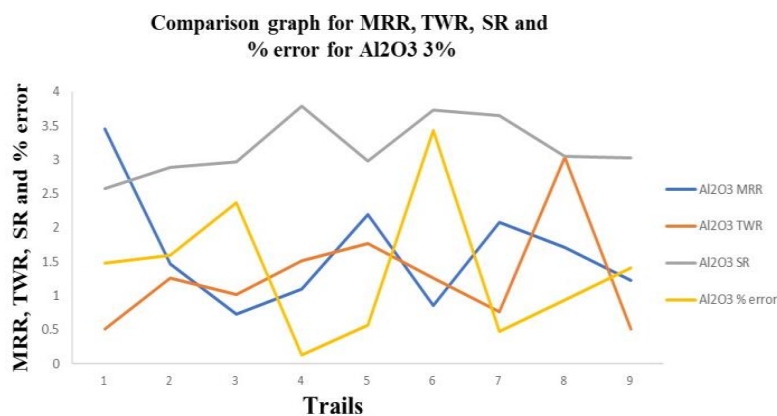


**FIGURE 49: Comparison graph for MRR, TWR, SR and % error for Al<sub>2</sub>O<sub>3</sub> 3%**

Higher Material Removal Rate is happens at higher current which in turn causing higher Roughness and all higher percentage error in geometry. The optimized condition for lower Roughness, lower TWR, lower Geometrical error and higher MRR is at Trail 1 (Parameters: current 4amps, pulse on time 100 $\mu$ s, pulse off time 50 $\mu$ s, voltage 30volts).

#### IV. CONCLUSION

From the experimental data and results obtained from the analysis the following conclusions may be drawn.

From the experimentation Al<sub>2</sub>O<sub>3</sub> 3% is found to be the optimum solution from all the cases (Al<sub>2</sub>O<sub>3</sub> 3%, Al<sub>2</sub>O<sub>3</sub> 6%, Al<sub>2</sub>O<sub>3</sub> 9% & Al<sub>2</sub>O<sub>3</sub> 12%)

- For 3% Al<sub>2</sub>O<sub>3</sub>, the Material Removal Rate is high (3.45 mm<sup>3</sup>/min), Surface Roughness is less in Trail 1 which is 3.955 $\mu$ m. Hence, the optimum condition for 3% Al<sub>2</sub>O<sub>3</sub> is in Trail 1 (Parameters: current 4amps, pulse on time 100 $\mu$ s, pulse off time 50 $\mu$ s, voltage 30volts).
- The optimized condition for lower Roughness, lower TWR, lower Geometrical error and higher MRR is in Trail 5 (Parameters: current 8amps, pulse on time 450 $\mu$ s, pulse off time 75 $\mu$ s, voltage 45volts).
- The main input parameter influencing the responses is current and its optimum value is 8amps.

#### FUTURE SCOPE

Aluminum Oxide (Al<sub>2</sub>O<sub>3</sub>) tool with Kerosene and Nano Fluid blend as a Dielectric.

#### ACKNOWLEDGMENT

The success of my project is a result of the hard work and technical expertise of many individuals, and I am grateful for their contributions. I would like to express my deep appreciation to my supervisor, **Dr. L. Siva Rama Krishna**, Professor & Department of Mechanical Engineering, Osmania University, for his guidance and suggestions throughout the project. I would like to express my deep appreciation to my co-supervisor, **Dr. S. Gajanana**, Professor & Dean of the Department of Mechanical Engineering, MVSR, for his guidance and suggestions throughout the project.

#### REFERENCES

- [1] H.M. Zawa, J.Y.H. Fuhb, A.Y.C. Neeb & L. Lub, Formation of a new EDM electrode material using sintering techniques. [https://doi.org/10.1016/S0924-0136\(99\)00054-0](https://doi.org/10.1016/S0924-0136(99)00054-0)
- [2] Z.Y. Yu, J.Kozak & K.P. Rajurkar, Modelling and Simulation of Micro EDM Process.
- [3] M.Rozenek, J.Kozak, L.Dąbrowski & K.Łubkowski, Electrical discharge machining characteristics of metal matrix composites.
- [4] K. M. Patel, Pulak M. Pandey & P. Venkateswara Rao, Determination of an Optimum Parametric Combination Using a Surface Roughness Prediction Model for EDM of Al<sub>2</sub>O<sub>3</sub>/Al<sub>2</sub>O<sub>3</sub>w/TiC
- [5] <https://doi.org/10.1080/10426910902769319>
- [6] M.R.Shabgard & R.M.Shotorbani, Mathematical Modeling of Machining Parameters in Electrical Discharge Machining of FW4 Welded Steel.
- [7] Sanjeev Kumar, Rupinder Singh, T.P. Singh & B.L. Sethi, Surface modification by electrical discharge machining: A review. <https://doi.org/10.1016/j.jmatprotec.2008.09.032>
- [8] Kuldeep Ojha, R. K. Garg & K. K. Singh, MRR Improvement in Sinking Electrical Discharge Machining: A Review.
- [9] Sharanjit Singh & Arvind Bhardwaj, Review to EDM by Using Water and Powder- Mixed Dielectric Fluid.
- [10] E. Weingärtnera, F. Kustera & K. Wegenera, Modeling and simulation of electrical discharge machining. <http://dx.doi.org/10.1016/j.procir.2012.05.043>.

# Properties of Symmetry of Space and Time, Hamilton's Principle and the Invariants

Korotkevich S.V.

RUP "Gomelenergo", Gomel, Belarus

Received: 02 August 2024/ Revised: 11 August 2024/ Accepted: 17 August 2024/ Published: 31-08-2024

Copyright © 2024 International Journal of Engineering Research and Science

This is an Open-Access article distributed under the terms of the Creative Commons Attribution Non-Commercial License (<https://creativecommons.org/licenses/by-nc/4.0>) which permits unrestricted Non-commercial use, distribution, and reproduction in any medium, provided the original work is properly cited.

**Abstract**—*This research investigates the fundamental role of symmetry properties in space and time in justifying the use of the principle of least action (PLA) to describe the creation and evolution of nanomaterials. By examining the kinetics of structural transformations in metals, we demonstrate that the PLA is a universal principle applicable to diverse physicochemical and biological processes. We explore the principle's ability to establish invariants at various structural-scale levels of metal deformation, including nano-, submicro-, micro-, meso-, and macroscale levels. Our findings highlight the significance of symmetry properties in understanding and predicting the behavior of nanomaterials.*

**Keywords**—*Symmetry properties, Space-time continuum, Principle of least action (PLA), Hamilton's principle, Invariants, Nanomaterials, Structural transformations.*

## I. INTRODUCTION

Structure determines the properties of materials under external influences. Establishing the causes, mechanisms and regularities of destruction of materials and, first of all, metals depends on the development of methods and technologies of their processing to increase reliable and safe operation. The complexity of the study of metal interface surface under external impacts and tribo-loading is determined by the lack of scientifically sound fundamental principles that can be applied at the junction of different sciences (physics, chemistry, mechanics, materials science, etc.) [1]. In addition, the complexity of the study of the metal interface surface is explained by the simultaneous occurrence of diverse processes (heat conduction, diffusion, mass transfer, hardening, fracture, amorphization, etc.) and the correct choice of the scale factor of external influence (load-velocity parameters, etc.). The latter makes it possible to divide a complex process into simpler constituent parts and to establish the course of the dominant process in their diversity [2]. The analysis of the dominant process makes it possible to identify and establish the main fundamental regularities describing this process [3].

All physicochemical [4] and biological processes [5] take place in a space-time continuum, the properties of which should be reflected in these processes as well. If this is so, then there must also exist a fundamental and universal principle of least action (PLA) to describe these processes. The existence of invariants is a direct proof of the existence of the PLA. Invariance in physics is a fundamental concept that means independence of physical regularities from specific situations in which they are established and from the way of description of these situations [6].

In chemistry, it is the law of conservation of mass of matter [7], Mendeleev's periodic table, where each chemical element has its own number with a set of certain parameters and properties that are invariant during chemical reactions [8], graph invariant [8], in biology it is Mendel's second law [10], in nuclear and quantum physics all processes occurring in the microcosm are subject to the law of conservation [11]. But where are these invariants in materials science, in condensed state physics, in technical sciences? Such a principle linking the symmetry of space and time properties with the properties of materials is the principle of least action or Hamilton's principle (HP). The latter determines the search and establishment of basic, fundamental invariants acting at all structural-scale levels of deformation of the metal.

The object of the study is the metal interface surface, namely the boundary lubricating layer of nanometer thickness, surface and subsurface layers. Rolling, quenching in different media, cavitation wear and longtime tribo-loading were selected as

external influence on the object of study - nickel surface. According to [12], the broadening  $\Delta H$  due to dislocations is proportional to  $\lambda^2/M^3$ , where  $M$  is the saturation state magnetization and  $\lambda$  is the magnetostriction constant. The ratio  $\lambda^2/M^3$  in nickel is about two orders of magnitude higher than in iron, so nickel was taken as the object of study. Mechanisms of hardening and fracture in the surface layer of metals having face-centered and volume-centered crystalline lattice have oscillatory character and time-localized lobe character of wear under tribo-loading [13, 14].

The aim of the work was to substantiate the application of the basic and universal principle of PLA describing the kinetics of structure formation of the metal interface surface and its use to establish invariants at nano-, submicro-, micro-, meso-, and macroscale levels of plastic deformation of the nickel surface layer, as well as to establish the structure, properties, and failure mechanisms of the steel interface surface under static and dynamic loading.

## II. EXPERIMENTAL DETAILS

Polycrystalline nickel of 99.99% purity, armco-iron, bearing steel, bronze, and cast iron were investigated. The nickel samples in the form of thin disks were polished electrolytically and annealed in a vacuum of 0.133 mPa at 973 K. The friction test of Ni – Mo pair was carried out on the machine AE-5 according to the finger-disk scheme with precise setting of the contact area at a specific load of  $\approx 84$  kPa and linear speed of  $\approx 0.5$  m/s. Electron microscopic studies of nickel were carried out on a microscope EVM-100AK and Hitachi-H800 by the method of thin foils on "lumen". The resolution of the Hitachi-H-800 is  $\approx 0.1$  nm. The technique of preparation of nickel samples for transmission electron microscopy is given in work [12]. Samples from steels: Ct 45, Ct 12X1, 65 Г, steel IIIХ-15, etc., which are used for the manufacture of rolling and sliding bearings, as well as cast iron (Cч-21-40); bronze (БрОЦС 5-5-5) were studied [3]. Studies have shown a time lobe flake mechanism of metal surface wear, which can only be explained using the theory of dislocation representations. There are no fundamental differences in the formation of dislocation structure for these metals [12]. References to monographs, articles, patents and materials of international conferences describing the idea of using HP, methods and ways of research of metal interfaces, rolling and sliding supports are described in the abstract [3].

## III. RESULTS AND DISCUSSION

It is known that the principle of least action (PLA) or Hamilton's principle is used to formulate the equations of motion of a material point in mechanics [4]. Why this fundamental principle cannot be used to describe kinetics of processes of structural transformations in materials occurring in the same continuum of space and time? A question naturally arises, namely: where there is symmetry, there should be invariants for describing the kinetics of various structural transformations at the multilevel, hierarchically organized processes occurring on the surface of metals? The kinetics of the transition of the system from one structural state (A) to another (B) is carried out in accordance with the principle of least action (Fig. 1).

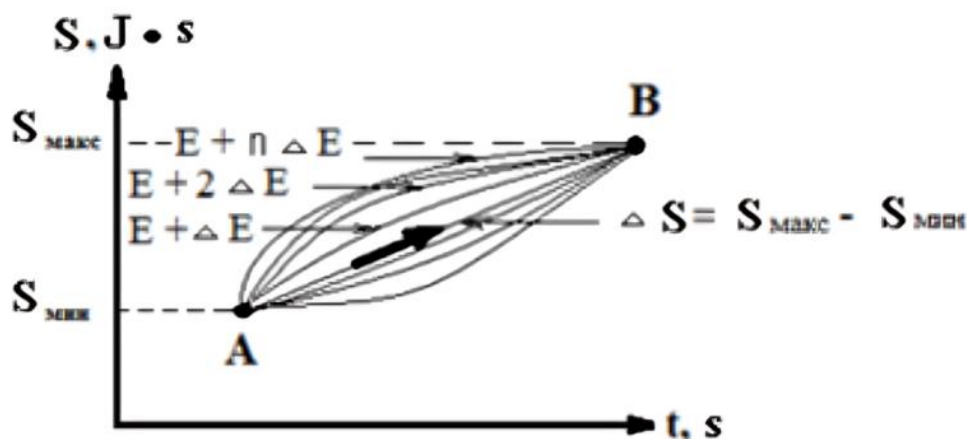


**FIGURE 1: Kinetics of system transition from one structural state (A) to another (B) in accordance with the principle of least action, where  $S$  – action,  $t$  – time**

It is known that the mathematical formulation of the PLA (or Hamilton's principle) has the form [4]:

$$\delta S = 0 \quad (1)$$

where

$$S = \int_{t_1}^{t_2} L(q, q', t) dt \quad (2)$$

where  $q, q'$  are independent parameters characterizing the system,  $t$  is time. Then the expression is valid:

$$\delta S = \int_{t_1}^{t_2} \left( \frac{\partial L}{\partial q} \delta q + \frac{\partial L}{\partial q'} \delta q' \right) dt = 0 \quad (3)$$

Suppose that the expression is true:

$$L = E_{\text{kin}} - E_{\text{pot}} \quad (4)$$

where  $E_{\text{kin}}$  – is the kinetic energy, a  $E_{\text{pot}}$  – is the potential energy of the material point under a given external influence.

The mathematical expression for the action of the electromagnetic field, together with the charged particles therein, is given in [15]. The general form of the Lagrangian for the system of particles (charges) forming the structure consists of the sum of Lagrangians taking into account the terms for free particles (the difference between kinetic and potential energy), the interaction of particles with the electromagnetic field and with each other, as well as the term for the electromagnetic field [15]. Obviously, the exact calculation of the Lagrangian for a system of particles is impossible due to the large number of particles constituting the defect as well as the elements of the defect structure. Nevertheless, a general form of the Lagrangian and the equation of motion (displacement) of the sublattices of positive and negative ions in a two-atom NaCl crystal are given in [16].

Entropy is given by the expression [17]:

$$H = \frac{\zeta(\nabla T)^2}{T^2} + \rho \frac{Z\Sigma}{T} \pm \frac{\rho}{T^2}([\alpha, \Omega], \nabla T, t) \quad (5)$$

where  $\zeta$  - thermal conductivity,  $\rho$  - material density,  $Z$  - defect flux density,  $\Sigma$  - hydrostatic stress in the defect phase formation zone, parameters  $\alpha$  and  $\Omega$  characterize the energy flux through the surface. The first summand in expression (5) is entropy production associated with heat generation. The second summand determines the work of defects flux when they move in the stress field. The third summand is related to the energy flow of the mechanical field of the crystal through the surface. The plus or minus sign determines the direction of the energy flow [17]. The change of the flow direction is determined by the energy advantage of the self-organization process or, in a broader sense, by the principle of least action. The latter implies the search and establishment of invariants [18, 19].

Correctly chosen scale factor of external influence or in this particular case soft mode of tribo-loading (or low-amplitude, alternating and multicycle external influence) allowed to analyze kinetic changes of hardening and softening of nickel surface (Fig. 2) [12]. Nickel was chosen as an object of study because its coefficient of magnetostriction is two orders of magnitude higher than, for example, that of armco-iron. The latter made it possible to see or analyze changes in the strength properties of the nickel surface using the ferromagnetic resonance (FMR) line broadening method [12]. Simultaneous study of nickel samples by weight method allowed to analyze their wear intensity (Fig. 2). Overlapping of two curves in one Fig. 2 allowed us to see their asynchronous dependence for one and each cycle of change in surface strength properties [20]. The multilevel system of deformation of a metal surface, for example, nickel (Fig. 2), ensures its stability [21]. The latter is confirmed by the fact that the selective mechanism covering a nickel layer hundreds of micrometers thick occurs only at time  $(t) \approx 108$  ks (Fig. 2) [20]. The self-organization of the system is expressed in 12 cycles of lobe fracture (Fig. 2), where lobe separation is an integral part of the evolution of structure formation of the multilevel system, since the time-localized separation of wear lobes reduces the level of stored energy (Fig. 2) and prevents cracks from propagating into deeper layers of nickel.



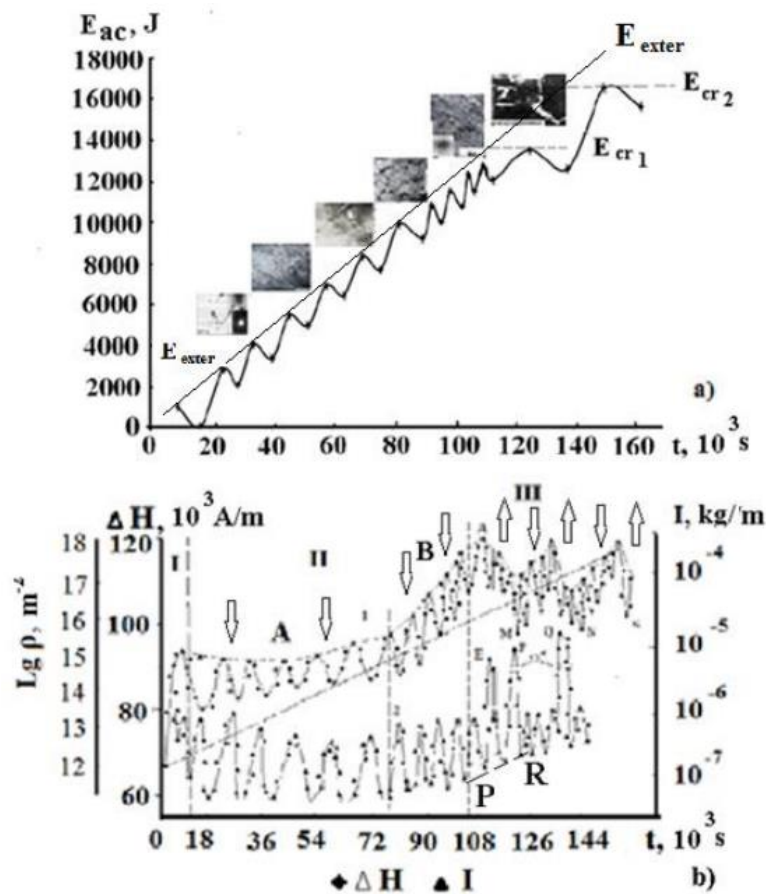


**FIGURE 2: Dependence of kinetics of structural changes of nickel surface layer under triboloading: a) – dependence of accumulated energy ( $E_{ac}$ ) on time ( $t$ ), where  $E_{cr1}$  and  $E_{cr2}$  are values of critical energy for destruction of meso- and macroscale level of deformation; b) – dependence of broadening of ferromagnetic resonance line ( $\Delta H$ ), dislocation density ( $\rho$ ), wear intensity ( $I$ ) on time ( $t$ ) of triboloading**

For one and each cycle of change in strength properties, an asymmetric dependence of the increase in dislocation density and wear intensity is established (Fig. 2), that is, the expression is fulfilled [3, 18]:

$$\rho \cdot I = const \quad (6)$$

where  $\rho$  is dislocation density,  $I$  is volumetric wear intensity,  $const \geq 0$ . The established relationship is confirmed by a number of articles [20, 22], which present model representations of lobe fracture of the surface layer. Experimental confirmation of hardening and lobe fracture is shown directly using the FMR method in our papers [13, 14]. Expression (6) is not invariant, as the constant changes with time, which may be due to both regular introduction of new lubricant into the friction zone (greasing) during each cycle of change in strength properties, and other reasons. It is necessary to carry out further research to find out the reasons for the constant change with time.

Fulfillment of the energy balance determines that part of the energy is spent on heat, deformation work, elastic field energy flow and energy determined by the mass of worn particles. Then, based on the law of conservation of energy, the expression will be fulfilled [23]:

$$E_{exter} - E_{ac} = H + M, \quad (7)$$

where  $E_{exter}$  - energy of external impact,  $E$  - energy accumulated in the surface layers of nickel,  $H$  is the entropy given by expression (6),  $M$  is the energy determined by the mass of worn particles. Entropy is a function describing the state of the system. Indeed, in the repeated 12 cycles of hardening of the nickel surface layer, the energy difference ( $E_{exter} - E_{ac}$ ) is minimal at the points of contact between the graphs of the functions  $E_{exter}(t)$  and the accumulated energy  $E_{ac}(t)$ , shown in Fig. 2. The formation of nanocrystalline (NC) structures occurs when dislocations exit to the surface and, accordingly, the dislocation

density increases, which occurs at the areas of maximum of the function  $E_{ac}(t)$ . Obviously, the formation of NC and SMC structures is accompanied by a decrease of the entropy (Fig. 2, a).

Let us quantitatively estimate the entropy value for the forming defect structures in Fig. 2, based on expression (7). The mathematical expression of entropy for the processes of structure formation kinetics depicted in Fig. 3 is given by expression (8):

$$H + M = \int_0^{160000} (\Delta(E_{exter}) - \theta(E_{ac})) dt \quad (8)$$

where  $\Delta(E_{exter})$  is a function defined by a directly proportional dependence on time, since the value of  $E_{vesh}$  is numerically equal to the work of tribo-loading forces, and the function  $\Theta(E_{ac})$  is defined by a monotonically increasing oscillating dependence in time (Fig. 2). The limits of integration vary from 0 to 160000 seconds according to Fig. 2. Since the definite integral of a function is numerically equal to the area of the figure bounded by the given function and integration limits, the numerical values of the smallest action were determined by the area of the figure bounded from above by a straight line and from below by a monotonically oscillating increasing dependence (Fig. 2, a). Table 1 quantifies the amount of entropy and energy determined by the mass of worn particles required to form a particular structure.

**TABLE 1**  
**THE QUANTITATIVE ESTIMATION OF ENTROPY AND ENERGY, DETERMINED BY THE MASS OF WORN PARTICLES, IN THE FORMATION OF A PARTICULAR STRUCTURE IN THE SURFACE LAYER OF NICKEL UNDER TRIBO-LOADING**

Type of structure	t, 10 <sup>3</sup> s	H+M, entropy plus energy determined by the mass of worn particles, 10 <sup>6</sup> J-s
NC structures	0.9	0.0972
Slip strips	6.5	2.51427
Fragmented NC and SMC structures	108	57.82821
Loose and porous surface layer	160	120.3802

As a result of long-term tribocharging of the nickel surface (more than  $150 \cdot 10^3$  s or 150 ks) the formation of a defective structure whose size varies from 30  $\mu$ m to 3 nm (Fig. 3) [23].

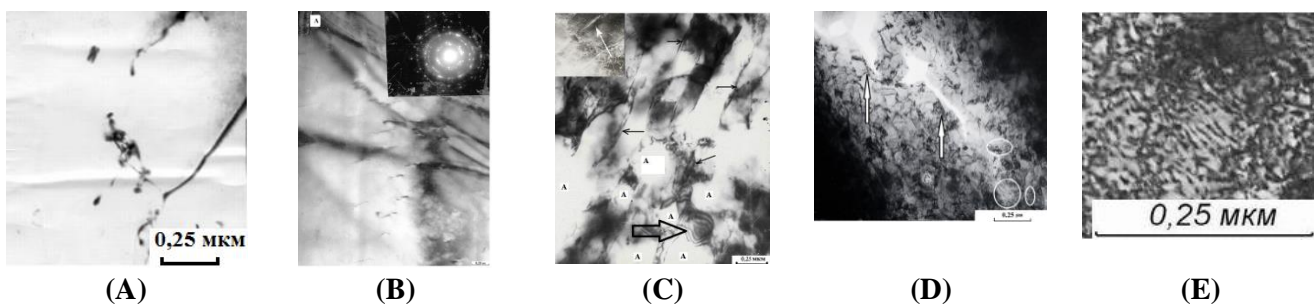


**FIGURE 3: Kinetics of the nickel surface structure under tribo-loading: A – initial structure of annealed nickel; B – structure corresponding to the minimum oscillation dependence of the ferromagnetic resonance line broadening ( $\Delta H(t)$ ); C – plate microstructure of slip bands; D – subgranular microstructure; E – nanocrystalline structure**

The grain size of the nickel annealed before triboloading was  $\approx 30 \mu$ m. The submicrocrystalline (SMC) and nanocrystalline (NC) structural states have a closed shape and are formed in areas with strongly disoriented crystal sections. The kinetics of defect structure formation can be simplified as a circle of decreasing diameter size (Fig. 4).

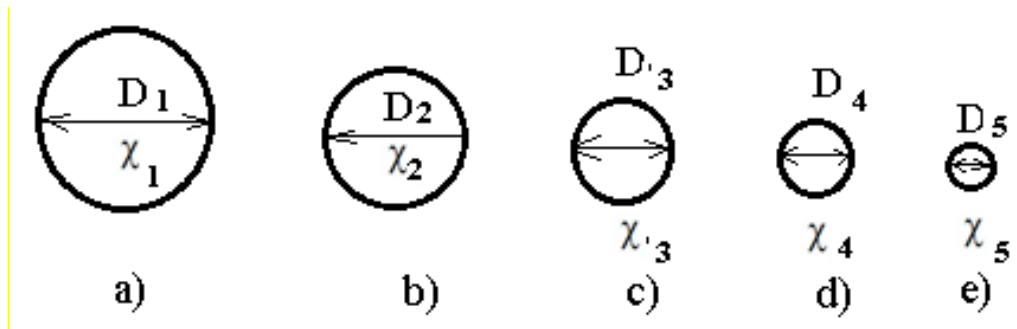


**FIGURE 4: Scheme of the formation of structural defects at different structural-scale levels of deformation: a) initial structure; b) – e) evolution of the structure under the action of external influences (triboloading), namely: b) formation of microstructure; c) submicro-; d) nanoscale and e) nanocrystalline structural states**

In Table 2, we summarize the parameters describing the structural states shown in Fig. 4.

**TABLE 2  
PARAMETERS DESCRIBING THE KINETICS OF STRUCTURAL STATES OF NICKEL SURFACE**

Size of structural elements (diameter (D)), 10 <sup>-6</sup> m	Angle (Δω), degree	Local curvature of nickel crystal structure (χ), degree/10 <sup>-6</sup> m
30	3600	12
3	3600	120
0,3	3600	1200
0,03	3600	12000

When the size of a structural element decreases by an order of magnitude, the value of local curvature of the nickel crystal structure increases by an order of magnitude. As the analysis of microdiffraction images shows, the disorientation of structures of  $\approx 3\div 10$  nm in size is  $\approx 10\div 20^\circ$  [12]. It is experimentally confirmed that the local curvature of the crystal structure of nickel increases by four orders of magnitude when the size of the structural element decreases by four orders of magnitude (table 2). The expression is fulfilled [24]:

$$\chi_{ij}(10^{-n}\cdot x_1; 10^{-n}\cdot x_2; 10^{-n}\cdot x_3) = 10^n \chi_{ij}^0(10^{-n}\cdot x_1, 10^{-n} x_2, 10^{-n} x_3), \tag{8}$$

where  $x_1, x_2,$  and  $x_3$  are spatial coordinates, and  $\chi_{ij}$  is the local curvature tensor of the nickel crystal lattice,  $n = 0, 1, 2, 3$   $\chi_{ij}^0$  is the local curvature tensor of the nickel crystal lattice corresponding to the initial structure. The local lattice curvature takes place at all structural levels of deformation, from the nano- to macrolevel of large-scale deformation, which indicates its fundamental importance in the formation and evolution of structures.

An example of fulfillment of expression (8) for three-dimensional space taking into account the values of parameters given in table 1, where  $n = 0, 1, 2, 3$ .

$$\begin{bmatrix} 12000 & 0 & 0 \\ 0 & 12000 & 0 \\ 0 & 0 & 12000 \end{bmatrix} (10^{-3}\cdot 0,03; 10^{-3}\cdot 0,03; 10^{-3}\cdot 0,03) = 10^3 \begin{bmatrix} 12 & 0 & 0 \\ 0 & 12 & 0 \\ 0 & 0 & 12 \end{bmatrix} (10^{-3}\cdot 0,03; 10^{-3}\cdot 0,03; 10^{-3}\cdot 0,03) \tag{9}$$

The scale invariance of the local curvature of the crystal structure of polycrystalline nickel at all structural strain levels is fulfilled [25].

It is necessary to emphasize the main and, at first sight, obvious fact that the formation and evolution of structural boundaries proceeds in accordance with the energy profitability [26]. As soon as it is physically possible to implement through one or another mechanism (twinning, formation of package defects, etc.), it is immediately launched according to the energy benefit, since the result of the process is the reduction of the energy accumulated as a result of the deformation in the material (Fig. 2).

The formation of nanocrystalline structures (NC) at the very beginning of triboloading ( $t = 0.9$  ks) is due to energy localization in a thin nickel surface layer and the absence of energy relaxation channels and mechanisms into the subsurface layer due to the juvenile pre-annealed nickel surface, where microcracks, pores and other elements of the defective structure are absent [27]. Energy localization allowed to reduce the time of formation of the same structures, but already at  $t \approx 140$  ks. Under prolonged triboloading a strongly thermodynamically nonequilibrium surface layer of nickel covering up to a hundred microns in depth was obtained [23]. There is an obvious relationship between time and energy, since the localization of energy reduces the time of realization of the process of formation of NC structures.

The process of stress localization in a thin surface layer of the order of  $\approx 1 \mu\text{m}$ , the formation first of rotational structures [25], and then of wear particles and their separation from the surface also proceeds in accordance with energy profitability. Petal separation of the thinnest surface layers up to 100 nm thick is shown in Fig. 2. It goes through 12 cycles of hardening and fracture before selective fracture occurs (point A in Fig. 2) [20, 22]. Each cycle of strength property change is characterized by the accumulation of dislocations up to a certain critical value, which determines the surface overlap. Then its destruction takes place. Approximately one tenth of the work or energy expended in friction for each cycle is accumulated in the subsurface. The accumulation of strain energy causes the formation of porosity (Fig. 5) and a highly nonequilibrium state of the nickel crystal lattice. The degree of porosity reaches more than 30 % of the entire observation area.

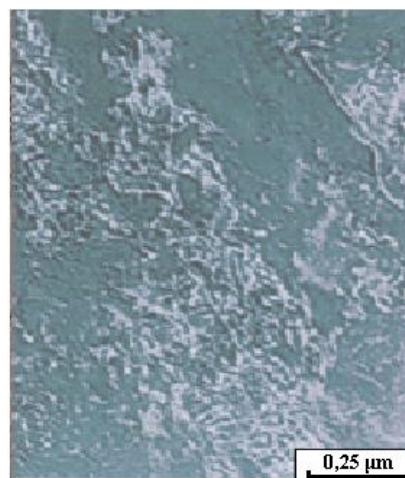


**FIGURE 5: Formation of the dispersed and porous (friable) layer during pre-destruction ( $t = 140$  ks).  
The image is invented for better contrast and clarity**

Analysis of the experimental data of the strongly nonequilibrium structure (Fig. 2, region III) shows that an increase in the total area of porosity also determines an increase in the volumetric wear rate (section PR in region III in Fig. 2). In the area of nonequilibrium deformation the gradient of the dislocation and point defects density flux has an oscillating character; the increase in the intensity of the gradient of upward and downward dislocation density fluxes causes an increase in the lower limit of wear intensity change in  $\approx 8$  times (area PR on Fig. 2 in area III), and the upper limit of wear intensity change at an avalanche-like selective mechanism of surface layer destruction – by three orders of magnitude (Fig. 2, area III). At the same time, in area III a decrease in the period of change of strength properties of the nickel surface by  $\approx 8$  times is noted in comparison with area II (Fig. 2). There is a complete coordination of change of strength properties and volumetric wear rate of nickel surface. Increase in 8 times of intensity of a gradient of ascending and descending flows of dislocation density causes both diffusion mobility of point defects and increase in porosity of a material [28]. Directly proportional increase of minimal value of volumetric wear intensity with increase in time of triboloading is established (Fig. 2, area III). The expression is fulfilled [29, 30]:

$$\frac{I}{S} = \text{const}, \quad (10)$$

where  $I$  is the volumetric wear rate,  $S$  is the total pore area,  $\text{const} \geq 0$ .

Further studies of non-dislocation mechanisms and the establishment of invariants in the self-organization of a highly nonequilibrium structure (Fig. 2, region III) are needed.

A method was developed to determine the wear of ferromagnetic materials under triboloading, where the frequency of oscillations of the FMR line width per unit time, obtained by the graduation dependence (Fig. 6), is used to infer the wear intensity of the ferromagnetic material [31].

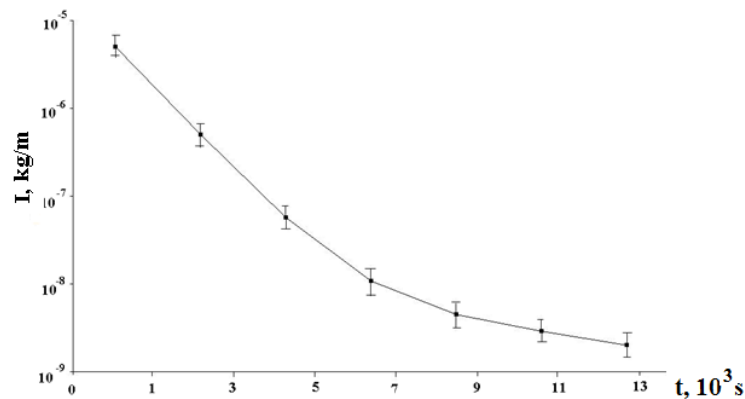


**FIGURE 6: Dependence of wear rate (I) on oscillation period (t) during triboloading with CYATIM-201 plastic lubricant**

An increase in the oscillation frequency of the ferromagnetic resonance line broadening or a corresponding decrease in the oscillation period determines an increase in the wear rate of the ferromagnetic material.

Separation of a highly fragmented layer up to  $\approx 100 \mu\text{m}$  thick occurs with a selective fracture mechanism (points E, F, Q, Fig. 2). The principle of least action is realized, where the separation of destruction is an energetically profitable process of preserving the integrity or durability of the material. The principle PLA is a broader fundamental concept as it describes not only equilibrium and non-equilibrium processes with a minimum [32] or maximum entropy production clause [33], but also implies the existence of invariants.

One of the main channels for reducing the strain energy accumulated by the material is grain boundary slip, which explains its plastic properties and conservation of its continuity. The law of conservation of the sum of stress moments, experimentally observed by V.E. Panin and formulated by him in the article [34].

$$\sum_{i=1}^N \text{Rot } J_i = 0 \quad (11)$$

where  $J_i$  are defect fluxes at the  $i$ -th structure-scale level. Under these conditions, all moment stresses in the material are compensated and the crystal lattice retains its translational invariance.

The analysis of experimental dependences of FMR line broadening on time for nickel samples subjected to triboloading after rolling at various degrees of deformation ( $\varepsilon \approx 0 \div 50 \%$ ), as well as after hardening in various media showed that the speed of surface hardening (coefficient  $K_1$ ) determines the speed of its softening (coefficient  $K_2$ ) [3, 18]. In other words, what quickly hardens, also quickly destroys. The latter is due to the dislocation nature of the formation of the stress fields and their interaction during the evolution of the structure.

$$\frac{K_1}{K_2} = \text{const}, \quad (12)$$

where  $K = \Delta H / \Delta t$  и  $0 \leq \text{const} \leq 1$ ;

There is an accumulation of dislocations up to some critical value, determined by the size of the formed wear particle and their number per unit volume. The latter is determined by boundary conditions, namely: strength properties of the boundary lubricating layer, surface of metals by intensity of external influence. To describe the different modes of boundary friction, an invariant criterion has been developed. The ratio of the registered contact resistance ( $R_c$ ) to the resistance of the initial metal surface (without lubrication and at the initial moment of triboloading time) taking into account the oxide film ( $R_{ok}$ ) characterizes the state of the interface and the expression is executed [35]:

$$\frac{R_c}{R_{ok}} = \text{const}, \quad (13)$$

where const depending on the mode of friction is much greater than unity ( $\gg 1$ ), greater than unity ( $> 1$ ), equal to unity ( $= 1$ ), less than unity ( $< 1$ ).

The local curvature of the nickel crystal lattice increases by an order of magnitude when the size of the structural element decreases by an order of magnitude. The conditions of scale invariance are fulfilled, namely [23]:

$$\chi_{ij}(10^{-n}\cdot x_1; 10^{-n}\cdot x_2; 10^{-n}\cdot x_3) = 10^n \chi_{ij}^0(x_1, x_2, x_3), \quad (14)$$

where  $x_i$  are coordinates of three-dimensional space,  $\chi_{ij}^0$  is the curvature tensor of the Ni crystal lattice in the state after annealing,  $n = 0, 1, 2, 3, 4$ . The local curvature of the crystal lattice, takes place at all structural levels of deformation, from the nano- to the macro-level of scale deformation, which indicates its fundamental importance in the formation and evolution of structures [25].

Directly proportional increase of minimal value of volumetric wear intensity with increase in time of tribo-loading is established (Fig. 2, area III). The expression is fulfilled:

$$\frac{I}{S} = \text{const}, \quad (15)$$

where  $I$  is the volumetric wear rate,  $S$  is the total pore area,  $\text{const} \geq 0$ .

Performing an energy balance [23]:

$$E_{\text{exter}} - E_{\text{ac}} = H + M \quad (16)$$

where  $E_{\text{exter}}$  - energy of external impact,  $E$  - energy accumulated in the surface layers of nickel,  $H$  is the entropy given by expression (6),  $M$  is the energy determined by the mass of worn particles.

Undoubtedly, there are also other invariants. The author hopes that the material presented in this paper, in accordance with the PLA, as well as in accordance with the analysis of the physical dimensionality of the parameters of invariants, will help researchers to identify them.

#### IV. CONCLUSION

The article convincingly shows that the symmetry of the properties of the continuum of space and time determines the use of the principle of least action to find and establish the invariants or the basic fundamental laws of the evolution of the structure of materials, regardless of the method by which they are obtained (rolling, tribo-loading, ultrasound, etc.). The establishment of invariants confirms the universality of using the scientifically sound fundamental principle of the least action for the creation, evolution, and destruction of materials, including nanomaterials of various functional purposes. The application of this principle, which describes various kinetic processes at the junction of different sciences: physics, chemistry, biology, mesomechanics, nonequilibrium thermodynamics, etc. determines not only the kinetics of evolution, but also the search and establishment of new fundamental, invariant laws for processes occurring in space-time continuum.

#### REFERENCES

- [1] "Problems of Wear of Solid Bodies in the Aspect of Mechanics, A. Y. Ishlinsky et al, Friction and wear, 1986, Vol. 7, № 4, pp. 581-591.
- [2] V. D. Kuznetsov, "Solid State Physics": in 4 vol., Tomsk : Krasnaya Znamya, 1937-1949, Vol. 4: "Materials on Physics of External Friction, Wear and Internal Friction of Solids", 1947, 543 p.
- [3] S. V. Korotkevich, Abstract of the Thesis for the Degree of Doctor of Physical and Mathematical Sciences in the Specialty 01.04.07 "Structure-Scale Levels of Deformation and Properties of Interfaces in Metals", Minsk: BSU, 2021, 54 p.
- [4] L. D. Landau, E. M. Lifshits, "Theoretical Physics in Ten Volumes. T. 1 Mechanics", Moscow: Nauka, 1988, 215 p.
- [5] V. I. Vernadsky, "Biosphere", M.: Mysl, 1967, 376 p.
- [6] G. Weil "Theory Groups and Quantum Mechanics", Moscow: Nauka, 496 p.
- [7] Ya. G. Dorfman, "Law of Conservation of Mass in Chemical Reactions and Physical Views of Lomonosov", Collection of Articles and Materials, M.-L.: Publishing House of the USSR Academy of Sciences, 1961, Vol. 5, pp. 182-193.
- [8] D. I. Mendeleev (1869). "On the Correlation Between the Properties of Atomic Elements and Their Atomic Weight", Journal of the Russian Physical and Chemical Society, 1869, 1, pp. 60-77 (note 2).
- [9] Chemical Applications of Topology and Graph Theory, Edited by R. King. - M.: Mir, 1987, 560 p.
- [10] I. B. Agafonova, V. I. Sivoglavov, E. T. Zakharova, "Biology, "General biology" 11th Grade. Basic Level", Drofa, corporation "Russian textbook", 2019, 208 p.
- [11] R. Feynman, C. Weinberg "Elementary particles and the laws of physics", Moscow: Mir, 2000, 138 p.

- [12] V. G. Pinchuk, S. V. Korotkevich, "Kinetics of Hardening and Fracture of Metal Surface under Friction", LAP Lambert Academic Publishing. Saarbrücken: LAP, 2014, 180 p.
- [13] V. G. Pinchuk, S. V. Korotkevich, "Microstructure and Strength Properties of Submicro and Nanocrystalline Nickel under Friction", Modeling and Numerical Simulation of Material Science, 2013, № 3, pp. 8–13.
- [14] V. G. Pinchuk, S. V. Korotkevich, "Microstructure Evolution in Friction-Loaded Layers of Nickel", Indian Journal of Research, 2015, Vol. 4, issue № 2, pp. 8–10.
- [15] L. D. Landau, E. M. Lifshits, "Theoretical Physics : in 10 vol.", Moscow : Main Editorial Board of Physical and Mathematical Literature, 1988, Vol. 2 : "Field Theory", 512 p.
- [16] C. Kittel, Quantum Theory of Solids, M.: Nauka, Gl. ed. Phys.-Mat. Litt., 1967, 492 p.
- [17] V. E. Panin, V. E. Egorushkin, "Deformable solid body as a nonlinear hierarchical organized system", Phys. Mesomechanics, 2011, Vol. 14, № 3, pp. 7-26.
- [18] S. V. Korotkevich, "Hamilton's Principle for to Search of Invariants at Creation, Evolution and Destruction of Nanomaterials", International Journal of Engineering Research and Science, 2018, Vol. 4, issue № 6, pp. 31-41.
- [19] S. V. Korotkevich, "The Principle of Least Action and Invariants", Scientific Research of the SCO Countries: Synergy and Integration: proc. of International Conference, Beijing, PRC, China, 31 March 2022, Part 2: Participants, Reports in English, pp. 34-42.
- [20] V. G. Pinchuk, S. V. Korotkevich, "Physical Patterns of Dislocation Structure Kinetics in Friction Loaded Surface Layers", Global Journal For Research Analysis, 2015, Vol. 4, issue № 5, pp. 255-257.
- [21] V. E. Panin, V. E. Egorushkin, "Deformable solid body as a nonlinear hierarchical organized system", Phys. Mesomechanics, 2011, Vol. 14, № 3, pp. 7-26.
- [22] V. G. Pinchuk, I. A. Buyanovskiy, S. V. Korotkevich, "Kinetics of Microstructure and Selective Mechanism of Fracture of Metal Surface Layer under Friction", Inorganic Materials: Applied Research, 2015, Vol. 6, № 4, pp. 355-362.
- [23] S. V. Korotkevich, "The Principle of the Least Action and Invariants of the Kinetics of Hardening and Fracture of the Surface Layer of Metals", "Actual Problems of Strength", V. A. Andreev [et al.], ed. by V. V. Rubanik, Mn.: Izd. "IVC of the Ministry of Finance", 2024, 470 p.
- [24] S. V. Korotkevich, "Multiscaling of Lattice Curvature of the Nickel", Scientific Research of the SCO Countries: Synergy and Integration: proc. of International Conference, Beijing, PRC, China, 20 April 2022, Part 1: Participants, Reports in English, pp. 174-182.
- [25] V. E. Panin, V. G. Pinchuk, S. V. Korotkevich, S. V. Panin, "Multiscaling of Lattice Curvature on Friction Surfaces of Metallic Materials as a Basic of Their Wear Mechanism", Physical Mesomechanics, 2017, Vol. 20, № 1, pp. 69-77.
- [26] R. Honicombe, "Plastic Deformation of Metals", R. Honicombe ; edited by B. Y. Lyubov, Moscow : Mir, 1972, 408 p.
- [27] S. V. Korotkevich, S. V. Panin Large-Scale Levels of Deformation and Destruction of the Surface Layer of Nickel under Localized External Impact, "Actual Problems of Strength", A. V. Alifanov [et al], under ed. by V. V. Rubanik, Mn.: Izd. "IVC of the Ministry of Finance", 2022, 540 p.
- [28] S. V. Korotkevich, V. V. Sviridova, "Analysis of Deformation Processes in the Surface Layer of Nickel", Problems of Physics, Mathematics and Engineering, 2020, № 4 (45), pp. 25-31.
- [29] S. V. Korotkevich, "Hamilton's Principle and the Invariants" Scientific Research of the SCO Countries: Synergy and Integration: proc. of International Conference, Beijing, PRC, China, 20 Oktober 2023, Part 1: Participants' reports in English, pp. 157- 164.
- [30] S. V. Korotkevich, "Lagrangian for Hamilton's principle" Scientific Research of the SCO Countries: Synergy and Integration: proc. of International Conference, Beijing, PRC, China, 23 December 2023, pp. 196– 205.
- [31] V. G. Pinchuk, S. V. Korotkevich, "Method for Determining the Average Wear Intensity of Ferromagnetic Material under Friction", patent. 19103 Republic of Belarus: MPKG 01 N 3/56; date of publication: 30.04.2015, Official Bulletin, National Center for Intellectual Property, 2015, № 2, pp. 83.
- [32] G. Nicolis, N. Prigogine, "Self-organization in nonequilibrium processes", Moscow: Mir, 1977, 512 p.
- [33] L. M. Martyushev, V. D. Seleznyov, "Principle of Maximum Entropy Production in Physics and Related Fields", Ekaterinburg: GOU VPO UGTU, 2006, 83 p.
- [34] V. E. Panin, V. E. Egorushkin, A. V. Panin, "Role of Local Nanostructural States in Plastic Deformation and Fracture of Solids", Phys. Mesomechanics, 2012, Vol. 15, № 5, pp. 5-18.
- [35] S. V. Korotkevich, V.G. Pinchuk, V.V. Kravchenko, "Diagnostics of Rolling and Sliding Supports by Physical Methods", Ministry of Education of the Republic of Belarus; Skorina State University, Saarbrücken: Lambert Academic Publishing, 2016, 267 p.

# Legal and Regulatory Structure Prevailing in the UK related to Data Privacy and Public Surveillance

Amarachukwu Grace Nwosu

School of Architecture, Computing and Engineering Department, University of East London

Received: 05 August 2024/ Revised: 10 August 2024/ Accepted: 16 August 2024/ Published: 31-08-2024

Copyright @ 2024 International Journal of Engineering Research and Science

This is an Open-Access article distributed under the terms of the Creative Commons Attribution Non-Commercial License (<https://creativecommons.org/licenses/by-nc/4.0>) which permits unrestricted Non-commercial use, distribution, and reproduction in any medium, provided the original work is properly cited.

**Abstract**— Over the years, the Internet has changed from a system essentially concerned with providing data, to a channel for communication and social cohesion (Fuchs et al.,2013). Criminals go fastidious to hide illegal activities, which is why surveillance is essential for the purpose of investigation. By carrying out surveillance, detectives can discover proof required to substantiate legal suit, or imprison a lawbreaker. This paper uses the IRAC method to explain the prevailing legal and regulatory structures in the EU and UK with respect to social media surveillance. It also gives an in-depth analysis of the rights of a person or citizen to social media privacy. It outlines the dangers of social media surveillance by authorities, and demonstrate different case laws and rulings regarding violations of citizens' right of privacy by different authorities.

**Keywords**— Social media surveillance, privacy rights, EU data protection, UK data protection, IRAC method, legal and regulatory framework, surveillance and crime, digital rights.

## I. INTRODUCTION

Surveillance can be used by detectives to track a person's movements, in search of activities that may implicate or vindicate them of skepticism. It can facilitate in identifying delinquent groups, as well as the connection between a suspected person, and their allies. It can ultimately provide helpful insights into the formation and strategies of criminal groups. There are basically six types of surveillance, and they include: electronic surveillance, physical surveillance, computer surveillance, social media surveillance, financial surveillance, and biometric surveillance.

Creation of social applications such as the X, TikTok, Facebook, was endorsed by Web 2.0, and it laid the foundation for Web 3.0, the succeeding initiation of the web which tackles glitches in a different way using same technologies (Will Kenton, 2023). It supports users to bring contents rather than merely watching it. With the arrival of these social applications, comes enormous supply and storage of individual data, which can in turn be methodically assessed, sold, or used for targeting users. The regulation of social media is a difficult and demanding issue as it comes with certain number of challenges like, (i) Outlining harmful content; establishing what forms a harmful content is complicated, as there is no distinct agreement on what content should be regulated, or permissible to stay on social media platforms. (ii) Implementing Regulations: enforcing regulations on social media platforms can be tough, because these platforms are situated in countries with diverse legal systems, and getting assistance from oversea governments can be challenging. (iii) Counterpoising uninhibited speech: striking a balance between the need to defend free speech, and the need to protect users from harmful content can be delicate while trying to regulate social media.

The degree of violation caused by social media surveillance by the government is overwhelming. There are reports of misuse even in countries with significant protections for basic freedoms. For instance, in the UK, London police seemingly monitored almost 9,000 advocates around the diplomatic field, using analysis based on emotions on information scratched from Facebook, X, and other social media platforms. Several of these advocates had no illegal background. Furthermore, there is a disturbing rise in the number of countries where social media users have been detained for their genuine online activities (Shahbaz & Funk, n.d).



## II. FACTS OF THE MATTER (ISSUES)

Authorities are progressively procuring state-of-the-art technologies to check the activities of their citizens on social media. Social media surveillance is the gathering, and managing of private information extracted from digital interaction platform, through mechanized skills, that permits evaluation of huge amounts of content, organization, and metadata. It cannot be discharged as not so much intrusive. Large number of people all over the world use this platform to connect with friends and loved ones. They also use it to voice their social, religious, and political views. China spearheads the generating, use, and distribution of social media surveillance devices (Shahbaz & Funk, n.d). As people continue to share pictures, videos, and posts, social media continues to grow.

Social media can put a person's personal information at risk without their knowledge, which is why information privacy is crucial as users set off digital tracks every day. For example, in July 2022, twitter was breached, and over 200 million users had their email addresses published on the dark web. These published emails can provide criminals with the information they require to carry out mischievous acts. A second example is, European Data Protection Board, fining Meta 1.3 billion dollars sometime in May 2023, because they violated European Union privacy laws by collecting, and transferring individual information of European Facebook users to United states servers. The consternation for privacy is at the foreground as cyberattack is in the news on a daily basis (Hetler, 2024). The concern for information privacy, triggered Federal Agencies, and U.S. states towards end of 2022, to prohibit workers from using TikTok on devices owned by government. They believe that since TikTok is owned by a Chinese company, they may likely use the app to acquire classified information about their government through these devices.

Majority of the information shared by users on social media platform through profile information and posts are done willingly. However, information can equally be unintentionally delivered through tracking cookies. These cookies trace the online activities of users, their acquisition record, and their webpage assessments. The information is afterwards collected and organized in sections, which in turn, is sold by information brokers for marketing intentions. Such sections may include: parents, fitness fanatics, animal lovers. Now with these sections, it is easy for organizations to modify advertising campaigns to social media users. In 2023, the information from Federal Trade Commission shows that people revealed losing over 10 billion dollars to scam, making it the largest scam losses so far recorded (Tressler, 2024). Scammers and promoters can still acquire the following information from a user on social media even when their account is private: location information, status updates, shared contents, employment details, personal interests, and religious beliefs.

Officials and scammers can obtain sufficient data to spy on user, or steal identities with the enormous amount of information on social media accounts. Certain ambiguities in privacy controls can place a user's data in jeopardy when using social media. Some social media privacy issues include:

- **Incorrect data:** Some individuals can disseminate misleading information on social media, while some trolls will seek to manipulate users' reactions by inciting them into intense arguments. It is therefore imperative to verify information from social media before utilizing it.
- **Privacy setting flaws:** Most private accounts on social media may not be as clandestine as users assume. For instance, a user may share information with a group of friends, once that information is reposted by those friends, it ends up before an entirely different audience.
- **Information exploitation:** Both cyberthieves and officials can begin spying on a target from information openly posted on social media. Cyberthieves can collect data such as email addresses, phone numbers, usernames, to plan phishing scams on users.
- **Setting of location:** A user's individual data, coupled with their location, is able to provide correct information to their profile. If a person turns off their location settings, the location app settings can still trace the person's location, because there are ways to aim their devices through phone turrets, websites, and public wi-fi.
- **Cyberbullying and harassment:** some mischievous persons can dox a person just for the intent of causing them harm.
- **Risk of viruses and malware:** When criminals hijack social media accounts, they use it to distribute malware to the contacts of the hijacked accounts. This can infect users with adverts, slow down their computers, and also steal delicate data.

Sometime in May 2013, Edward Snowden, a 29-year-old former technical assistant for the CIA, disclosed the worldwide surveillance activities of large parts of the web, most especially the social networks, organized by the National Security Agency. This action, has thus, raised privacy concerns on the internet. Do social media users actually care about their online privacy?

Do they believe that their online information is secure? Are users truthful about the information they post? The answer to these questions could be obtained by analyzing the empirical study conducted by Knautz and Baran (2016), between 22 July and 11 August 2014, on 304 people categorized by age, sex, and academic background, using an online questionnaire. The people who participated in the study, were queried about their conduct on social media, as well as their individual view about online privacy. The study shows a strong connection between the extent of people's divulgence on social media and age. The academic background of a person does not appear to influence their behavior in respect to their social media divulgence. However, the knowledge of the harms associated with abuse of privacy, has small connection with a person's maturity and education (Knautz & Baran, 2016). Regulating the kind of data shared to groups remains one of the most conventional ways of protecting a person's online privacy. Social media users know about the dangers of privacy violation, but appear willing to disregard them, especially when evaluated against the profit they get from using it.

Big Brother Watch, the UK civil rights group has made public, a key document about the UK government's social media surveillance. The 106-page article titled 'Ministry of Truth', reconnoiters at least five sinister divisions inside the UK government: the 77<sup>th</sup> Brigade, the Government Information Cell, the Intelligence and Communications Unit, the Rapid Response Unit, and the Counter Disinformation Unit. Each of these divisions, prevalingly use social media to collect data about people (Moody, 2023). The article specifies the behaviors of these divisions, and also proves that their evidence is gotten by means of liberty of data demand. According to the information made available to Big Brother Watch, by a whistleblower, about the comment made by the 77<sup>th</sup> brigade: "home observation of citizens online appeared not to be determined by a wish to tackle the fears and interests of the public, rather to discover forces for conformity with debatable government policies", typically explains the damage social media surveillance activities brings to privacy (Moody, 2023).

"The dangers that surveillance causes to privacy and equality are often spoken in the abstract, practical expressions, or as imminent dangers". Though, the effect of disproportionate surveillance in the UK is being experienced now, just that oftentimes, the opinions of those impacted the most are not heard (Hurfurt, 2023). Some of the issues of social media surveillance includes:

- **Destroys right:** Social media surveillance gradually destroys a person's right; fairness entails exciting open space devoid of continuous surveillance.
- **Infringes privacy:** Officials can save and study personal details of individuals like, their religious beliefs, sexual inclination, individual relationships through surveillance, and disclose them to authorities.
- **Impends immigrants' rights:** Individuals can be denied entry by immigration officers on the basis of their religious, political, and social views conveyed on their social media platforms.
- **Allows discrimination:** Analytical and human predisposition can enable untrue and dangerous ideas, hence, inexplicably affecting relegated groups.
- **Limits uninhibited expression:** Social media surveillance can cause individuals to desist from frankly making known their positions on political, religious, and social issues, for fear that their communication could be documented by officials, and possibly used against them.
- **Restraints right of association:** Surveillance of social media by authorities can make individuals more unlikely to join certain parties or groups.
- **Challenges integrity:** Social media surveillance disavows independent legal standards of "justified suspicion", and "good reason", and handles everybody as a crime suspect.

### III. RELEVANT ACT, DIRECTIVES (RULES)

As technology improvements have made monitoring actions simpler, surveillance laws in the UK have also become even more significant currently. It is essential to know what the laws say about surveillance in the UK and EU, amidst the use of surveillance cameras, CCTV systems, and other methods of monitoring. Some of the laws governing surveillance in the UK include: Investigatory Powers Act 2016 (IPA), Data Protection Act 2018 (DPA), Human Rights Act 1998 (HRA), General Data Protection Regulation (GDPR) as amended, Regulation of Investigatory Powers Act 2000 (RIPA), alongside the published codes of practice from the Home Office, Investigatory Powers Commissioner's Office (IPCO), previously the Office of Surveillance Commissioners (OSC), and the Information Commissioner's Office. The Privacy and Electronic Communications Regulations (the PECR) 2003 (EC Directive), execute the prerequisites of Directive 2002/58/EC, (the "ePrivacy Directive" as amended by Directive 2009/136/EC), which specifies a precise number of privacy rules to integrate the management of individual information by the telecommunications section. The essence of these policies is to explain how the Authorities may use social media when performing investigations, or carrying out other duties. This includes scrutinization of child protection, examination of trading paradigms, preemptive assessments in comparison to profits and incomes, and violations of the

Authorities' guideline. It ensures that any surveillance, investigation, or data collection requiring the use of social media is performed properly and lawfully in conformity with a person's human right. Social media, otherwise known as Social Networking Service (SNS), is a web-based resource which permits individuals, or businesses to create a public profile. Few of its characteristics include: the capacity to display a list of other people whom a user has association with, capacity to permit posting of photos and videos which can be viewed by many, and the capacity to surf and see list of associations made by other people in the platform.

The Center for Democracy & Technology (CDT), identifies an interconnected threat to privacy, resulting from individual data on social media posts. This moves beyond just data extraction of shared posts; it is an outcome of current attempts to permit researchers to have understanding of social media dynamics, by providing them authorized access to huge data. Example is the Article 40 of the EU's Digital Services Act (DSA), which requires organizations that are labelled as big online platforms, to provide appropriately evaluated researchers access to information, though hinged on some specific conditions. One of the confusing issues in this matter according to CDT report, is that while the Digital Service Act took effect in November 2022, a lot of facts are still indistinct. These will be fixed using "delegated acts"; extra stipulations released by the European Commission. The way to resolve the new right to access social media with the European Union's supreme GDPR (General Data Protection Regulation), is one of the paramount concerns at the moment. This simply shows that many social media posts include individual data that is subject to the GDPR.

RIPA was passed to determine ways by which the authorities may interfere with privacy rights in agreement with the law, and also in order to integrate the stipulations of Article 8(2) in English law. The aim is to shield the administrators and Commission in an investigation. The structure of RIPA is to affirm that an approval for covert surveillance, shall be legally recognized for every purpose, but that such legal recognition, could be approved, only if the officer is convinced that what is intended, is required and fair. If the approval methods presented by RIPA are adhered to, they offer shield to local authorities, and also to officials, with regards to difficulties associated with acceptability of evidence, applications under the Human Rights Act 1998, and objections to the Investigatory Powers Tribunal. The Act is backed by latest statutory Codes of Practice issued in 2018. They are the 'Covert Surveillance and Property Interference' and the 'Covert Human Intelligence Sources' (CHIS) Code of Practice. RIPA demands the local authorities to respect the stipulations of the Codes, which are admissible in any court as proof in criminal and civil actions. Although, the modifications which was operational on 1<sup>st</sup> November 2012, imply that a district authority may only approve directed surveillance under RIPA, to identify or avert illegal crimes punishable by full term of 6 months incarceration, whether on accusation or sentence. District authorities cannot approve directed surveillance for the aim of stopping chaos, except when it concerns unlawful crime punishable by a full 6 months incarceration term.

In May 2001, Investigatory Powers Commissioner's Office; an Inspectorate, was created in the Office of Surveillance Commissioners (OSC), to retain the evaluation of the practice and implementation of the powers, and responsibilities enforced by RIPA. In October 2017, this Office was substituted, and is presently called the IPCO (Investigatory Powers Commissioner's Office), and is controlled by the Investigatory Powers Commissioner. In August 2018, the latest Procedures and Guidance record, was released by the Investigatory Powers Commissioner, and is accessible on the Council's network. Authorities generally are obligated by RIPA to release all such records to the Investigatory Powers Commissioner, to enable him perform his tasks. Duly, the local authorities' custom and procedure is to conform entirely, and also conciliate between defending a person's basic privacy right, and carrying out a covert surveillance. One may ask, what is meant by covert surveillance? In accordance with RIPA section 48(1), surveillance is covert, only if it is executed in a way that is intended to ensure that the individuals who are being surveilled are unaware that they are under surveillance. Act 2000 outline, does not apply if surveillance is exposed to a person under examination. Furthermore, when surveillance is covert but not invasive, it is said to be 'directed'. Directed surveillance is any prearranged surveillance movement, embarked covertly, for the aim of a precise scrutinization, in a manner that is apt to end in getting a person's private data.

Whereas an individual may have a minimal expectation of privacy on social media, covert surveillance of the person's public activities can still result in getting their personal data. This is most likely the situation where the individual has a logical presupposition of privacy though acting in public. In an event where covert surveillance is executed under 'immediate response', in a manner that it is satisfactorily impracticable to get approval, it will not require a directed surveillance approval according to the Covert Surveillance and Property Interference Code of Practice of the 2000 Act. For example, a policeman who just stumbled on a suspect while on guard, would not need an approval to hide himself and surveil the individual. While using social media for research and investigations, officials should be careful not to drift into surveillance. They should not assume that because social media is an open space, it exempts the need for an approval before surveillance can take place. The use of social media in situations that require logical expectation of privacy, requires approval especially when the surveillance

will take longer than one week. Furthermore, certain actions like opening a fake or unknown account, and entering locked groups with the intention of investigation is also most likely to need an approval, except the official's identity is disclosed from the beginning.

The Human Rights Act 1998 regulates surveillance in the UK, it integrates the European Convention on Human Rights (ECHR) into UK law, together with right to privacy. This implies that local authorities should make sure that any surveillance they perform is essential and fair, and does not unjustifiably breach the rights of a person. Regulation (European Union) 2016/679; GDPR (General Data Protection Regulation), was the primary data protection legislation in the United Kingdom prior to their exit from the EU on the 31st December, 2020. The GDPR voided the Data Protection Directive 95/46/EC, and this resulted in better compliance with the data protection law throughout the European Union member states. Certain conditions in the GDPR, can be modified in the national laws of the European Union member states. Hence, the Government of the United Kingdom issued the Data Protection Act 2018 (DPA 2018), and a number of successive modifications that encompasses those sections of the GDPR which are not included in the EU law, but could be added by the European Union member states. The Data Protection Act 2018 became operational on 25th May, 2018. The Investigatory Powers Act 2016 (IPA) is correspondingly another important UK law on surveillance, that strengthens and revises the prerogatives of local authorities to perform surveillance. However, IPA demands that local authorities must get approval through the secretary of state or a Judge before conducting surveillance.

Protection of information is a basic right in the European Union (Article 8 of the Charter of Fundamental Rights). It is matched by various other mediums like, the Data Protection Regulation (EU) 2018/1725, which sets off the information protection constraints with respect to managing of individual information by the EU organizations and agencies, relevant to the European Research Executive Agency (REA). People whose individual information is managed by REA, could apply some rights set up in Articles 14-24 of Regulation 2018/1725. In some cases, REA can constrain a person's information right, in conformance to the rules of Article 25 of the Regulation, centered on its evaluation of the Steering Committee, on internal rules regarding constrain of certain rights of a person's information. A person can be notified of their rights through DPN (Data Protection Notices), communicated by the data controllers and the DPR (Data Protection Records), accessible in the Central Public Register of Records. Directive (EU) 2016/680, defends a resident's basic right to information protection, anytime delicate information is being used by law enforcement government department, for the intent of prosecution. It ensures that the individual information of accused persons, witnesses, and targets are protected accordingly as well as aid international cooperation, in the battle against criminality and violence.

Directive (EU) 2016/680 became operative on 5 May, 2016 and was transferred into EU countries' national law on 6 May, 2018. Countries in EU have raised national bodies in charge of protecting individual's information in agreement with Article 8(3) of the Charter of Fundamental Rights of the EU. The GDPR regulation purposes to restructure collaboration between Data Protection Authorities when implementing the GDPR in international cases. The EDPB (European Data Protection Board), is a self-regulating body, that ensures the coherent implementation of information protection rules in every part of the European Union. EDPB is instituted by the GDPR, and is comprised of the spokespersons of the national data protection authorities of the EU/EEA (European Economic Area), and the directors of the European Data Protection. The basic tasks of the EDPB include: directing the European Commission on subjects connected to the protection of individual data, and any fresh recommended legislation in the EU, offering help on basic models of the Law Enforcement Directive and the GDPR, and finally approving mandatory resolutions in disagreements between the national managerial authorities. A Data Protection Officer, as selected by The European Commission is in charge of monitoring and implementation of information protection rules in the European Commission. The officer objectively ensures the domestic implementation of information protection rules in collaboration with the European data protection directors.

The European ePrivacy Regulation is a crucial amendment to the current ePrivacy directive of 2002, and it is the "lex specialis" to the GDPR. Lex specialis means "law governing a specific matter". The legal doctrine "lex specialis derogat legi generali" (a special law overrides laws that govern general matter), is welcomed by the European Union. According to Article 1, Subject matter, the regulation draws up rules concerning the protection of basic rights and freedom of an individual, with regards to the use of electronic interaction service in managing personal data. It also draws up the rules regarding the protection of the basic rights of the authority, in the use of electronic interaction services, especially their rights to acceptance of interactions. EU member states, in February 10 2021, settled on a bargaining order for amended rules on the protection of privacy and discretion, in the use of electronic interaction services. The amended ePrivacy rules, outline the circumstances in which internet access providers are permitted to process or access information saved on consumer's machines. The rules also include information conveyed on networked devices, to ensure complete protection of privacy rights and to encourage a reliable IoT

(Internet of Things). The rules apply when consumers are in the European Union, and also include situations where the processing or the service provider is situated outside the European Union. Therefore, as a principal rule, any information through electronic interaction is private, so any form of interference, monitoring or processing of such information by anybody apart from the consumer is illegal, except when approved by the ePrivacy regulation.

#### IV. ANALYSIS OF RELEVANT CASE LAWS

The assimilation of Article 8 into the UK law through the Human Rights Act 1998 simply implies that a public or government agency involved in any interference practice with a person's privacy should be able to prove that the said surveillance is: required, lawful, commensurate to the intention, and performed in agreement with one of the legal objectives laid out in Article 8(2) of the ECHR. In the case of *Prismall v. Google UK Limited and Deepmind Technologies Limited* [2023] EWHC 1169 (KB); about the alleged abuse of medical reports of 1.6 million patients. The reports were moved to DeepMind, a subdivision of Google focusing on artificial intelligence research and development. The aim of moving the reports was to help in creating an app intended to assist health care specialists to discover and treat people with severe kidney damage. The plaintiff, Andrew Prismall was one of the patients impacted. He argued that moving the reports without the consent of the patients was an abuse of private information, and requested for costs over loss of control of his personal data, and that of the other impacted patients. Although the court acknowledged Prismall's worries, it dismissed the claim, establishing the fact that there was no reasonable outlook of proving a logical expectation of privacy among the patients. It also states that the diverse nature of the patients' conditions disallows pursuing an action.

In the survey by the International Association of Chiefs of Police (IACP), "2011 IACP (2011, p.3 as cited in Brunty & Helenek, 2012), 88.1% of law officers use social media among the 800 law officers surveyed. Greater part of them stated that social media has assisted them in solving crime. From the investigation conducted by Privacy Internation, David Feldman, who is Rouse Ball English law professor from the university of Cambridge, disputed that before the passing of the Human Rights Act 1998 (HRA), there was no recognized right to privacy in UK law. Though people could petition to the European Court of Human Rights, if they suffered any violation of their right to privacy under the Article 8 of the ECHR (European Convention on Human Rights). Following the passing of the Human Rights Act, the ECHR turned out to be part of an established home law, and also an over-all right to respect for family and private life under Article 8 in the UK. As a result, it became illegal for any public agency to act in a way that intrudes a person's privacy, except the public agency can indicate any particular exceptions enclosed in Article 8.

Also, In the case of a popular model Naomi Campbell and Mirror Group Newspaper [2004] UKHL 22; Mirror Group Newspaper published an article about her drug addiction, and successively backed it up with some photographs of the model exiting a gathering for drug addicts. The model requested costs for violation of privacy relative to the covertly taken photographs. However, she acknowledged that the newspaper was permitted to publish the evidences of her addiction and treatment, following her earlier public statement. She won the trial where it was held that the information objected was private, and publication was not in the interest of the public. The court of appeal however, agreed that the respondent's petition, on the ground that the extra information of the model's medical treatment, was required to prove the integrity of the story, and in the interest of the public. Campbell however appealed to House of Lords. The House of Lords maintained that the appropriate experiment to establish if information was private, was to consider whether a random sensible individual, subjected in the exact situation as the Model, would find the exposure of the information invasive. The Court stated that guarantee of privacy, was a necessary part of Campbell's treatment therapy in relation to her physical and mental health, and that details of her therapy, consequently formed private information which resulted in privacy obligation. The press exceeded their editorial boundary. Meanwhile, regarding the photographs taken outside the gathering, the Court acknowledged that a person may have a logical privacy expectation in public, and that this expectation was unreasonably violated in this case.

The establishment of HRA has assisted in making sure that the privacy of the people is well secured. However, right to privacy alone is incapable of providing enough base for the protection of people against intrusive surveillance, or processing of information. For example, in the landmark judgement in relation to UK's mass surveillance, European Court of Human Rights (ECtHR) ruled that the UK's mass surveillance, violated the people's right to privacy. The mass surveillance was revealed by Edward Snowden. UK's negligence to use protections of identity, location, and address violated the people's right to privacy under Article 8 ECHR. Though the ruling involved the Regulation of Investigatory Powers Act 2000 (RIPA), which has been significantly overtaken by the Investigatory Powers Act 2016 (IPA), much of the court's reflections relate to the new law. The UK's surveillance system subject to RIPA was unsolicited, simply implying that the UK people's individual information was collected indiscriminately, without any hint of suspicion, or proof of crime, and the system was indefinitely operative.

Furthermore, in the case of *Bekoe v. Islington LBC* [2023] EWHC 1668 (KB), concerning the abuse of private information by a local authority. Islington LBC, a local authority abused the private information and confidential details of Bekoe's finances, by retrieving and distributing them during legal trials, thereby breaching the GDPR. Bekoe stated that his information was gotten illegally, and claimed that Islington had breached the GDPR by abusing a Data Subject Access Request (DSAR), which he tendered. He stated that Islington was responsible for loss of legal documents following an unfinished confession, a four-year delay, and negligence in providing sufficient protection over personal data. The court resolved that Islington had failed to show that the misuse of Bekoe's private information was commensurate to the intention. The expectation of privacy, outweighs other interests, consequently violating Bekoe's GDPR rights. The court awarded him 6,000 pounds in costs.

Also, in the case of *ZXC v Bloomberg* [2022] UKSC 5; a pivotal privacy case resolved by the UK Supreme Court. It was contemplated whether an individual under criminal investigation, prior to being arraigned, has a logical hope of privacy, about information concerning the investigation. ZXC is a regional CEO of a Plc overseas, and in charge of operations. An Editorial was published regarding the Plc's operations for which ZXC was liable. The Editorial was centered on subjects of a letter sent to a foreign law enforcement agency, by a law enforcement agency in the UK, investigating the activities of the Plc within the district. ZXC demanded a logical hope of privacy, based on the details of the criminal investigations into his activities, revealed through the letter. He also claimed that the publication of the editorial by Bloomberg resulted in violation of that confidential information. There were three subjects before the court:

- A) If the Court of Appeal was mistaken to maintain that there is a common rule, relevant in the current lawsuit, that an individual under criminal investigation has, prior to being arraigned, a logical hope of privacy regarding information relating to that investigation.
- B) If the Court of Appeal was mistaken to maintain that, in a lawsuit where a claim for violation of confidence was not followed, for the fact that the information printed by Bloomberg about the investigation, came from the confidential records of the law enforcement, made the information private thereby weakening Bloomberg's power to bank on the public interest in exposing it.
- C) If the Court of Appeal was mistaken to maintain the findings of one Nicklin J, that the plaintiff had a logical hope of privacy with respect to the printed information complained of, and that Article 8 and 10 correspondingly went down in support of the plaintiff.

The Appeal was dismissed by the court on all three bases, hence, the practice is established that there is, as a lawful basis, a supposition that there is a logical hope of privacy relative to facts of a criminal investigation prior to arraignment.

## V. CONCLUSION

The use of social media surveillance for investigative purposes is more consistent across forces than it is for communication purposes. A study of the internal policy documents, by Egawhary (2019), of UK Law Enforcement Agencies' use of social media in surveillance, finds that they deliberate five surveillance aspects of social media: common surveillance of the residents, inciting residents to surveil each other, supervisory surveillance, homologous surveillance and surveillance with the intention of investigation. Several of the cases involving surveillance begins with a concern of the actions' agreement with Article 8(2) in accordance with the requirements of the law. For example, the Article states that, "there shall be no interference by a public authority with the exercise of this right except such as is in accordance with the law and is necessary in a democratic society in the interests of national security, public safety or the economic well-being of the country, for the prevention of disorder or crime, for the protection of health or morals, or for the protection of the rights and freedoms of others".

In my analysis however, I observed that Article 8(2) has failed in attaining sufficient amount of clarity regarding the limit which surveillance methods can be used, and this has intensified the danger of using surveillance in an illogical manner.

I recommend that in a situation whereby Article 8(2) cannot be amended to provide more clarity, then, in addition to whatever training is being given to public authorities entrusted with implementing Article 8(2), they should be made to understand in clear terms, the importance of moral and integrity, in ensuring that the implementation of the Article is free, fair, credible, in good fate and without bias.

## REFERENCES

- [1] Fuchs, C, Boersma, K, Albrechtslund, A & Sandoval, M (2013). *Internet and Surveillance: The Challenges of Web 2.0 and Social Media*. Routledge. New York.

- [2] The Washington Post & O' Harrow, Jr (2014, Jan 9). Zero day: the threat in cyberspace. Diversion books. (kindle edition).
- [3] Shahbaz, A., & Funk, A. (n.d). Social Media Surveillance, Freedom on the Net 2019 Key Finding: Governments harness big data for social media surveillance Freedom House. <https://freedomhouse.org/report/freedom-on-the-net/2019/the-crisis-of-social-media/social-media-surveillance>
- [4] Brunty, J & Helenek, K (2012). Social Media Investigation for Law Enforcement. Taylor & Francis group.
- [5] Types of Surveillance for Investigations Explained. (April 25, 2023). NITA. <https://investigativeacademy.com/6-types-of-surveillance-for-investigations-explained/#:~:text=Surveillance%20takes%20many%20forms%2C%20including,threats%2C%20and%20investigate%20criminal%20activity>
- [6] Will, K (2023, July 30). What is Web 2.0? Definition, Impact, and Examples. Investopedia. <https://www.investopedia.com/terms/w/web.20.asp#:~:text=Web%202.0%20describes%20the%20current,aftermath%20of%20the%20dotcom%20bubble>.
- [7] Jake Hurfurt (2023). State of Surveillance in 2023. Big Brother Watch. <https://bigbrotherwatch.org.uk/wp-content/uploads/2023/12/State-of-Surveillance-Report-23.pdf>
- [8] Home Office Covert Surveillance and Property interference, August 2018. (2020, May 24). PI. <https://privacyinternational.org/long-read/3532/home-office-covert-surveillance-and-property-interference-august-2018>
- [9] Moody, G (2023, February 1). UK Government Is Engaged in Large-Scale Surveillance of Social Media. Private Internet Access. <https://www.privateinternetaccess.com/blog/uk-social-media-surveillance/>
- [10] Henson, B., Reyns, B. W., & Fisher, B. S. (2011). Security in the 21st Century: Examining the Link Between Online Social Network Activity, Privacy, and Interpersonal Victimization. *Criminal Justice Review*, 36(3), 253-268. <https://doi.org/10.1177/0734016811399421>
- [11] What Laws Are There on Surveillance in the UK? (2023, March 24). Able Investigations and Enforcement Services. <https://ableinvestigations.com/what-laws-are-there-on-surveillance-in-the-uk/#:~:text=Under%20the%20IPA%20and%20RIPA,rights%20of%20individuals%20are%20protected>
- [12] Regulation of Investigatory Powers Act 2000 <https://proceduresonline.com/trixcms2/media/8508/ripa-2000-using-social-media-as-a-surveillance-tool.pdf>
- [13] History of the UK Regulator's concerns regarding Local Authority use of social media monitoring. (2020, May 24). PI. <https://privacyinternational.org/long-read/3531/history-uk-regulators-concerns-regarding-local-authority-use-social-media-monitoring>
- [14] Kouvakas, L (2023, August 22). Changes to UK Surveillance Regime May Violate International Law. Just Security. <https://www.justsecurity.org/87615/changes-to-uk-surveillance-regime-may-violate-international-law/>
- [15] Methodology: Social Media Monitoring by Local Authorities. (2020, May 24). PI. <https://privacyinternational.org/report/3530/methodology-social-media-monitoring-local-authorities>
- [16] Surveillance: Citizens and the State- Constitution. (2009). <https://publications.parliament.uk/pa/ld200809/ldselect/ldconst/18/1806.htm>
- [17] Teacher, Law. (November 2013). Campbell v Mirror Group Newspapers - 2004. Retrieved from <https://www.lawteacher.net/cases/campbell-v-mirror-group.php?vref=1>
- [18] The use of social media monitoring by local authorities- who is a target? (2020, May 24). PI. <https://privacyinternational.org/explainer/3587/use-social-media-monitoring-local-authorities-who-target>
- [19] Use of social media in investigations policy and procedure 2020-21. (n.d). <https://www.colchester.gov.uk/info/cbc-article/?catid=policy-framework-local-choice&id=KA-01480>
- [20] Egawhary, E.M (n.d). Surveillance and Society: The surveillance Dimensions of the Use of Social Media by UK Police Force. <https://ojs.library.queensu.ca/index.php/surveillance-and-society/article/view/12916/8481>
- [21] When Local Authorities aren't your Friends. (2020, May 24). PI. <https://privacyinternational.org/report/3584/when-local-authorities-arent-your-friends>
- [22] Article 8: Respect for your private and family life. (2021, June 24). Equality and Human Rights Commission. <https://www.equalityhumanrights.com/human-rights/human-rights-act/article-8-respect-your-private-and-family-life#:~:text=and%20family%20life-,Article%208%20protects%20your%20right%20to%20respect%20for%20your%20private,and%20emails%2C%20for%20example>
- [23] Head of Law and Governance Stratford-on-Avon District Council. (2020, December). Use of Social Media in Investigations Procedure. <https://www.stratford.gov.uk/doc/210080/name/SDC%20Use%20of%20Social%20Media%20in%20Investigations%20Procedure%20Version2%20.pdf>
- [24] The Regulation of Investigatory Powers Act (RIPA) Policy and Procedure. (2020, November 25). Lancaster City Council. <https://committeeadmin.lancaster.gov.uk/documents/s82166/RIPA%20and%20Social%20Media%20Policy%20v3%201.1.pdf>
- [25] REA privacy policy and social media use. (n.d). European Commission. [https://rea.ec.europa.eu/rea-privacy-policy-and-social-media-use\\_en](https://rea.ec.europa.eu/rea-privacy-policy-and-social-media-use_en)
- [26] Hetler, A (2024, April 23). 6 common social media issues. TechTarget. <https://www.techtarget.com/whatis/feature/6-common-social-media-privacy-issues>

- [27] Clarke, L (2024, January 3). Britain's got some of Europe's toughest surveillance laws, Now it wants more. Politico.  
<https://www.politico.eu/article/uk-bulking-up-spying-regime-breakneck-speed/>
- [28] Data protection in the EU. (n.d). European Commission. [https://commission.europa.eu/law/law-topic/data-protection/data-protection-eu\\_en](https://commission.europa.eu/law/law-topic/data-protection/data-protection-eu_en)
- [29] The European ePrivacy Regulation. (2021, February 10). <https://www.european-eprivacy-regulation.com/>
- [30] Overview- Data Protection and the EU. (n.d). ICO. [https://ico.org.uk/for-organisations/data-protection-and-the-eu/overview-data-protection-and-the-eu/#:~:text=in%20the%20EEA.,Does%20the%20GDPR%20still%20apply%3F,Act%202018%20\(DPA%202018\)](https://ico.org.uk/for-organisations/data-protection-and-the-eu/overview-data-protection-and-the-eu/#:~:text=in%20the%20EEA.,Does%20the%20GDPR%20still%20apply%3F,Act%202018%20(DPA%202018))
- [31] Sachowski, J (2016). Ensure Legal Reviews. In J. Sachowski (Eds.), *Implementing Digital Forensic Readiness*. (pp. 143-149). Syngress. <https://www.sciencedirect.com/science/article/pii/B9780128044544000149>
- [32] Osborne, M (2006). Information Security Laws and Regulations. In M. Osborne (Eds.), *How to Cheat at Managing Information Security/* (pp. 71-86). Syngress. <https://www.sciencedirect.com/science/article/pii/B9781597491105500117>
- [33] Zorzetto, S (2012, September 3). The Lex Specialis Principle and its Uses in Legal Argumentation. *An Analytical Inquire*.
- [34] The final text of the Digital Services Act (DSA). (2022, October 19). Cyber Risk GmbH. [https://www.eu-digital-services-act.com/Digital\\_Services\\_Act\\_Article\\_40.html](https://www.eu-digital-services-act.com/Digital_Services_Act_Article_40.html)
- [35] UK: Europe's top court rules UK mass surveillance regime violated human rights. (2021, My 25). Amnesty International.  
<https://www.amnesty.org/en/latest/press-release/2021/05/uk-surveillance-gchq-ecthr-ruling/>
- [36] UK: Stop social media monitoring by local authorities. (2020, June 10). EDRI. <https://edri.org/our-work/uk-stop-social-media-monitoring-by-local-authorities/>
- [37] Nakutavičiūtė, J (2024, January 01), What are the most common social media privacy issues?. NordVPN.  
<https://nordvpn.com/blog/social-media-privacy-issues/>
- [38] Hickman, T & Devine, J (2023, July 20). Data Protection Laws and Regulations UK 2023-2024. <https://iclg.com/practice-areas/data-protection-laws-and-regulations/united-kingdom>
- [39] The Human Rights Act Is A Vital Defense Against Surveillance. (2018, November 8). <https://eachother.org.uk/the-human-rights-act-is-a-vital-defence-against-surveillance/>
- [40] Jeanis, Michelle & Muniz, Caitlyn & Molbert, Courtney. (2019). Law Enforcement and Social Media Usage: An Analysis of Engagement. *Policing: A Journal of Policy and Practice*. 15. 10.1093/police/paz026.
- [41] Todd, E, Andrews, J.J & Lysik, A (2024, February 20). 2023 UK Data Protection and Privacy Case Law Update. ReedSmith.  
<https://www.reedsmith.com/en/perspectives/2024/02/2023-data-protection-and-privacy-case-law-overview>
- [42] Lipschultz, J.H (2023). *Social Media Communication: Concepts, Practices, Data, Law and Ethics*. Routledge. (Fourth edition).
- [43] Top 10 Privacy and Data Protection Cases 2022. (2023, January 1). The Privacy Perspective.  
<https://theprivacyperspective.com/2023/01/01/top-10-privacy-and-data-protection-cases-2022/>
- [44] European Convention on Human Rights- Article 8 (nd). FRA. <https://fra.europa.eu/en/law-reference/european-convention-human-rights-article-8-0>
- [45] Egawhary, E.M (2019). *Surveillance & Society. The Surveillance Dimensions of the Use of Social Media by UK Police Forces*.  
<https://eu.docs.wps.com/l/sIHW88LHlAb7vwrIG?v=v2>.



# Enhancing Material Removal Rate in EDM with Green Dielectrics: A Regression Modeling Approach

M. Sirisha<sup>1\*</sup>, Dr. S. Gajanana<sup>2</sup>, Dr. P. Laxminarayana<sup>3</sup>

<sup>1</sup>Research Scholar, Mechanical Engineering Department, University College of Engineering, Osmania University, Hyderabad, India

<sup>2</sup>Professor, Department of Mechanical Engineering, MVSR Engineering College, Hyderabad, India

<sup>3</sup>Professor, Mechanical Engineering Department, University College of Engineering, Osmania University, Hyderabad, India

\*Corresponding Author

Received: 05 August 2024/ Revised: 10 August 2024/ Accepted: 14 August 2024/ Published: 31-08-2024

Copyright © 2024 International Journal of Engineering Research and Science

This is an Open-Access article distributed under the terms of the Creative Commons Attribution

Non-Commercial License (<https://creativecommons.org/licenses/by-nc/4.0>) which permits unrestricted

Non-commercial use, distribution, and reproduction in any medium, provided the original work is properly cited.

**Abstract**— *Electrical Discharge Machining (EDM) is one of the electrical based advanced machining method where electrical energy is used as a source to cut or remove material. Green dielectrics are utilized in machining to make the process extremely competent and secure. Hybrid aluminum 2021 tools with different copper percentages are utilized for super alloy superalloy 909 machining research in an effort to further lower manufacturing costs. The impact of different input parameters Investigations are conducted on the work material for material removal rate as a reaction to changes in pulse on time, pulse off time, current, voltage, and tool material. A mathematical model is created and the influence of process parameters on response is determined using the Taguchi design of experiments. Each factor's percentage contribution is calculated. The goal of this research is to provide a substitute dielectric that can be machined in an environmentally friendly and sustainable manner while producing a satisfactory output at the lowest possible tooling cost.*

**Keywords**— *EDM, material removal rate, process parameters, regression equation.*

## I. INTRODUCTION

EDM supports a persuasive manufacturing method that authorizes production of components made of hard matters accompanying difficult geometry that are troublesome to manufacture by a normal machining method. EDM does not form direct contact across the tool and the workpiece, eliminating mechanical stresses, chatter, and vibrations while machining. The talent to control process limits to obtain the necessary precision and surface texture has established this build movement in an outstanding position in industrialized requests. The outstanding interest in EDM has upshot excellent bettering in its field and concedes it as main non-traditional machining method, widely used in automobile, aerospace, die and tool industry. Applications vary from simple die and tool making to producing complicated components. Surface characteristic damage on account of machining operations is straightforwardly had connection with the strength used to eliminate the metal. The major determinants effecting machining in EDM are electrical parameters (discharge current, and voltage), material characteristics of tool and workpiece, and the dielectric fluid used.

The main research concern in advancing the status of EDM process is to have a better understanding of the relation between the input parameters and the responses.

### 1.1 Material Removal Mechanism:

In EDM the electric sparks strike the electrically conductive materials immersed in a dielectric medium and divided by a tiny gap, which erodes and removes material. The electrodes receive electric energy in the form of brief impulses with a predetermined shape. Spark generators made specifically for this purpose are a good way to provide the necessary energy, which is often needed as rectangular pulses. An electric spark discharge takes place inside the interelectrode gap, when the electrodes are subjected to such a voltage pulse. It is commonly recognized that the heat action of an electrical discharge is primarily responsible for erosion on the electrode surfaces. A spark generator's induced charge on electrodes produces a powerful electric field. Where the electrodes are nearest to one another, this field is strongest. The dielectric fluid's molecules and ions are polarized and directed between these two peaks. Anode and cathode electron avalanche strikes generate a low

resistance discharge channel when the dielectric strength of the liquid in the gap surpasses a natural limit. Heat and pressure are produced during this collision event, which changes the kinetic energy of the atomic particles. Even for brief pulse durations, heat produced within the discharge channel is expected to reach 1017 W/m<sup>2</sup>, which might elevate electrode temperatures locally to as high as 20000K. There isn't a machining technique that produces comparable high temperatures in such small dimensions. Current density in the interelectrode gap reduces as a result of the pressure rise in the plasma channel, which also drives the discharge channel borders to expand. The pressure rise is usually so great that heated metal on electrode surface cannot evaporate. A sudden drop in channel pressure upon the cessation of the pulse voltage starts a severe erosion. The superheated cavities burst into the dielectric liquid. Ultimately, the surfaces instantly cool, with all of the evaporated material being carried away by the dielectric liquid along with a portion of the molten material in the form of hollow or ragged particles. The end effect is a small crater where some of the residual molten material has spilled across both electrode surfaces. Applying rapid high-frequency spark discharges one after the other and pushing one electrode in the direction of the other progressively erodes the workpiece.

## II. DEVELOPMENT OF MODEL

A Mathematical model is formed to improve the input limits for every tool used for machining by Design of Experiments(DOE). In DOE, numbers of trails expected attended are contingent upon Taguchi DOE and design matrix is built for five input parameters with four distinct levels. Experiments are completed activity according to the design model. Once the design matrix is developed, regression coefficients are computed. Adequacy of model is proven by fisher test at 5% significance level. For every regression coefficient Student's t-test is carried to find out its importance. The mathematical model is generated after ignoring unimportant coefficients. Finally Analysis of Variance (ANOVA) is carried to find the contribution of each determinant to the MRR.

### 2.1 Taguchi DOE:

Taguchi envisioned a brand-new approach to experiment design that is predicated on clearly laid out rules. A unique class of arrays known as orthogonal arrays is used in this technique. These standard arrays specify how to carry out the fewest tests necessary to fully understand every element influencing the performance parameters. Standard orthogonal arrays come in a variety of forms, and each one is intended for a particular quantity of independent design variables and values. L16 orthogonal array, for instance, would be the best option if one wishes to carry out an experiment to determine the influence of five distinct independent variables, each of which has four level values. This array makes the assumption that no two factors interact. While there are numerous situations in which the interaction model premise is not met, there are other instances in which interaction is amply demonstrated. Such example of such interaction would be the relationship between temperature and material properties.

### 2.2 Postulation of Mathematical Model:

The relationship between the responder and predictor variables is described by the regression expression, which is an algebraic description of the regression line. The general form of regression equation looks like this:

$$\text{Response} = \text{constant} + \text{coefficient} * \text{predictor} + \dots + \text{coefficient} * \text{predictor}$$

$$\text{or } Y = C_0 + C_1X_1 + C_2X_2 + \dots + C_kX_k$$

Where:

(Y) is the response numeral.

(C<sub>0</sub>) is the response variable when the predictor variable(s) is zero. The constant is known as intercept because it determines where the regression line cuts the Y-axis.

(X) is the predictor variable(s) value. It can be a polynomial term.

Coefficients (C<sub>1</sub>, C<sub>2</sub>, ..., C<sub>k</sub>) represent the change in mean response for each unit variation in the predictor value. In other words, it is the variation in Y that happens when X rises by one unit.

In order to create a mathematical model that predicts the MRR, the EDM process variables are determined. These include current (I), pulse on time (T<sub>on</sub>), pulse off time (T<sub>off</sub>), voltage (V), tool electrode (Tool). It is assumed that the first order model has two, three, and four interactions.

Regression models and examines the connection between a predictor (X) and response (Y). Although categorical and continuous predictors are both acceptable, the response must be continuous. Both polynomial and linear relationships can be modeled.

Regression analysis is particularly useful for figuring out how the response variable changes in response to changes in a given predictor variable. For every response variable, Minitab keeps track of the most recent regression model you fitted. Predictions, overlaid contour plots, and optimum responses can all be produced rapidly with saved models. You must fit a model for every response in analyses that make use of numerous responses.

### III. EXPERIMENTATION

The Electrical Discharge Machine, Die-Sinking Type SYCNC PC-60 as shown in figure 1, is used for the experimentation. Its electrode polarization is situated as negative, while the work piece polarization is located as positive. The workpiece in figure 3 is 66.8 mm in diameter and 6 mm thick, and it is shaped like a cylinder made of superalloy Superni 909. Four distinct tool electrodes in figure 2 are employed, with the proportion of copper varied and aluminum 2021 serving as the foundation material. The regenerated dielectric liquid had a specific gravity of 0.763 and was EDM oil. Using a stopwatch, the machining time for each experiment is maintained at 10 minutes. To determine the MRR, the workpiece is thoroughly cleaned and its weight is recorded both before and after each trial. Table 1 displays the process parameters and their corresponding levels. The machine's capability is taken into account when choosing the range of parameters for the trials. In order to ensure more accurate optimization, a wide range is used. For this investigation, an L16 orthogonal array with 8 columns and 16 rows was chosen.



**FIGURE 1: Die-sinking EDM machine**



**FIGURE 2: Al2021 Electrodes with varying % of Cu**



**FIGURE 3: Workpiece machined**

**TABLE 1  
INPUT PARAMETERS AND THEIR VALUES**

Parameter	Units	Level 1	Level 2	Level 3	Level 4
Current(A)	A	10	20	30	40
Pulse on Time( $\mu$ s)	$\mu$ s	250	500	750	1000
Pulse off Time ( $\mu$ s)	$\mu$ s	100	200	300	400
Voltage (V)	V	30	40	50	60
Electrode		T1	T2	T3	T4

Three dielectric fluids were tested in the experiments: used vegetable oil, used gear oil, and EDM oil. MRR was computed for each trial. Before beginning the studies, the dielectric tank was thoroughly cleaned and emptied. To carry out the studies, fresh EDM oil was added to the tank. Similar to this, used vegetable and used gear oil were added to the tank after it had been emptied and cleaned. 48 trials in all were conducted, 16 runs of each using used gear oil, used vegetable oil, and EDM oil. While machining with each of the three dielectric fluids, results have been noted. Figure 4(a-b) displays dielectric fluid samples.



**FIGURE 4(a): Used gear oil sample**



**FIGURE 4(b): Used gear oil sample**

#### IV. RESULTS AND DISCUSSIONS

The Fisher Test was then used to see if the model was adequate. According to this method, the produced model's F-ratio do not surpass the tabulated value of F-ratio at a 95% confidence level. Therefore the model was suitable. Student's T-test was performed to determine the significance of the coefficients, and only significant coefficients were employed to create the mathematical model. The final model for the MRR for used vegetable oil, used gear oil, and EDM oil is provided below in coded form.

Regression equation for material removal rate developed for EDM oil as dielectric fluid.

$$\text{MRR} = -1.89 + 0.00408 T_{\text{on}} + 0.00150 T_{\text{off}} + 0.1050 I + 0.0099 V + 0.0487 T_{\text{ool}} \quad (1)$$

Regression equation for material removal rate developed for used gear oil as dielectric fluid.

$$\text{MRR} = 1.93 + 0.00326 T_{\text{on}} - 0.00438 T_{\text{off}} + 0.0648 I - 0.0567 V + 0.0942 T_{\text{ool}} \quad (2)$$

Regression equation for material removal rate developed for used vegetable oil as dielectric fluid

$$\text{MRR} = 3.46 + 0.00202 T_{\text{on}} - 0.00747 T_{\text{off}} + 0.1056 I + 0.0267 V - 0.0639 T_{\text{ool}} \quad (3)$$

The calculated material removal rates and regression coefficients for MRR are shown in the tables 2 and 3.

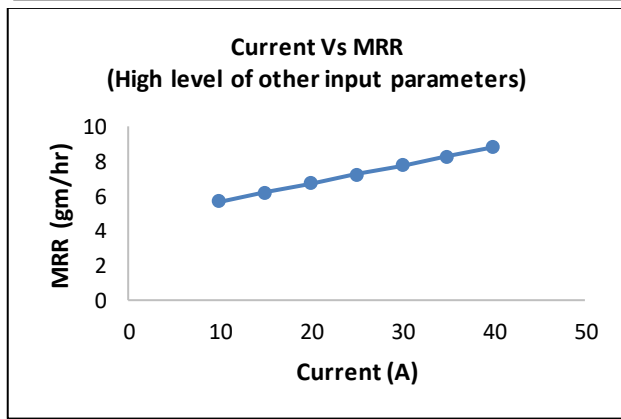
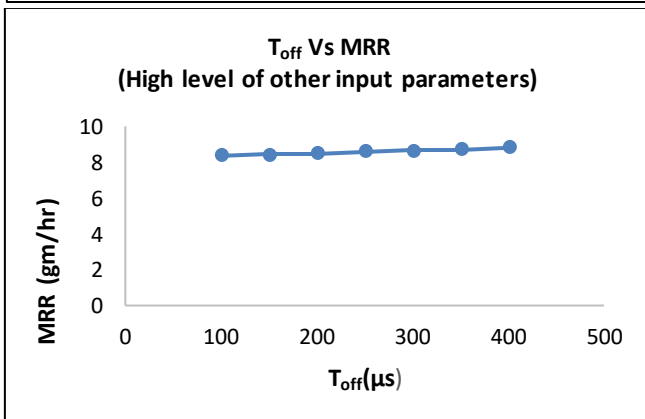
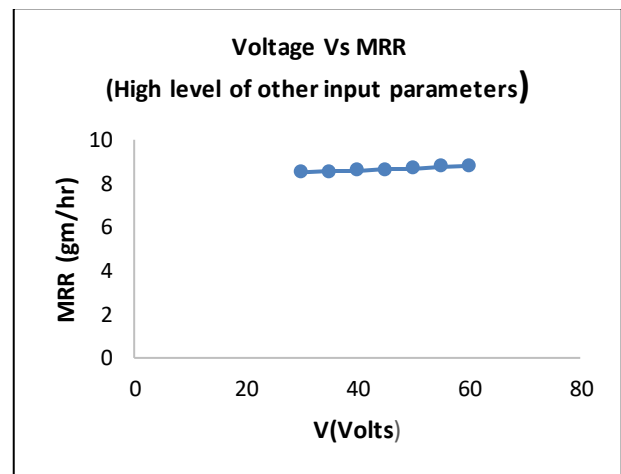
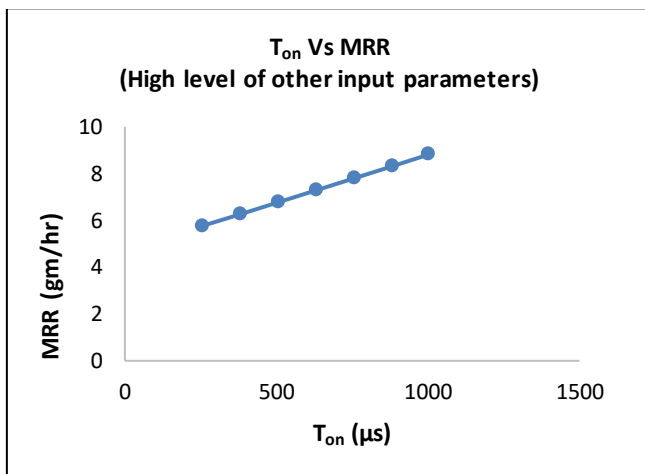
**TABLE 2**  
**CALCULATION OF REGRESSION COEFFICIENTS FOR MRR**

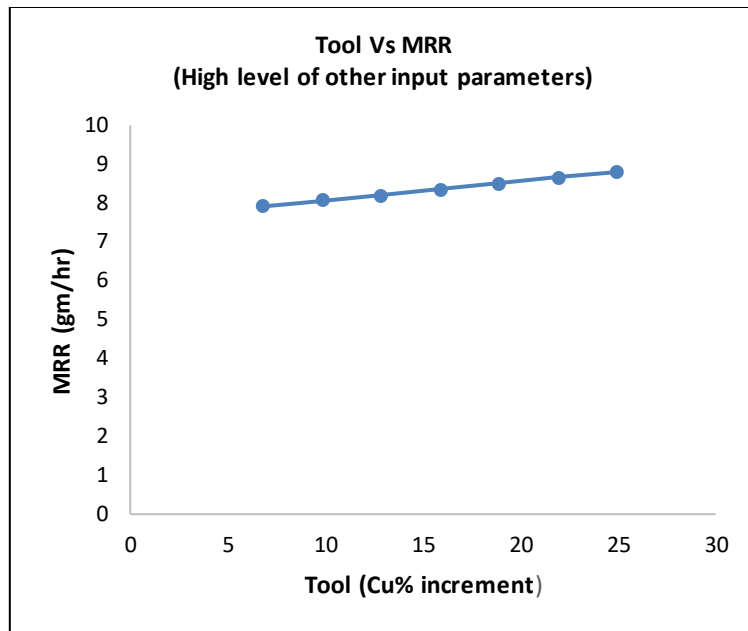
Regression coefficients	EDM oil	Used gear oil	Used vegetable oil
constant	-1.89	1.93	3.46
<b>T<sub>on</sub></b>	0.00408	0.00326	0.00202
<b>T<sub>off</sub></b>	0.0015	-0.00438	-0.00747
<b>I</b>	0.105	0.0648	0.1056
<b>V</b>	0.0099	-0.0567	0.0267
<b>T<sub>ool</sub></b>	0.0487	0.0942	-0.0639

**TABLE 3**  
**CALCULATED MRR FOR EDM OIL, USED GEAR OIL AND USED VEGETABLE OIL**

S No	Ton	Toff	I	V	Tool	MRR gm/hr		
						EDM oil	Used gear oil	Used vegetable oil
1	250	100	10	30	T1	2.82	1.56	4.32
2	250	200	20	40	T2	1.02	3.84	5.4
3	250	300	30	50	T3	3.6	2.1	4.32
4	250	400	40	60	T4	7.32	2.82	5.16
5	500	100	20	50	T4	4.92	3.36	5.28
6	500	200	10	60	T3	2.46	2.64	3.96
7	500	300	40	30	T2	6.12	3.24	7.32
8	500	400	30	40	T1	3.84	3.3	4.68
9	750	100	30	60	T2	5.34	2.4	10.26
10	750	200	40	50	T1	5.52	2.82	7.44
11	750	300	10	40	T4	2.46	2.82	2.82
12	750	400	20	30	T3	5.04	3.48	4.86
13	1000	100	40	40	T3	8.4	9	9.36
14	1000	200	30	30	T4	7.2	7.14	4.68
15	1000	300	20	60	T1	5.7	2.64	5.4
16	1000	400	10	50	T2	6.72	2.76	5.1

**4.1 Experimentation with EDM oil:**

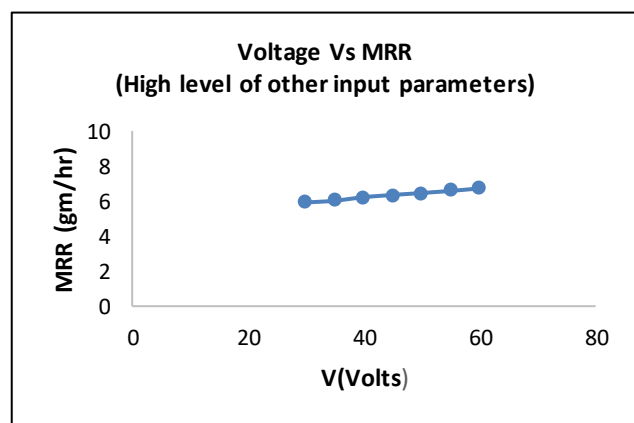
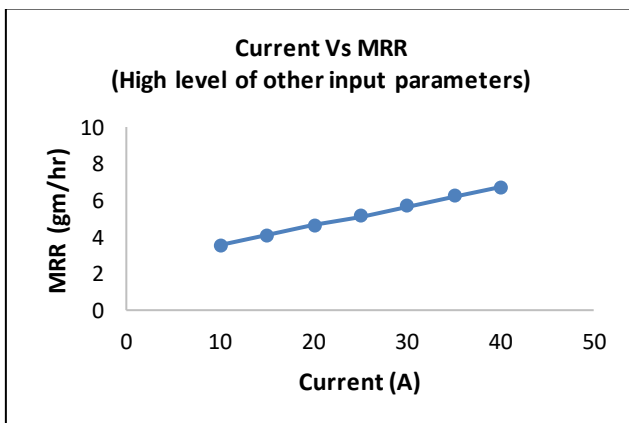
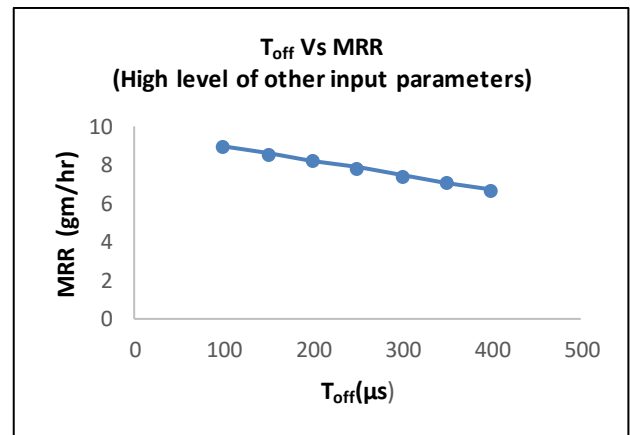
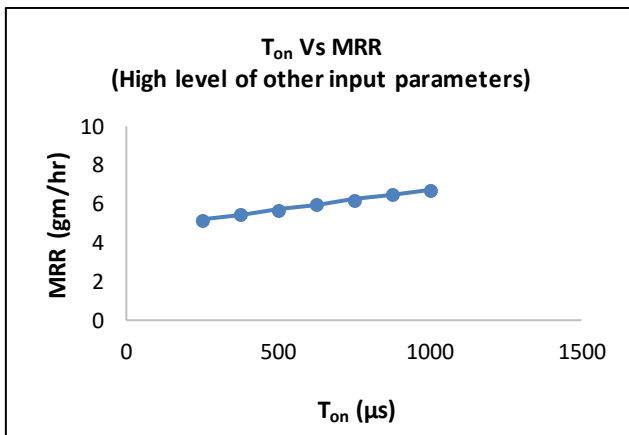


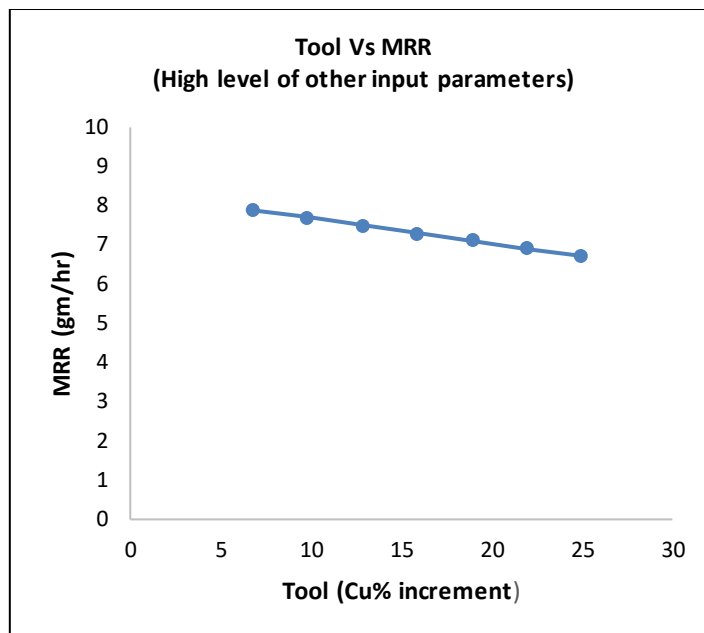


**FIGURE 5: Response behavior of MRR (EDM oil as dielectric)**

Under the impact of the chosen control settings, the response behavior of MRR was recorded and is depicted in the figure 5. A higher MRR is necessary in order to produce more economically. It's a crucial variable in this process economy. We can infer from the figure that the MRR falls with pulse-off time but rises with pulse-on time and current. voltage doesn't have much impact on MRR. It is noticed that MRR is rising with increasing percentage of Cu in the Al2021 tool.

**4.2 Experimentation with used vegetable oil:**

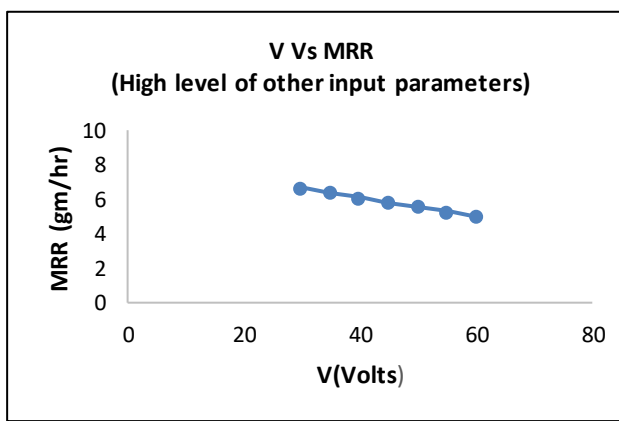
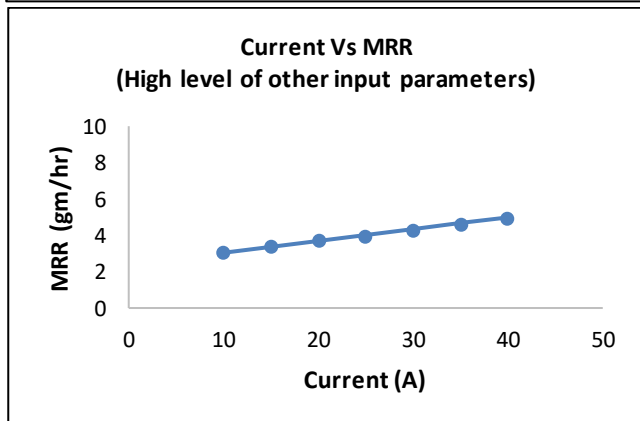
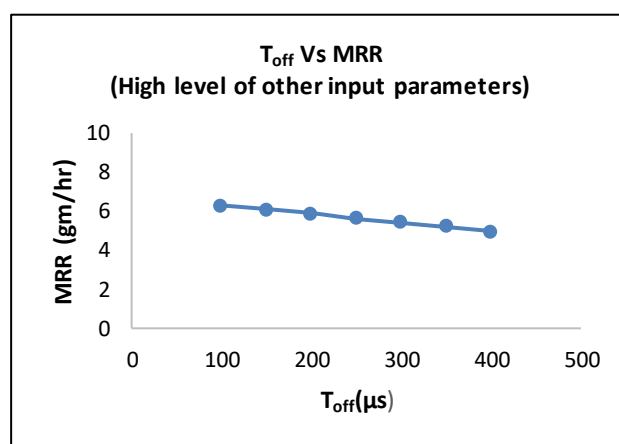
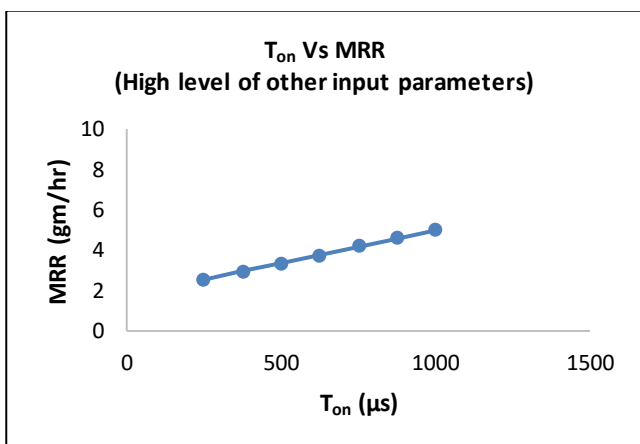




**FIGURE 6: Response behavior of MRR (used vegetable oil as dielectric)**

Figure 6 illustrates how response variable MRR is impacted by process factors. The MRR is found to increase linearly as current and voltage rise, and the energy applied used by pulse-on-time directly relates to the removal of metal. More metal from the workpiece will melt away with a longer pulse length. The elimination of metal is inversely correlated with the pulse-off-time and increase in cu percentage in Al2021 tool.

**4.3 Experimentation with used gear oil:**



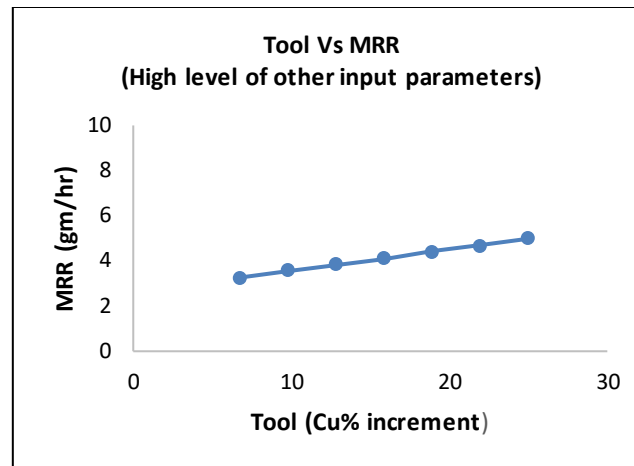


**FIGURE 7: Response behavior of MRR (used gear oil as dielectric)**

The impact of process factors on MRR is depicted in Figure 7. It has been found that when pulse-on time and current increase, the metal removal rate rises linearly. More metal melts when the pulse-on-time is raised because the same heating temperature is applied for more time. It is evident from the figure that voltage and pulse off time have negative bearing on MRR. Tool T4 exhibits the highest rate of metal removal with 25% weight copper.

## V. CONCLUSIONS

The trials were conducted using the Taguchi methodology's design matrix. The work completed leads to the following findings.

- When testing with EDM oil as the dielectric, the highest metal removal rate of 8.4 gm/hr was achieved for input values Ton 1000, Toff 100, I 40, V 40, and T3 tool.
- Maximum metal removal rate of 10.26 gm/hr was obtained for input values Ton 750, Toff 100, I 30, V 60 and T2 tool when experimentation was conducted with used vegetable oil as dielectric.
- When testing with used gear oil as the dielectric, highest metal removal rate of 9 gm/hr was achieved for input values Ton 1000, Toff 100, I 40, V 40, and T3 tool.
- According to the aforementioned observation, used vegetable oil utilized as a dielectric resulted in a maximum metal removal rate of 10.26 grams per hour.

## REFERENCES

- [1] G. S. Prihandana, M. Mahardika, M. Hamdi, Y. S. Wong, and K. Mitsui, "Accuracy improvement in nanographite powder-suspended dielectric fluid for micro-electrical discharge machining processes," *Int. J. Adv. Manuf. Technol.*, Volume: 56, no. 1–4, pp. 143–149, doi: 10.1007/s00170-011-3152-6. (2011)
- [2] Sandeep Kumar S. Dhanabalan, "Influence on machinability and form tolerance of Inconel 718 in EDM using different diameter multi hole Cu electrodes" *SN Applied Sciences* 1-396 48 (2019)
- [3] Vishal Kumar Jaiswal Amitesh Paul, Vikas Yadav Vijay Singh Literature "Review on Electrical Discharge Machining (EDM)" *IJSRD - International Journal for Scientific Research & Development* Vol. 6, Issue 05, 2018
- [4] Somu C.1 and Ranjith R. "Electric Discharge Machining of Inconel 718 Under a Distinct Dielectric Medium" *ECS Journal of Solid State Science and Technology*, Volume 11, Number 5, 2022
- [5] Rajesh S., Patnaik P.K., Sharma A.K., Kumar P., "Surface integrity evaluation of electro discharge machined Inconel 718", *Proceedings of the 3rd International 24th AIMTDR Conference*, pp. 259-264, 2010.
- [6] Bharti P.S., Maheshwari S., Sharma C., "Experimental investigation of Inconel 718 during die-sinking electric discharge machining", *International Journal of Engineering Science and Technology*, Vol. 2(11), pp. 6464-6473, 2010.
- [7] Shirsendu Das, Swarup Paul, Biswanath Doloib, "Feasibility assessment of some alternative dielectric mediums for sustainable electrical discharge machining: a review work", *Journal of the Brazilian Society of Mechanical Sciences and Engineering* (2020)
- [8] Shirsendu Dasa, Swarup Paula, Biswanath Doloib, "An experimental and computational study on the feasibility of bio-dielectrics for sustainable electrical discharge machining", *Journal of Manufacturing Processes* Volume: 41, pp 284–296 (2019)
- [9] Harlal Singh Mali and Nitesh Kumar, "Investigating Feasibility of Waste Vegetable Oil for Sustainable EDM", *Proceedings of 6th International & 27th All India Manufacturing Technology, Design and Research Conference (AIMTDR-2016) College of Engineering, Pune, Maharashtra, INDIA December 2018*



- [10] Rajesh Bajaj, Amit Rai Dixit, Arun Kumar Tiwari, "Machining performance enhancement of powder mixed electric discharge machining using Green dielectric fluid, Journal of the Brazilian Society of Mechanical Sciences and Engineering 42:512, Page 2 of 20, (2020)
- [11] Singh, N.K. Singh, Y. Sharma, A. Singla, A. Negi, P. "An environmental- friendly electrical discharge machining using different sustainable techniques: a review". Adv. Mater. Process. Technol., (2020).
- [12] Umair Arif a Imtiaz Ali Khan b and Faisal Hasan "Green and sustainable electric discharge machining: a review" Advances in Materials and Processing Technologies (2022)
- [13] Mohsen Soori, Mohammed Asmael, "A Review of the Recent Development in Machining Parameter Optimization" Jordan Journal of Mechanical and Industrial Engineering Volume 16, Number 2, March. 2022 ISSN 1995-6665 Pages 205 – 223 (2022)
- [14] Rouniyar, A. K. & Shandilya, P. "Study on Powder Mixed Electrical Discharge Machining Process: A Review" DAAAM International Scientific Book pp. 123-142(2019)
- [15] Bharat Singh, "Influences of Powder mixed Dielectric Fluid on Machining Characteristics of EDM processed parts: A review" IOP Conf. Series: Materials Science and Engineering 1116 012099(2021)
- [16] R. Toshimitsu, A. Okada, R. Kitada, and Y. Okamoto "Improvement in Surface Characteristics by EDM with Chromium Powder Mixed Fluid," Procedia CIRP, vol. 42, no. Isem Xviii, pp. 231–235, (2016)
- [17] Singh H and Singh A, "Effect of Pulse on/Pulse Off Time on Machining of AISI D3 Die Steel Using Copper and Brass Electrode in EDM", International Journal of Engineering and Science, Vol. 1, No. 9, pp. 19-22(2012)
- [18] Rajesh Choudhary, Parlad Kumar and Jagdeep Singh, "Analysis of Electro Discharged Machined Surfaces of AISI D3 Steel by Composite Tool Electrode", International Journal of Surface Engineering & Materials Technology, Vol. 2 No. 2, 2012.

# Solving the Node-Weighted Steiner Tree Problem using Reinforcement Learning

Zongbo Yang

Department of Big Data Statistics, Guizhou University of Finance and Economics, Guizhou

Received: 09 August 2024/ Revised: 16 August 2024/ Accepted: 20 August 2024/ Published: 31-08-2024

Copyright @ 2024 International Journal of Engineering Research and Science

This is an Open-Access article distributed under the terms of the Creative Commons Attribution Non-Commercial License (<https://creativecommons.org/licenses/by-nc/4.0>) which permits unrestricted Non-commercial use, distribution, and reproduction in any medium, provided the original work is properly cited.

**Abstract**—The node-weighted Steiner tree problem is a significant issue in network design, with broad applications including telecommunications network construction, offshore oilfield development planning, and wireless ad-hoc networks. The objective of the node-weighted Steiner tree problem is to find a subtree within a given undirected graph that has the minimum total weight and includes all specified terminals. This problem is NP-hard, typically requiring complex algorithm design and exponential time. We have combined graph neural networks and deep reinforcement learning techniques to propose a new solution method. By encoding the structural information of the graph into vector form through graph neural networks and self-attention networks, and optimizing decisions using a reinforcement learning strategy network, we efficiently construct the desired node-weighted Steiner tree. To validate the model's effectiveness, we conducted extensive experiments on various types and sizes of generated graphs, covering different numbers of endpoints. The results show that in scale-free networks (BA), our algorithm performs equivalently to SCIP, with both achieving a Gap value of 0. In small-world networks (WS) and complete graphs (K), our algorithm closely matches SCIP's performance, with the highest Gap values being 0.3% and 1.76%, respectively, indicating that our algorithm can closely approximate SCIP's performance in handling these network structures. In random graphs (ER) and random regular graphs (RR), while there is a performance discrepancy between our algorithm and SCIP, the maximum gap does not exceed 5.76%. These findings demonstrate that our algorithm performs well in solving the node-weighted Steiner tree problem.

**Keywords**—Node-Weighted Steiner Tree; Reinforcement Learning; Graph Neural Networks; Combinatorial Optimization.

## I. INTRODUCTION

Network design problems are prevalent across various practical applications, with the Node-Weighted Steiner Tree Problem (NWSTP) being a particularly significant one. The NWSTP was first introduced by Segev A<sup>[1]</sup> in 1987 and has found extensive applications in real-world scenarios. For example, in logistics and transportation, companies can use NWSTP to optimize delivery routes by identifying the most efficient transfer points and routing paths, thereby reducing transportation time and costs. In offshore oil field development<sup>[2]</sup>, the problem can be modeled where edges represent pipelines and nodes represent potential platform locations. Here, the rewards indicate the net difference between expected revenue from a site and the construction cost, while edge costs represent installation and maintenance expenses. In the field of network communications<sup>[3]</sup>, multicast communication often employs tree structures known as multicast trees. When modeling a network as a graph, a multicast tree can be seen as a node-weighted Steiner tree. In this model, the multicast sender and receivers correspond to the endpoints of the Steiner tree, while other nodes involved in constructing the tree are referred to as Steiner nodes. These diverse applications underscore the importance of the NWSTP in optimizing complex networks and resources, highlighting the need for effective solutions and advancements in algorithmic strategies.

The definition of the Node Weighted Steiner Tree Problem (NWSTP) is as follows: In an undirected graph  $G = (V, E, \omega)$ , each node  $v \in V$  and each edge  $e \in E$  are assigned a non-negative weight  $\omega(v)$  and  $\omega(e)$ , respectively. Given a graph  $G$  and a set of terminal nodes  $T$ , where  $T \subseteq V$ , the task is to find a subtree  $G'$  with the minimum total weight such that  $G'$  includes all the terminal nodes in  $T$ ,  $T \in G'$ . The formula representation is as follows:

$$C(S, G)_{min} = \sum_{e \in E_S} \omega(e) + \sum_{v \in S} \omega(v) \quad (1)$$

Where  $S$  represents the set of nodes used to construct the Node Weighted Steiner Tree.

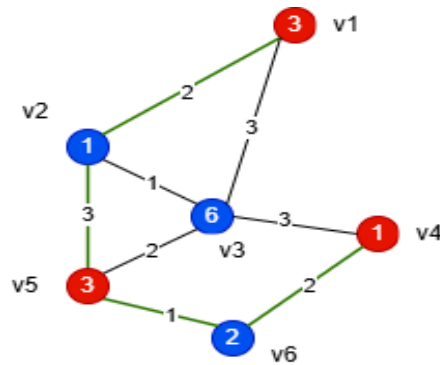


**FIGURE 1: Node weighted Steiner Tree**

The optimal solution diagram for the Node Weighted Steiner Tree, with endpoints represented by red nodes, and the optimal solution connected by green edges, connecting nodes  $\{v1, v2, v5, v6, v4\}$  with a total weight of  $1+2+2+1+3+3+1+2+3 = 18$ , where  $\{v2, v6\}$  are Steiner points.

In recent years, numerous algorithms have been proposed to solve the Node Weighted Steiner Tree Problem (NWSTP). For instance, Y Sun and S Halgamuge<sup>[4]</sup> introduced a Physarum-inspired heuristic algorithm for solving NWSTP; S Angelopoulos<sup>[5]</sup> proposed an approximation algorithm with a ratio of  $o(\min\{\log \alpha, \log k\})$ , where  $\alpha$  is the ratio of the maximum to minimum node weights, and  $k$  is the number of terminals; E D Demaine<sup>[6]</sup> developed an approximation algorithm with a ratio of 3; T Erlebach and A Shahnaz<sup>[3]</sup> offered an approximation algorithm with a ratio of  $0.775d$ , where  $d$  is the maximum degree; A Buchanan et al.<sup>[7]</sup> extended the Steiner tree algorithm by Dreyfus and Wagner<sup>[8]</sup>, proposing an exact algorithm with a provably worst-case runtime of  $O(n^3)$  in instances with a finite number of terminals and  $n$  nodes; R Cordone and M Trubia<sup>[2]</sup> suggested an exact algorithm, however, their experiments did not involve graphs with degrees greater than 2. Despite the progress made by existing methods, they have limitations in dealing with highly complex graphs, providing approximate solutions only under specific conditions, and longer computational times. With the advancement of graph neural networks and reinforcement learning technologies, new solution strategies have emerged. This paper will explore an efficient and precise method to solve the NWSTP by leveraging the strengths of these two technologies, aiming to break through the limitations of traditional algorithms.

## II. DEEP REINFORCEMENT LEARNING

Due to the NP-hard nature of the Node Weighted Steiner Tree Problem (NWSTP) and the challenges in obtaining accurate node labels, we have chosen to employ the Actor-Critic algorithm from deep reinforcement learning<sup>[9]</sup> to address the NWSTP. In this algorithm, the agent's decision-making for the next step does not depend on information about future actions because all necessary information is already contained in the current state, which is directly determined by previous actions. In reinforcement learning, the Actor-Critic algorithm features two key roles: the Actor selects actions based on the current state, while the Critic evaluates these actions and provides feedback to optimize the choices. This cooperative mechanism is central to many successful reinforcement learning algorithms and enables the agent to continuously make wise decisions and improve performance.

When addressing the NWSTP, we treat it as a sequential decision-making problem, starting from a node and incrementally building the tree with the minimum weight sum while ensuring all specified endpoints are included. To handle different types and sizes of graphs, we define six core elements: state space, state transitions, action space, rewards, policies, and termination conditions.

**State Space:** At time  $t$ , the state is a tensor describing the current environment, including the graph  $G$ , the partial solution set  $S$ , the set of unadded endpoints, and node features. When an endpoint is added to the solution set, the related node features change, and each addition of a node updates the state, collectively forming the state space.

**Action Space:** At time  $t$ , the actions that the agent can execute are the set of candidate nodes at that moment. Candidate nodes are required to connect with nodes in the partial solution set and not be part of it, ensuring the tree structure does not form a cycle. The action space at the initial moment  $t = 0$  is set as the endpoint set  $T$ , thus defining the action space representation at time  $t$  as:

$$A_t = \begin{cases} \{v \in T | T \in V\}, & \text{if } t = 0 \\ \{v | v \notin S \wedge \exists u \in S : (u, v) \in E\}, & \text{otherwise} \end{cases} \tag{2}$$

**State Transitions:** The state transitions for the NWSTP on the graph are deterministic, without any probabilistic elements. When a node  $v$  is added to the partial solution  $S$ , the state changes accordingly.

**Rewards:** The reward mechanism in our model is designed based on the current state and actions taken, aiming to guide the agent toward finding the path with all endpoints included and the minimum weight. When a new node  $v$  is added to the partial solution set  $S$ , moving the state from  $s_t$  to  $s_{t+1}$ , rewards are calculated based on the type of node  $v$  (endpoint or non-endpoint) considering, the reward function  $r(S, v)$  considers two main factors: (1) The change in the cost function  $C(S, G)$ , which measures the overall path cost after adding the new node  $v$ ; (2) The path weights from node  $v$  to other endpoints, reflecting the cost from the current node to reach endpoints. The design aims to incentivize the model to achieve the minimum weight tree, with the specific reward function as follows:

$$R(s, v) = \begin{cases} C(S', G) - C(S, G) + |x_v| + N, & v \in T \\ C(S', G) - C(S, G) + |x_v| + N + c, & v \notin T \end{cases} \tag{3}$$

Where  $S'$  represents the partial solution set after adding node  $v$ ,  $|x_v|$  is the sum of distances from the node to the endpoints,  $N$  is the weight of the currently added node, and  $c$  is a constant.

**Policy:**  $a_t \sim \text{Categorical } \pi_\theta(v|s; \theta)$ , where the policy network computes the probability distribution of actions given the state  $S$ ,  $\pi_\theta(v|s; \theta)$ , and  $\theta$  represents the network parameters. Subsequently, actions are sampled from the discrete categories based on the probability distribution. This method of action selection balances exploration and exploitation during training. Traditional greedy algorithms tend to get stuck in local optima, while the sampling method based on probability distribution introduces randomness, allowing the policy network to explore the state space more effectively. Introducing randomness permits the policy to attempt various possible action paths at different training stages, thereby increasing the likelihood of finding the global optimal solution.

**Termination Condition:** The process terminates when all endpoints are added to the solution set  $S$ ,  $T \in S$ .

### III. MODEL

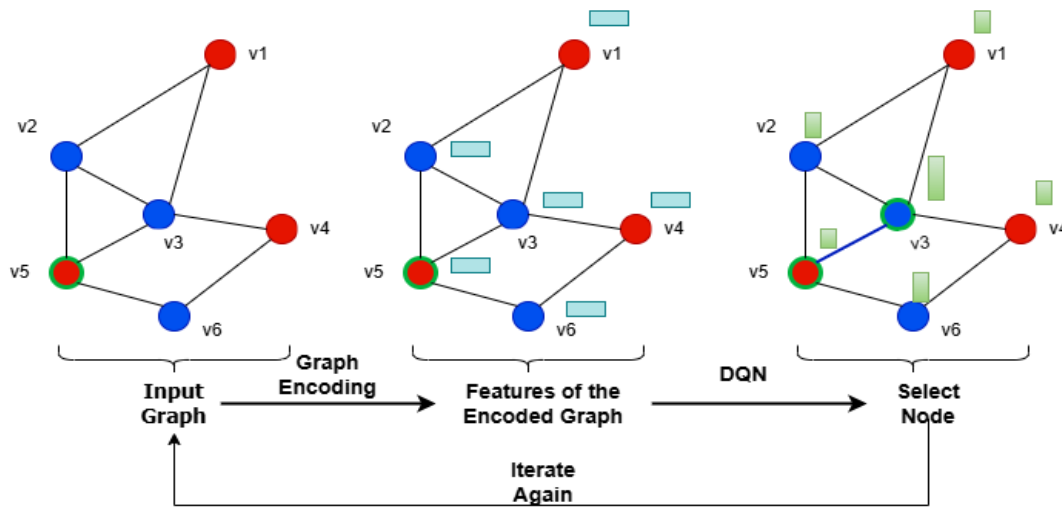


FIGURE 2: MODEL DIAGRAM

#### 3.1 Model overview:

Figure 2 provides an overview of the model. Initially, a graph is input where endpoints are represented by red nodes. Subsequently, the graph's information, the partial solution set, and predefined node feature information are fed into the model. The model employs a novel graph encoding method to compactly encode the input information into node state tensors (as shown by the colored bars next to the nodes in the diagram). The encoded tensor is then input into a DQN, which outputs scores for candidate nodes, represented by green bars. The height of the bar indicates the node's score, with higher bars representing higher scores. Finally, the model incrementally adds the highest-scoring nodes according to a greedy strategy to construct the solution set. The specific construction process is shown in Algorithm 1.

**Algorithm 1**

**Input:** In the graph  $G$ , a random initial node  $v_0 \in T$ .

$S = \{v_0\}$ ,  $V(G, t) = S$

**While**  $T \notin S$  **do** :

    Obtain the action space  $A_t$ .

$a_t \in A_t$ :  $a_t \sim \text{Categorical}(\pi(v|s; \theta))$ , Select an action  $a_t$ .

$S = S + a$

**end while**

**return**  $S$

**3.2 Node feature construction:**

Node features have a direct impact on model performance. Therefore, we constructed 20 initial features for each node in the graph. The specific features are detailed in Table 1.

**TABLE 1**  
**FEATURES**

index	feature description
0	Whether it is in the partial solution: 1 if the node is in the solution, otherwise 0.
1	Whether it is an endpoint: 1 if the node is an endpoint, otherwise 0.
2	Node weight.
3	Edge weight of the node.
4	PageRank: Reflects the importance of the node in the graph based on connection quality and structure.
5	Degree centrality: The number of direct connections of the node.
6	Clustering coefficient: Measures the density of connections between the node's neighbors.
7	Closeness centrality: The reciprocal of the average distance from the node to all other nodes.
8	Betweenness centrality: The number of shortest paths passing through the node.
9	Eigenvector centrality: The influence of the node in the graph.
10	Distance to the nearest endpoint.
11	Distance to the second closest endpoint.
12	Distance to the third closest endpoint.
13	Minimum weight of neighboring nodes.
14	Second smallest weight of neighboring nodes.
15	Edge weight to neighbor node 1.
16	Edge weight to neighbor node 2.
17	Edge weight to neighbor node 3.
18	Weight of second-order neighbor node 1.
19	Weight of second-order neighbor node 2.
20	Weight of second-order neighbor node 3.

We constructed features for each node, including commonly used graph theory metrics such as degree centrality, PageRank, and clustering coefficient. When solving the NWSTP problem, we particularly focus on the shortest distance from the nodes to the endpoints. These distances are represented in the matrix  $X \in R^{|V| \times |T|}$ , where  $V$  denotes the number of nodes  $v$ , and  $T$  denotes the number of endpoints  $T$ . To maintain consistent matrix dimensions and to eliminate the influence of endpoints that are too far away from the nodes, we set  $T$  in  $X \in R^{|V| \times |T|}$  to a constant parameter  $k$ . Since constructing the tree is a Markov decision process, once an endpoint is added to the partial solution set, it loses its value. Therefore,  $k$  refers to those endpoints that have not been added to the partial solution set. When the number of unadded endpoints is less than  $k$ , we pad with zeros. Experimental analysis shows that the model performs best when  $k = 3$ .

Next, we considered the edge weights of nodes and their first-order neighbors, as these weights are crucial for constructing the solution set. Therefore, we selected the three neighbors with the smallest weights and their edge weights as features, padding

with zeros if there were fewer than three. Additionally, to enhance the model's ability to capture longer path information, we introduced the weights of each node's second-order neighbors. Specifically, we chose the weights of the three second-order neighbors with the smallest weights as features.

Finally, the topology of the subgraph formed by the partial solution set influences the selection of the next node. To enable the model to recognize this structure, we encoded the subgraph information into feature tensors. By integrating the graph tensor and subgraph tensor through a fully connected neural network, we extracted more comprehensive information about the graph.

### 3.3 Encoding and decoding:

Due to the STP problem involving unstructured data, the probability of selecting candidate nodes is influenced by multiple factors, including the graph's structure, the positions of the terminals, and their weights. Our goal is for the network to accurately understand the current state at any given time and calculate the selection probability for each candidate node. To achieve this, we designed an encoding-decoding architecture aimed at effectively handling these complex factors. This architecture is mainly divided into two parts: the encoder and the decoder.

**Encoder:** The encoder is responsible for converting the current state information into a representation suitable for processing by a machine learning model. Its role is to transform the graph structure, terminal positions, and other relevant information into tensors. The encoder's input consists of the graph, the partial solution set, and features, and its output is a state tensor that contains all the key information of the current state.

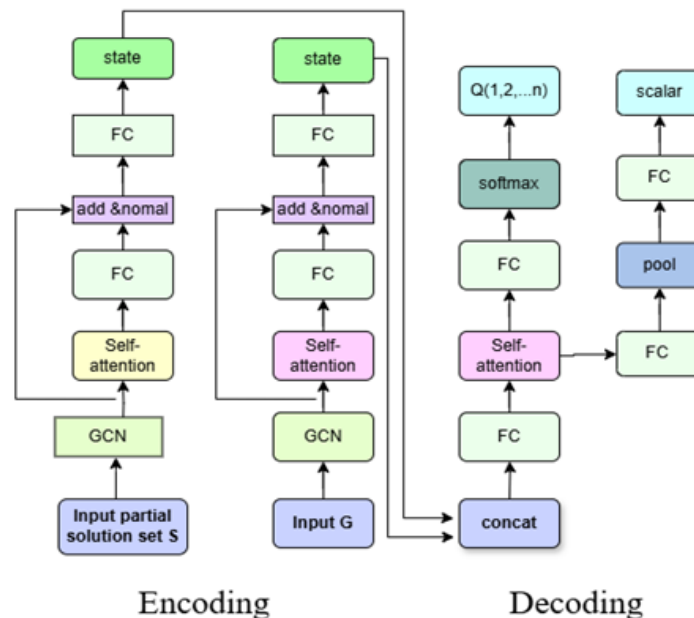


FIGURE 2: Encoding-Decoding architecture diagram

**Decoder:** The task of the decoder is to learn and understand the state vector generated by the encoder, in order to predict the selection probability and reward for each candidate node. It receives the state tensor provided by the encoder as input and outputs the selection probability and reward for each candidate node.

The encoder-decoder architecture enables deep reinforcement learning models to effectively utilize the complex structures and multiple influencing factors in graph-structured data, thereby enhancing the accuracy and efficiency of solving the node-weighted Steiner tree problem. This approach is not only applicable to addressing the node-weighted Steiner tree problem but also provides a methodology for solving other combinatorial optimization problems.

#### 3.3.1 Encoding process:

Our model takes a graph's feature matrix  $X$  and adjacency matrix  $A$  as inputs. Initially, we utilize a Graph Convolutional Network (GCN) to propagate features, with the layer-to-layer propagation rule defined as follows:

$$H^{(l+1)} = \sigma \left( \tilde{D}^{-\frac{1}{2}} \tilde{A} \tilde{D}^{-\frac{1}{2}} H^{(l)} W^{(l)} \right) \quad (4)$$

where  $H^{(l)}$  is the feature matrix at layer  $l$ ;  $H^{(0)} = X$ ;  $\tilde{A} = A + I$  is the adjacency matrix (including self-connections);  $\tilde{D} = \text{diag}(\sum_j \tilde{A}_{ij})$  is the degree matrix;  $W^{(l)}$  is the weight matrix learned by the convolution layer;  $\sigma$  represents the activation function.

To enhance the nonlinear transfer capability, several fully connected layers (FC) are added after the convolution to more effectively learn the graph's feature embeddings.

$$H^{(l+1)} = H^{(l)} W + b \tag{5}$$

where  $W$  is the weight matrix of the linear layer,  $b$  is the bias vector, and  $H^{(l)}$  is the feature matrix output from the convolution layer.

To better capture the complex relationships between nodes and their neighbors, we employ a multi-layer, multi-head attention network. In this network, we take the output of the previous layer  $X = H^{(l)}$  as input, and process it through multiple attention heads, each with its own query, key, and value matrices  $W_{Q_i}, W_{K_i}, W_{V_i}$ . For the input features  $X$ , where  $X$  is the output from the previous layer, the attention computation for each head is as follows:

$$Z^i = \text{softmax}\left(\frac{Q^i(K^i)^T}{\sqrt{d_k}}\right)V^i \tag{6}$$

where  $Q^i = XW_{Q_i}$ ,  $K^i = XW_{K_i}$ ,  $V^i = XW_{V_i}$ , and  $d_k$  represents the dimension of the key. Next, we concatenate the outputs from all heads and then apply a linear transformation to obtain the final multi-head attention output:

$$H^{(l)} = \text{Concat}(Z^1, Z^2, \dots, Z^h)W \tag{7}$$

To address the problems of vanishing and exploding gradients in deep neural networks, we introduce residual connection technology. The residual connection formula is as follows:

$$y = F(X, W) + X \tag{8}$$

where  $F(X, W)$  represents the features computed through several layers, and  $X$  is the input feature.

To enhance the stability and training efficiency of the model, we use layer normalization. The layer normalization process includes calculating the mean and variance of the input features, normalizing the input, and finally scaling and shifting:

$$\hat{x} = \frac{x - \mu_L}{\sqrt{\sigma_L^2 + \epsilon}} \tag{9}$$

$$y = \gamma \hat{x} + \beta \tag{10}$$

where  $\mu_L$  and  $\sigma_L^2$  are the mean and variance of the input features,  $\epsilon$  is a small constant to prevent division by zero, and  $\gamma$  and  $\beta$  are learnable parameters.

### 3.3.2 Decoder process

Our decoding section employs two network structures and shares some parameters between them. This design aims to improve computational efficiency by reducing the number of model parameters and to lower the risk of overfitting when handling similar tasks or inputs. The specific structure is shown as Figure 4.

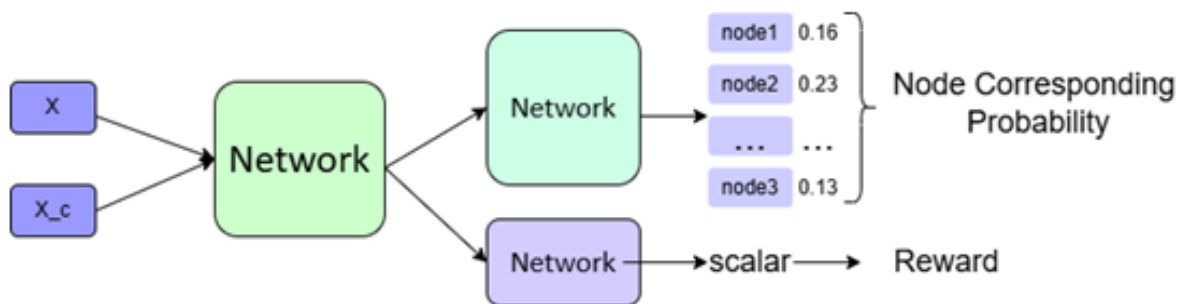


FIGURE 3: Structure of shared parameters in the decoding network

First, we input the graph  $G$  and its adjacency matrix  $A$ , along with the graph  $G_c$  composed of partial solution sets and its corresponding adjacency matrix  $A_c$  into the decoder, thus obtaining the encoded feature representations  $X$  and  $X_c$ .

Next, we combine the feature information of graph  $G$  and graph  $G_c$  to obtain the current state information of the graph:

$$X = \text{Concat}(X, \text{tile}(\text{mean}(X_c, \text{axis} = 0), (N, D))) \quad (11)$$

where  $N$  is the number of nodes,  $D$  is the dimension of features,  $\text{Concat}$  represents concatenation, and  $\text{tile}$  indicates replicating the feature  $N$  times, resulting in  $\in R^{N \times 2D}$ .

Subsequently,  $X$  is passed through a fully connected layer and a multi-head self-attention layer to further extract features, concluding the sharing of network parameters.

Following this, the feature matrix obtained from the previous step undergoes various processes to produce different outputs. First, it outputs the probability of a node being selected:

$$Q(S, \theta) = \text{softmax}(X \cdot W + b) \quad (12)$$

Next, it outputs the predicted expected reward:

$$R_{\text{total}} = \text{sum}(\text{Pool}(X \cdot W_1 + b_1) \cdot W_2 + b_2) \quad (13)$$

Where  $\text{Pool}$  represents average pooling.

### 3.4 Strategy optimization:

After sampling  $N$  node-weighted Steiner trees using strategy  $\pi_\theta$ , we obtained  $N$  sets of trajectories:

$$\{P_t, R_{t-1}, r_t, m_t\}_{t=0}^{\sum_0^n T_n} \quad (14)$$

where  $T_n$  is the final time step of the  $n$ th trajectory,  $R_t$  is the expected reward at time  $t$ ,  $r_t$  is the actual reward received after executing an action at time  $t$ , and  $m_t$  indicates whether a solution set has been found at time  $t$ , if found,  $m_t = 0$ ; otherwise,  $m_t = 1$ .

The gradient of the average reward  $J(\theta)$  can be approximated using the policy gradient theorem:

$$\nabla J(\theta) = \sum_{t=0}^{\sum_0^n T_n} (r_t + m_t * R_t - R_{t-1}) * P_t \quad (15)$$

We use the Adam optimizer, and the training process is detailed in Algorithm 2.

#### Algorithm 2

```

For _ in 1 to N do:
  Initialize three empty lists
  e_n = [], Record the logarithm of the probability of choosing each action, log p_t
  rewards = [], Record the rewards obtained from executing each action
  mask = [], Record whether a Steiner tree is completed, with the mask for the last action set to 0 and the rest set to 1.
  For episode in range (batch, batch + N):
    Read graph G, randomly initialize node v_0 ∈ T and construct subgraph
    V(G_t) = S
    While T ∉ S do:
      Obtain the action space A_t
      a_t ∈ A_t: a_t ~ Categorical π(v|s; θ), Select a node and record the output R of the evaluation network.
      Execute action a_t, record the actual reward r_t, and the probability p_t of choosing action a_t.
      Record the expected reward V^θ(s_t) output by the network
    s = s + a
  end while
end for
batch += N, N as a parameter
Loss = ∑_{t=0}^{\sum_0^n T_n} (r_t + m_t * V^θ(s_t) - V^θ(s_{t-1})) * P_t
θ ← Amda(θ, ∇_{Loss})
end for

```



## IV. EXPERIMENT AND ANALYSIS

### 4.1 Dataset:

In evaluating our model, we used a variety of graph generation rules, including Random Regular graphs (RR)<sup>[11]</sup>, Erdős-Rényi graphs (ER)<sup>[12]</sup>, small-world networks (WS)<sup>[13]</sup>, scale-free networks (BA)<sup>Error! Reference source not found.</sup>, and complete graphs (K). For each generation rule, we generated instances with a node count of  $n$ . These generation rules are widely applied in solving various graph combinatorial optimization problems, such as Minimum Vertex Cover (MVC) and Maximum Cut (MAXCUT). For the Node Weighted Steiner Tree problem, the number and positions of terminals in the graph significantly influence the instances; thus, we introduced a parameter  $m$ , representing the probability of each vertex becoming a terminal. We set  $m$  values at 0.3, 0.6, and 0.9, and node counts  $n$  at 20, 30, 40, and 50. By varying  $m$  and  $n$ , we generated different instances to increase the complexity of the generated graph instances. Lastly, we randomly assigned a weight between 1 and 3 to each edge and node in the graph. Through this method, we were able to generate test instances of certain complexity, effectively evaluating the performance of the model, as shown in Table 2.

TABLE 2  
EXPERIMENTAL DATA

Type of Graph	Number of Nodes	Node Weight Range	Edge Weight Range	Terminal Ratio
RR/WS/BA/ER/K	20	1,3	1,3	0.3, 0.6, 0.9
	30	1,3	1,3	0.3, 0.6, 0.9
	40	1,3	1,3	0.3, 0.6, 0.9
	50	1,3	1,3	0.3, 0.6, 0.9

### 4.2 Comparison methods:

SCIP-Jack<sup>[10]</sup> is a software package designed for the classic Steiner tree problem in graphs. It is also capable of solving fourteen related Steiner tree problems, such as prize-collecting Steiner trees, node-weighted Steiner tree problems, etc. Currently, SCIP-Jack is the optimal solver for the Node-Weighted Steiner Tree Problem.

### 4.3 Parameter settings:

During the graph embedding phase, we extract features using three layers of Graph Convolutional Networks (GCN), one fully connected neural network layer, and one multi-head self-attention network layer (with eight heads). In the subgraph embedding phase, feature extraction is performed using two layers of GCN, one fully connected neural network layer, and one multi-head self-attention network. Subsequently, the features from these two phases are merged and further processed through one convolutional layer and two fully connected network layers to enhance feature expression. To improve the model's nonlinearity, we have chosen the hyperbolic tangent function ( $\tanh$ ) as the activation function.

Considering the limitations of computational resources, we trained graphs with a node count ranging from 20 to 50, totaling 20,000 graphs. The experimental settings include: a random seed set to 42 to ensure reproducibility; a decay factor  $\gamma$  set at 0.99, used to regulate the learning rate; parameter  $N$  set at 5, and parameter  $C$  set at 2. The model optimization is managed by the Adam optimizer, with an initial learning rate  $\eta$  of 0.01, which is gradually reduced to 0.00001, implementing a progressively decaying learning rate strategy.

### 4.4 Comparison of Experimental Results:

In the experiment, we evaluated the gap between the model proposed in this paper and SCIP-Jack. To eliminate random errors, we tested 100 instances for each type of graph generated. We used the formula  $\text{Gap} = (\text{RL}/\text{obj} - 1) \times 100\%$  to determine the gap, where  $RL$  is the result calculated by our algorithm, and  $\text{obj}$  represents the result calculated by the *SCIP* algorithm. We calculated the mean of these instance results as the outcome to measure the performance of each algorithm.

**TABLE 3**  
**EXPERIMENTAL RESULTS**

Number of Nodes	Terminal Ratio	RR_Gap	WS_Gap	BA_Gap	ER_Gap	K_Gap
20	0.3	2.47%	0.19%	0.00%	0.53%	0.99%
	0.6	2.50%	0.03%	0.00%	0.55%	1.47%
	0.9	3.90%	0.11%	0.00%	3.13%	1.72%
30	0.3	2.74%	0.26%	0.00%	1.51%	1.17%
	0.6	4.07%	0.04%	0.00%	2.51%	1.76%
	0.9	4.94%	0.20%	0.00%	4.20%	1.71%
40	0.3	3.22%	0.07%	0.00%	2.55%	1.51%
	0.6	5.18%	0.02%	0.00%	4.12%	1.76%
	0.9	4.56%	0.01%	0.00%	5.76%	1.47%
50	0.3	3.62%	0.03%	0.00%	3.81%	1.75%
	0.6	5.71%	0.01%	0.00%	5.62%	1.62%
	0.9	4.62%	0.34%	0.00%	0.83%	0.99%

The experimental results from Table 3 show that our algorithm performs on par with SCIP in solving scale-free network graphs (BA), with a Gap value consistently at 0. In small-world network graphs (WS), our algorithm generally performs better, with Gap values very low, the highest being only 0.3%, indicating that our algorithm closely approximates the performance of the SCIP algorithm in handling small-world networks. For random graphs (ER) and random regular graphs (RR), although our algorithm shows some difference from SCIP, the largest gap does not exceed 6%. In complete graphs (K), our algorithm's performance is close to SCIP, with the largest Gap value at 1.76%, which is not significant, and the Gap does not increase notably with more nodes. These comparisons indicate that our algorithm is effective in solving the Node Weighted Steiner Tree problem.

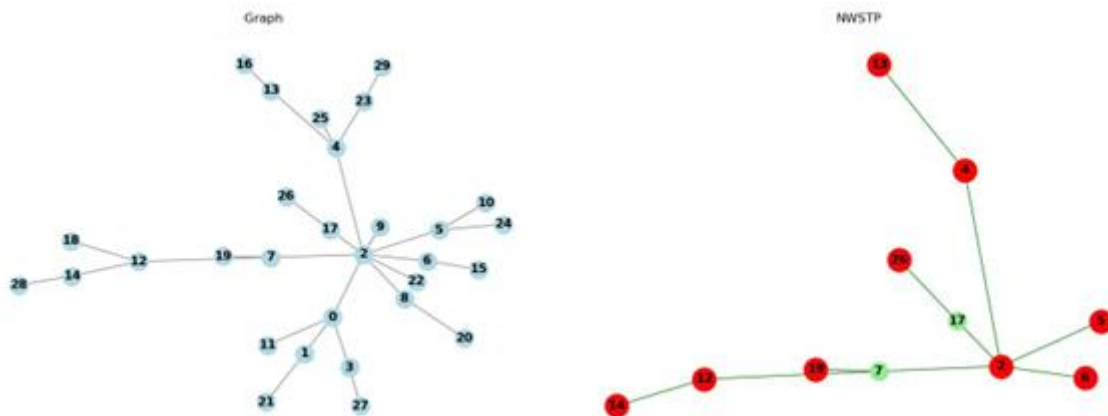


**FIGURE 4: Display of solution results in BA graphs**

Figure 5 demonstrates the solution of a scale-free Barabási–Albert (BA) network instance with 30 nodes where the terminal ratio is 0.3. In this figure, the red nodes are terminals, and the green nodes are Steiner points. This visualization helps in understanding how the algorithm identifies and utilizes Steiner points to effectively connect all the terminals in the most optimal manner.

## V. CONCLUSION

We have proposed an innovative solution method for the node-weighted Steiner tree problem by integrating graph neural networks and reinforcement learning techniques. Initially, we employ graph neural networks and multi-head self-attention networks to encode complex graph structure data into tensor representations, aimed at capturing the deep relationships between nodes in the graph. Subsequently, by combining reinforcement learning techniques, we optimize the decision-making process

through policy networks, progressively constructing node-weighted Steiner trees, thus achieving efficient solutions for the NWSTP.

To validate the effectiveness and robustness of our proposed method, we conducted experiments using five different types of generated graphs. These graphs not only include various types and sizes but also simulate different terminal count scenarios, ensuring the complexity and comprehensiveness of the experimental conditions. The results indicate that our algorithm has achieved satisfactory outcomes.

Looking ahead, although this research has already achieved certain results, there is still room for improvement in the scalability and universality of the algorithm. Future work may include: first, exploring more types of graph neural network architectures to adapt to more complex structural changes in graphs; second, optimizing reinforcement learning strategies to enhance the model's adaptability to different tasks; and third, applying the model to more practical scenarios such as social network analysis and bioinformatics to verify its practicality and effectiveness. Through ongoing research and improvement, we hope to achieve deeper breakthroughs in solving graph optimization problems.

#### ACKNOWLEDGEMENTS

we would like to extend special thanks to D. Rehfeldt, who provided the SCIP-Jack binary files, allowing us to compare our algorithm with SCIP-Jack.

#### REFERENCES

- [1] Segev A. The node-weighted Steiner tree problem[J]. *Networks*, 1987, 17(1): 1-17.
- [2] Cordone R, Trubian M. An exact algorithm for the node weighted Steiner tree problem[J]. *4OR*, 2006, 4: 124-144.
- [3] Erlebach T, Shahnaz A. Approximating node-weighted multicast trees in wireless ad-hoc networks[C]//*Proceedings of the 2009 International Conference on Wireless Communications and Mobile Computing: Connecting the World Wirelessly*. 2009: 639-643.
- [4] Sun Y, Halgamuge S. Fast algorithms inspired by physarum polycephalum for node weighted steiner tree problem with multiple terminals[C]//*2016 IEEE Congress on Evolutionary Computation (CEC)*. IEEE, 2016: 3254-3260.
- [5] Angelopoulos S. The node-weighted Steiner problem in graphs of restricted node weights[C]//*Scandinavian Workshop on Algorithm Theory*. Berlin, Heidelberg: Springer Berlin Heidelberg, 2006: 208-219.
- [6] Demaine E D, Hajiaghayi M T, Klein P N. Node-weighted Steiner tree and group Steiner tree in planar graphs[C]//*Automata, Languages and Programming: 36th International Colloquium, ICALP 2009, Rhodes, Greece, July 5-12, 2009, Proceedings, Part I 36*. Springer Berlin Heidelberg, 2009: 328-340.
- [7] Buchanan A, Wang Y, Butenko S. Algorithms for node-weighted Steiner tree and maximum-weight connected subgraph[J]. *Networks*, 2018, 72(2): 238-248.
- [8] Dreyfus S E, Wagner R A. The Steiner problem in graphs[J]. *Networks*, 1971, 1(3):195-207.
- [9] Konda V, Tsitsiklis J. Actor-critic algorithms[J]. *Advances in neural information processing systems*, 1999, 12.
- [10] Rehfeldt D, Koch T. Implications, conflicts, and reductions for Steiner trees[J]. *Mathematical Programming*, 2023, 197(2): 903-966.
- [11] Molloy, M.; and Reed, B. 1995. A critical point for random graphs with a given degree sequence. *Random Structures and Algorithms*, 6(2): 161–180.
- [12] Erdos, P.; and R " enyi, A. 1960. On the evolution of random graphs. *Publ. Math. Inst. Hung. Acad. Sci*, 5(1): 17–60.
- [13] Watts, D. J.; and Strogatz, S. H. 1998. Collective dynamics of 'small-world' networks. *nature*, 393(6684): 440.
- [14] Barabási, Albert-László, and Réka Albert. "Emergence of scaling in random networks." *science* 286.5439 (1999): 509-512



**AD Publications**

**Sector-3, MP Nagar, Bikaner,  
Rajasthan, India**

**[www.adpublications.org](http://www.adpublications.org), [info@adpublications.org](mailto:info@adpublications.org)**